Constraints on the Dynamic Contribution to 21st-Century Sea Level Rise from Greenland Outlet Glaciers

by

Elizabeth Ultee

A dissertation submitted in partial fulfillment
of the requirements for the degree of
Doctor of Philosophy
(Atmospheric, Oceanic, and Space Sciences)
in the University of Michigan
2018

Doctoral Committee:

Associate Professor Jeremy N. Bassis, Chair
Associate Professor Eric Hetland
Assistant Professor Gretchen Keppel-Aleks
Professor Maria Carmen Lemos
Professor Emeritus Henry N. Pollack
Professor Richard B. Rood

Elizabeth Ultee
ehultee@umich.edu
ORCID iD: 0000-0002-8780-3089

For you.

ACKNOWLEDGMENTS

This work would not be what it is without innumerable contributions, small and large, from those around me. I am deeply grateful for them all—for you all—but am bound to forget some thank-yous that really should be included here. Please take this as a reflection of my imperfect memory rather than a sign of ingratitude.

Jeremy Bassis was a truly excellent supervisor. He took my ideas and questions seriously, demonstrating a great deal of patience while I puzzled through things. His considerate mentorship helped me develop as a confident, independent scientist. It has been a joy to work with him.

My dissertation committee met my broad interests with their own. Gretchen Keppel-Aleks asked thoughtful questions and gave insight from her own experience. Eric Hetland shared helpful thoughts about academic careers and always had good book recommendations. Henry Pollack drew on his wealth of experience to shape who and how I wanted to be as a scientist. Ricky Rood listened carefully to my needs and helped me refine my career plans. Maria Carmen Lemos helped me delve as deep into science usability as I was willing to go, and she was brilliant as a manuscript co-author.

Members of the Ice Dynamics research group were invaluable in shaping my understanding of my field. They listened to hours of my practice talks and scientific musings, sent along interesting articles, and helped me design visualizations for my results. Mac Cathles, in particular, has been an incredible help in many areas, not least by encouraging me to keep having fun. Morgan Whitcomb shared delights, absurdities, and challenging times with me; when I really needed someone, Morgan was there (with a bag of googly eyes).

The wider glaciology community has given me a great deal of data, mentorship, and encouragement. I could not have produced any of these results without data supplied and/or suggested by Shad O'Neel, Bob McNabb, Christian Kienholz, Matthias Huss, Leigh Stearns, and Ruth Mottram. A special thank you to Regine Hock and the instructors and students of the 2016 International Summer School in Glaciology, which remains a highlight of my time in graduate school.

Many distinct groups at U-M have made my time here more pleasant and enriching. Campus Symphony Orchestra forced me to spend at least one evening a week not even

thinking about work. Michigan Sustainability Cases allowed me to think and write about pedagogy in new ways. The office for Community-Engaged Academic Learning were tireless in finding niches for me to develop as a community-engaged instructor. The Residential College made space for me to teach a semester-long course of my own design, which I deeply appreciate as an uncommon opportunity for graduate students. Justin Schell, Toly Rinberg, and Jake Wylie were partners in course design and management. Climate Blue gave me the incomparable experience of attending COP21 and allowed me to explore the intersection of my nonprofit-management background with my academic interests. The Michigan University-wide Sustainability & Environment Initiative brought interdisciplinarity to my doctoral education, and the people I worked with there are delightful. I am especially thankful that MUSE introduced me to my thoughtful collaborator and friend, James Arnott. Tim NeCamp, Andrew Schwartz, and Jeff Shi are community-engaged scientists, but mostly my friends.

Groups in the wider Ann Arbor community made this place a home conducive to doing good work. Ashtanga Yoga: Ann Arbor was an important source of clarity and stability; I hope I was able to offer back the same energy. The Eco Book Club of Literati Bookstore is a really bright group of people, and every time I saw them I emerged with new ideas. The Zen Buddhist Temple was my literal home for a summer and always welcomed me.

Previous experiences helped me develop skills and attitudes that served me well throughout these four years of research. Queen's University Department of Mathematics and Statistics offered intellectual rigor and genuine excitement about theory during my undergraduate studies. Dick Peltier and the University of Toronto Centre for Global Change Science let me preview what it would be like to work in this field. AIESEC UK made me a public speaker, a manager, and a person who reflects deeply on my values.

Friends including Simone Arvisais-Anhalt, Ariella Wolkowicz, Paige Barton, Emily Burdo Gray, Ed Belk, Luke Power, Dan Bregha, Leo Szivo, Ilma Ibrisevic, Sebastian Trenckmann, Larissa Becirovic, Peter Gallivan, and Kai Ip Wong showed genuine interest in my work and my graduate school experience. Jana Fey is the perfect academic mate. My family and Nick Perlongo's family cared for me often and well.

Finally, a kind of philosophical note: scientists are whole people, not robots. A number of people, including but not limited to the following, have been especially important in my developing as a whole person during the past four years: Nick Perlongo, Mayank Vikas, Angela Jamison, Rebecca Hardin, Denise Galarza Sepúlveda, Sara Soderstrom, John Ware, Liza Degtiarenko, Ezana Zewede, Lisa Wolf, and Sergio Tarazona.

Thank you.

PREFACE

The body of this dissertation consists of the text of three published papers and one manuscript in preparation for publication. Each chapter includes a short header paragraph to explain its role in the dissertation as a whole. With the exception of such headers, and any necessary changes in format, chapters whose text has already been published are presented unaltered, out of respect for the peer-review process that produced their final form.

In Chapters 2 and 3, we refer to the large outlet glacier near Ilulissat by its Danish name, Jakobshavn Isbræ, as is common elsewhere in the glaciological literature. Between the publication of Chapter 3 and the writing of Chapter 4, we contacted Oqaasileriffik, the Language Secretariat of Greenland, to ask about preferred nomenclature for that and other glaciers we study. They responded encouraging us to use the Greenlandic name, Sermeq Kujalleq; we implement that change in Chapter 4. In this dissertation, "Jakobshavn Isbræ" and "Sermeq Kujalleq" refer to the same glacier.

TABLE OF CONTENTS

LIST OF FIGURES

LIST OF TABLES

ABSTRACT

Numerical models currently in use for projections of future ice sheet mass balance lack a mechanistic description of iceberg calving, introducing uncertainty in the future glaciological contribution to global sea level. Constraining dynamic mass loss associated with particular future scenarios can help us parse that uncertainty. We have modified the plastic approximation of Nye (1952) to apply to ocean-terminating glaciers (published derivation: Ultee & Bassis, 2016) and generate physically consistent constraints on dynamic mass loss. Our approach accounts for the interaction of multiple glacier tributary branches (published methods: Ultee & Bassis, 2017) and their contribution to sea level. For four large Greenland outlet glacier catchments—Sermeq Kujalleq (Jakobshavn Isbræ), Koge Bugt, Helheim, and Kangerlussuaq Glaciers—we find an upper bound of 29 mm on dynamic contribution to sea level after 100 years of warming. This bound accounts for dynamic loss only and can be summed with surface mass balance projections to bound the total glaciological contribution to sea level from those catchments. The convergence of upper bounds derived from our two strongest forcing scenarios agrees with studies that suggest surface mass balance will dominate future mass loss from Greenland.

Although our work is motivated by coastal communities' exposure to rising seas, the constraints we produce here are unlikely to be immediately usable for coastal adaptation. Intermediaries such as extension agents, climate consultants, or regional science-policy boundary organizations may be able to tailor our results for use in local adaptation contexts (published commentary: Ultee, Arnott, Bassis, & Lemos, 2018). Understanding the landscape of science intermediation, as well as working directly with stakeholders, can help

researchers produce more usable sea level information.

CHAPTER 1

Introduction

The future of global sea levels is of worldwide societal concern. Global mean sea level has been on the rise at least since 1900, with considerable acceleration since 2000 (Hay et al., 2015). The 2014 U.S. National Climate Assessment found that vulnerable populations, including indigenous people, elderly people, and people living in poverty, were already at that time being displaced by rising seas (Melillo et al., 2014), and in the intervening years popular media have amplified stories of coastal community relocation (e.g. Davenport and Robertson, 2016; Rytz, 2018).

Climate research can respond to this widespread societal concern by producing and sharing sea level information that supports decision-making. Constraining the rate of sea level rise in the 21st century, for example, can help to construct best- and worst-case scenarios for coastal planners to incorporate into their work. In this century, the most important factor determining the rate of sea level rise will be the rate of mass loss from glaciers and ice sheets worldwide.

This dissertation aims to constrain the rate of mass lost from glaciers and ice sheets due to iceberg calving, the process by which blocks of solid ice detach from glaciers where they meet the ocean. We develop a simple numerical model for ocean-terminating glaciers and apply it to glaciers in Greenland and Alaska. The projections of dynamic mass loss we generate complement existing estimates of ice loss due to melting. In the final dissertation chapter, we discuss how this work and broader sea-level research can better support decision-making.

Because each chapter of this dissertation is or aims to be a self-contained, published article, the chapters appear with their own introductions. The sections of this introductory chapter give a very brief summary of the problem of iceberg calving, how other authors have approached it, and how our approach differs.

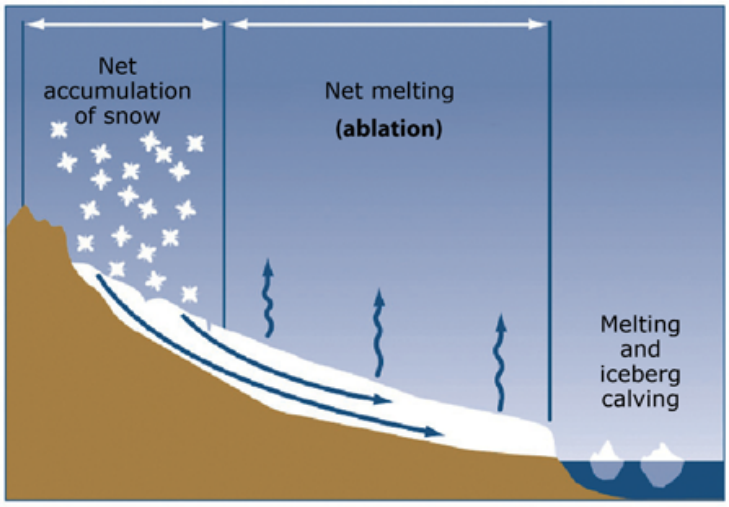

Figure 1.1: A diagram of glacier mass balance processes, showing a mountain in brown, glacier ice in white, with direction of ice flow indicated by blue arrows. Image credit: U.S. Geological Survey.

1.1 Processes of ice mass loss and gain

When a region receives sufficient frozen precipitation that does not melt during the summer, it can build up year after year and compress into glacier ice. Continued accumulation of frozen precipitation on the surface of a glacier adds to its mass. The glacier flows slowly under the force of gravity, and when it reaches a warmer area at lower elevation, it can lose mass by melting and sublimation. A glacier that reaches a body of water can also lose mass when icebergs break off the glacier front and float away. Figure 1.1 illustrates these processes for an idealized marine-terminating glacier.

On the Greenland Ice Sheet, meltwater runoff and iceberg calving are each responsible for about half of annual mass loss (van den Broeke et al., 2009). When a marine-terminating glacier loses mass to the ocean, it contributes directly to changing global sea levels. Land-terminating glaciers also contribute to sea level change by returning water to the hydrological cycle, but additional factors such as terrestrial water storage affect how much of that water ends up in the ocean. The sea level contribution of land-terminating glaciers is beyond the scope of this work.

Ice loss due to melting is well understood and included in models (e.g. Huss and Hock, 2015; Marzeion et al., 2012). The details of the iceberg calving process remain more difficult to capture. Most ice sheet models — including e.g. the Simulation Code for Polythermal Ice Sheets ("SICOPOLIS", Greve and Hutter, 1995), the Parallel Ice Sheet Model ("PISM", Winkelmann et al., 2011), the Ice Sheet System Model ("ISSM", Larour et al.,

2012), Elmer/Ice (Gagliardini et al., 2013), the Community Ice Sheet Model ("CISM", Price et al., 2015), and PennState3D (DeConto and Pollard, 2016) — and global-scale glacier models (including Huss and Hock, 2015; Marzeion et al., 2012) represent ice flow as viscous continuum deformation, which cannot easily accommodate discontinuities from ice fracture and iceberg detachment. Furthermore, ice fracture itself has several physical modes (Colgan et al., 2016) and various mathematical descriptions (Rice, 1968; Reeh, 1968; Vaughan, 1993). Section 1.2 describes existing approaches to account for calving in numerical glacier and ice sheet models.

1.2 Previous modeling approaches

We are interested in bounding the contribution of iceberg calving to global mean sea level within this century. This means we seek a numerical model that finds (rather than pre-sets) the rate of iceberg calving, can be validated against multi-annual observations from our glaciers of interest, and is practical to implement on the century time scale. Given the importance of ice dynamics for the mass balance of glaciers and ice sheets (Velicogna et al., 2014; Khan et al., 2014, 2015), many groups have developed approaches to the problem that are suitable for assorted applications. We review them here to demonstrate the need for the new modelling approach we develop for this particular problem.

The simplest model approach to account for iceberg calving is to set the calving rate with an empirical parametrization (Benn et al., 2007). For example, one configuration available in the Community Ice Sheet Model imposes a set fraction of ice lost per time step from each grid cell at the ice-ocean interface (Price et al., 2015). One of the many calving parametrizations included in the Parallel Ice Sheet Model removes all marine ice thinner than a user-input threshold value. Both CISM and PISM solve equations of ice flow in three dimensions, across entire ice sheets, and pre-set calving fractions help manage computational expense. However, the use of an empirical relation assumes that statistics such as temporal rate and size distribution of iceberg calving will persist unchanged into the future. That assumption is not necessarily supported by physics, and changes in local environment may affect the relevant statistics. In short, directly setting the rate of iceberg calving limits the future scenarios we can consistently simulate.

Several models use more physics-motivated calving parametrizations. The "eigencalving" parametrization available in the Parallel Ice Sheet Model, for example, sets an iceberg calving rate proportional to the product of the principal strain rates wherever that product is positive (Winkelmann et al., 2011; Albrecht and Levermann, 2012). Another popular parametrization allows ice to calve when surface crevasses have penetrated down to

a threshold depth. In the flowline model of Nick et al. (2013b), parameters controlling crevasse penetration (as well as other physical processes) are tuned such that the glacier terminus position matches observations. Although these parametrizations have a stronger connection to underlying physics, the tuning of parameters to current observations still relies on an assumption that the environment of the future will be like the one we observe today. We prefer a model formulation in which the only adjustable parameters are physical quantities that can be directly determined from experiment or observation.

Much more detailed models represent glacier ice as a granular material, a flowing collection of ice particles that can break apart and produce icebergs of varying sizes (e.g. Åström et al., 2013; Bassis and Jacobs, 2013). Benn et al. (2017a) couple the granular model HiDEM with the continuum model Elmer/Ice and find terminus evolution and iceberg size distribution consistent with observations at Store Glacier, Greenland. Those models' primary applicability is in exploring detailed relationships between calving rate and variables such as fjord water depth or depth of water in surface crevasses. Model validation, accordingly, considers daily-to-monthly observations (e.g. iceberg size distribution in a fjord) rather than the multi-annual loss of mass or change in terminus position of observed outlet glaciers. Further, both Åström et al. (2013) and Benn et al. (2017a) state that their models are too computationally expensive to implement on wide spatial or temporal scales. To project century-scale changes for multiple Greenland outlet glaciers, we need a more streamlined model.

We can streamline a numerical model by solving equations of ice flow in fewer dimensions, essentially averaging dynamics across the width and/or depth of the glacier. Streamlined "flowline models" as described in Oerlemans (2008), solve only along lines that follow the glacier flow. Nick et al. (2013a) use a flowline model with a single line for each of four large glacier catchments in Greenland. The simplicity of flowline models makes them computationally efficient and suitable for simulations of century scale or longer. Ice loss from glaciers undergoing prolonged retreat may expose underlying topography that divides catchments into dynamically disconnected regions (Enderlin et al., 2018), however, which are less easily represented by a single flowline. We are not aware of any previously published flowline models that are able to handle dynamic separation of glacier catchments. The bed topography underlying major Greenland catchments such as Helheim and Kangerlussuaq Glaciers suggests that dynamic separation may take place over century-scale retreat, so we would like to account for that effect in our model.

1.3 Our approach

In this work, we introduce a width-averaged, vertically-integrated model applied to networks of interacting flowlines. It accounts for the effect of iceberg calving without directly controlling the calving rate. Instead, the yield strength of ice τ_y, which can be constrained within an order of magnitude by laboratory and field observation (O'Neel et al., 2005; Cuffey and Paterson, 2010), describes where ice should break at the glacier terminus. We validate the model with observations of marine-terminating glaciers in Greenland and Alaska, demonstrating that we capture observed terminus advance, retreat, and multi-annual cycling. Our model keeps the computational efficiency of a flowline model while accounting for dynamic separation of glacier catchments. It is well-suited to estimating upper bounds on outlet glacier sea level contribution at the century time scale under a variety of future forcing scenarios.

CHAPTER 2

An extension of the perfect plastic approximation to calving glaciers

N.B.: This chapter was published in 2016 as

Ultee, L. and Bassis, J. N. (2016). The future is Nye: an extension of the perfect plastic approximation to tidewater glaciers. *Journal of Glaciology*, 62(236), pp. 1143–1152. http://dx.doi.org/10.1017/jog.2016.108.

It describes the physical basis and historical context for our work, and we derive the fundamental equations applied in later chapters.

2.1 Introduction

Global mean sea level rise (SLR) threatens coastal and island populations worldwide, but large uncertainties remain in near-term projections of the threat (e.g. Horton et al., 2015; Church et al., 2013). Ice sheets and glaciers provide the largest—and most uncertain—contribution to projected 21st century SLR (Church et al., 2013), with integrated mass loss from Greenland, Antarctica, and the large number of smaller glaciers worldwide each responsible for about one third of the sea level contribution observed at present (Gardner et al., 2013). The Greenland Ice Sheet sheds mass to the ocean through a drainage network of tidewater glaciers, and the sea level contribution from Alaska glaciers is especially large (Larsen et al., 2015). Tidewater glaciers such as Alaska's Columbia Glacier are susceptible to instability that can drive rapid retreat and loss of ice mass to the ocean. Thus, improving understanding of tidewater glacier dynamics is crucial to decreasing uncertainty in SLR projections. This is especially important given that about half of recently observed acceleration of Greenland mass loss is attributed to dynamic discharge of solid ice to the ocean

through iceberg calving (Straneo et al., 2013), a mechanism that also dominates mass loss from Alaska tidewater glaciers (McNabb et al., 2012; Larsen et al., 2007; O'Neel et al., 2003).

Despite the dominant role iceberg calving plays in current and projected mass loss from ice sheets and glaciers, calving remains poorly understood. Part of the difficulty in understanding stems from the large number of factors influencing calving (e.g. local meteorology, ocean temperature and circulation, glacier geometry) for which available data are limited (Straneo et al., 2013; Benn et al., 2007). Even when data are available, observations show contradictory behavior for glaciers in different environments. For example, Alaskan tidewater glaciers very rarely form floating ice tongues, but when they do (as in the case of Columbia Glacier in later stages of its ongoing retreat) they may show more large-scale and fewer small-scale calving events (Bassis and Jacobs, 2013; Walter et al., 2010). This suggests another challenge to understanding calving: the wide variety of spatial and temporal scales involved. Different styles of iceberg calving may be observed at sub-hourly, multi-weekly, and decadal time scales (Bassis and Jacobs, 2013; Amundson and Truffer, 2010). Further, the calving contribution from small glaciers is difficult to capture at the model resolutions typical of continental-scale ice sheet models (e.g. Bassis, 2011).

Current ice sheet models treat glacier ice as a viscous fluid, without a physically-consistent method for simulating iceberg calving. Several parameterizations for calving are used, varying in complexity according to the intended application of the model. One relatively simple approach treats calving rate and/or the calving fraction of total ice loss as a directly adjustable parameter (e.g. Price et al., 2015). Another approach requires ice to calve from an ice sheet margin when it thins below a given thickness; the threshold ice thickness can be constrained by observations, such as the 150-m minimum ice shelf thickness observed in present-day Antarctica (Peyaud et al., 2007).

Recently, more continuum based calving criteria have begun to be implemented in ice sheet models. One such approach is damage mechanics, which introduces ice "damage" from fracturing as a state variable that affects ice flow (Duddu et al., 2013; Borstad et al., 2012; Pralong and Funk, 2005). Calving can be set to occur once damage reduces the load-bearing capacity of the ice by a certain percentage, constrained by analysis of large calving events such as the Larsen B ice shelf collapse (Borstad et al., 2012). Significant controversy remains, however, about how to formulate the damage evolution law. A related approach ties calving to penetration of surface and basal crevasses. This crevasse-depth criterion assumes that glacier ice calves off once surface crevasses reach the waterline or surface and basal crevasses connect, and further that the calved ice immediately ceases to interact with the rest of the glacier (Nick et al., 2010; Bassis and Walker, 2012; Benn et al., 2007).

These models, however, typically require the addition of surface meltwater into crevasses to trigger calving and treat meltwater as a parameter that is adjusted to approximate observations (as in Nick et al., 2010). Newer methods, based on discrete particles (e.g. Bassis and Jacobs, 2013; Åström et al., 2013) or self-organized criticality (Astrom et al., 2014) of glacier termini are promising, but too computationally expensive to be routinely used in prognostic ice sheet models.

Here we propose a different approach that integrates some of the advantages of particle-based methods and continuum-based methods, but which is much simpler than previously proposed approaches. We assume that above a yield strength, fractured glacier ice deforms much more rapidly than intact glacier ice. Because the flow of ice is rapid above the yield strength, the yield strength provides an upper bound on state of stress within the glacier. Assuming that the glacier is everywhere near this critical state of stress corresponds to the perfect-plastic approximation, first derived by Nye (Nye, 1951, 1952, 1953). Nye's formulation deduces the length of glaciers from the surface mass balance profile by assuming that the ice thickness at the terminus vanishes, limiting the application of the model to terrestrial environments. Here we extend Nye's solution and show that if yielding also occurs at the calving front, a reasonable assumption for calving glaciers, then this provides a boundary condition that allows us to self-consistently determine the terminus position and rate of advance/retreat of the glacier. Application of the model to Columbia Glacier shows that, despite the model's simplicity, it is able to reproduce the observed pattern of retreat.

2.2 Model development

The perfect plastic flow presented here is a special case of viscoplastic flow. A viscoplastic fluid flows with some nonzero viscosity until its maximum principal stress exceeds a given yield strength, after which point it flows much more rapidly (Nye, 1951). In the perfect plastic case, the material is rigid below the yield strength. Examples of geophysical fluid flows exhibiting plastic or viscoplastic rheology include avalanches, lahars, and rockslides (e.g. Balmforth et al., 2006; Remaître et al., 2005). Applied to glacier ice, a viscoplastic rheology may offer a unified treatment of intact and fractured ice, in contrast to existing models relying on purely viscous ice flow that ignores the effect of fractures on glacier flow.

Here we explore a simple generalization of Nye's perfect plastic approximation, supplementing the assumption that shear stress at the bed is at the yield with the additional criterion that longitudinal stress at the calving front is also at the yield stress. This simple criterion provides a self-consistent means of computing steady-state profiles of glaciers in

marine environments in addition to terrestrial environments. Moreover, we show that the perfect plastic approximation not only produces realistic steady-state profiles of glaciers, but also predicts retreat patterns that mimic observed patterns.

2.2.1 Theory

To develop the model, we start from the conservation of mass and momentum in a 2-D incompressible fluid. For a fluid with velocity field $\vec{u} = [u(x,z,t),\ w(x,z,t)]$ and pressure $p(x,z,t)$ flowing down a plane inclined at angle φ to the horizontal, conservation of mass and momentum imply:

$$\frac{\partial u}{\partial x} + \frac{\partial w}{\partial z} = 0 \tag{2.1}$$

$$\rho \frac{\mathrm{D}u}{\mathrm{D}t} = -\frac{\partial p}{\partial x} + \frac{\partial}{\partial x}\tau_{xx} + \frac{\partial}{\partial z}\tau_{xz} + \rho g \sin\varphi \tag{2.2}$$

$$\rho \frac{\mathrm{D}w}{\mathrm{D}t} = -\frac{\partial p}{\partial z} + \frac{\partial}{\partial x}\tau_{xz} + \frac{\partial}{\partial z}\tau_{zz} - \rho g \cos\varphi, \tag{2.3}$$

where τ_{ij} are the components of the deviatoric stress tensor $\boldsymbol{\tau}$. For the case $\varphi \approx 0$, common for ice sheets and low sloping regions of marine-terminating-glaciers, $\rho g \sin\varphi \to 0$ and $\rho g \cos\varphi \to \rho g$ in the equations above.

Instead of the usual power-law creep flow often used in modeling ice, we model ice as a plastic material with no basal slip. When the effective stress, $\tau_{\mathrm{e}} \equiv \sqrt{\tau_{xx}^2 + \tau_{xz}^2}$, is beneath a material dependent yield strength, τ_{y}, we assume the glacier ice is rigid. In reality glaciers are not rigid beneath a yield strength. However, in our model we assume that the deformation of intact glacier ice is much slower than the deformation of yielded ice—effectively rigid. Above the yield strength τ_{y}, we assume the ice is disarticulated and flows like a granular material. We model this regime as power-law creep, but with a much smaller effective viscosity then the viscosity of intact ice. Hence, our rheology can be written in the form:

$$\tau_{ij} = \frac{1}{\dot{\gamma}} \left(B_{\text{gran}}\, \dot{\gamma}^{1/n} + \tau_{\mathrm{y}} \right)\ \dot{\varepsilon}_{ij} \qquad \text{for } \ \tau_{\mathrm{e}} \geq \tau_{\mathrm{y}}, \tag{2.4}$$

and $\dot{\varepsilon}_{ij} \equiv 0$ otherwise. Here B_{gran} represents the softness parameter for yielded (granular) ice, the components of the strain rate tensor are $\dot{\varepsilon}_{ij} = \left(\frac{\partial u_i}{\partial x_j} + \frac{\partial u_j}{\partial x_i} \right)$, and

$$\dot{\gamma} = \sqrt{4\dot{\varepsilon}_{xx}^2 + \dot{\varepsilon}_{xz}^2} \equiv 2\dot{\varepsilon}_{\mathrm{e}}, \tag{2.5}$$

defining $\dot{\varepsilon}_{\mathrm{e}}$ as the effective strain rate.

We impose two boundary conditions: the upper surface must be traction-free, and for simplicity we require no slip at the bed. The no-slip boundary condition means simply that both velocity components vanish at the bed $b(x)$, i.e.

$$u = w = 0 \quad \text{wherever } z = b(x). \tag{2.6}$$

The ice/air interface $z = h(x,t)$ is a material surface subject to net snow accumulation, $\dot{a}$. Imposing the traction-free condition on this material surface gives the boundary conditions:

$$\frac{\partial h}{\partial t} + u\frac{\partial h}{\partial x} = w + \dot{a}, \tag{2.7}$$

$$\left(1 - \left(\frac{\partial h}{\partial x}\right)^2\right) p + \left(1 + \left(\frac{\partial h}{\partial x}\right)^2\right) \tau_{xx} = 0, \tag{2.8}$$

$$\left(1 - \left(\frac{\partial h}{\partial x}\right)^2\right) \tau_{xz} - 2\frac{\partial h}{\partial x}\tau_{xx} = 0. \tag{2.9}$$

We now nondimensionalize our equations using a characteristic thickness H, a characteristic length scale L, and the aspect ratio $\epsilon = H/L$. Then

$$u = V\tilde{u} \qquad w = \epsilon V\tilde{w} \qquad t = \frac{L}{V}\tilde{t} \tag{2.10}$$

$$p = \rho g H\tilde{p} \qquad \dot{\gamma} = \frac{V}{H}\tilde{\dot{\gamma}} \qquad \tau_{ij} = \rho\nu\frac{V}{H}\tilde{\tau}_{ij} \tag{2.11}$$

$$\frac{\partial}{\partial x} = \frac{1}{L}\frac{\partial}{\partial \tilde{x}} \qquad \frac{\partial}{\partial z} = \frac{1}{H}\frac{\partial}{\partial \tilde{z}} \qquad \frac{\partial}{\partial t} = \frac{V}{L}\frac{\partial}{\partial \tilde{t}} \tag{2.12}$$

where $\rho = \rho_{\text{ice}}$ (assumed constant), $V = \frac{gH^3}{\nu L}$ is a characteristic flow speed, $\nu = \frac{B_{\text{gran}}}{\rho}\left(\frac{V}{H}\right)^{(1/n)-1}$ is a characteristic viscosity, and tildes denote dimensionless variables. This nondimensionalization corresponds to a model where the characteristic time scale is determined by the (assumed) much faster time scale associated with rapid flow of yielded ice. On this fast time scale, unyielded ice appears to be quasi-rigid.

In the final dimensionless equations, we drop the tilde markers for ease of notation. The conservation equations become:

$$\frac{\partial u}{\partial x} + \frac{\partial w}{\partial z} = 0 \tag{2.13}$$

$$\epsilon\mathcal{R}\left(\frac{\partial u}{\partial t} + u\frac{\partial u}{\partial x} + w\frac{\partial u}{\partial z}\right) = -\frac{\partial p}{\partial x} + \epsilon\frac{\partial}{\partial x}\tau_{xx} + \frac{\partial}{\partial z}\tau_{xz} \tag{2.14}$$

$$\epsilon^3\mathcal{R}\left(\frac{\partial w}{\partial t} + u\frac{\partial w}{\partial x} + w\frac{\partial w}{\partial z}\right) = -\frac{\partial p}{\partial z} + \epsilon^2\frac{\partial}{\partial x}\tau_{xz} + \epsilon\frac{\partial}{\partial z}\tau_{zz} - 1 \tag{2.15}$$

and the rheology

$$\begin{pmatrix} \tau_{xx} & \tau_{xz} \\ \tau_{xz} & \tau_{zz} \end{pmatrix} = \frac{1}{\dot{\gamma}} \left[\dot{\gamma}^{\frac{1}{n}} + \mathcal{B} \right] \begin{pmatrix} 2\epsilon \frac{\partial u}{\partial x} & \frac{\partial u}{\partial z} + \epsilon^2 \frac{\partial w}{\partial z} \\ \frac{\partial u}{\partial z} + \epsilon^2 \frac{\partial w}{\partial z} & 2\epsilon \frac{\partial w}{\partial z} \end{pmatrix} \tag{2.16}$$

for $\tau_{\mathrm{e}} \geq \mathcal{B}$, with the aspect ratio $\epsilon = H/L$ as above; and $\dot{\varepsilon}_{ij} \equiv 0$ for $\tau_{\mathrm{e}} < \mathcal{B}$. In the above we have introduced the dimensionless Reynolds and Bingham numbers

$$\mathcal{R} = \frac{HV}{\nu}, \qquad \mathcal{B} = \frac{\tau_{\mathrm{y}} H}{\rho \nu V}. \tag{2.17}$$

For glaciers and ice sheets, we have $\mathcal{R} \ll 1$.

2.2.2 Thin film approximation

We take the thin film approximation $\epsilon \ll 1$ and drop all terms of order ϵ or higher to find the simplified equations:

$$\frac{\partial u}{\partial x} + \frac{\partial w}{\partial z} = 0 \tag{2.18}$$

$$\frac{\partial p}{\partial x} = \frac{\partial}{\partial z} \tau_{xz} \tag{2.19}$$

$$\frac{\partial p}{\partial z} = -1 \tag{2.20}$$

$$\tau_{xz} = \frac{1}{\dot{\gamma}} \left[\dot{\gamma}^{\frac{1}{n}} + \mathcal{B} \right] \frac{\partial u}{\partial z}. \tag{2.21}$$

We integrate Eqns. (2.19) and (2.20) in z, using the boundary conditions $p = \tau_{xz} = 0$ on $z = h(x,t)$, to find

$$p = h - z \qquad \tau_{xz} = -\frac{\partial h}{\partial x}(h - z), \tag{2.22}$$

and substitute into the simplified Eqns. (2.18-2.21) to find the velocity components.

Velocity components described by the rheology (Eqn. (2.16)) are distinct above and below a yield surface,

$$z = Y(x,t) = \max \left(h - \frac{\mathcal{B}}{|\frac{\partial h}{\partial x}|}, b(x) \right) \tag{2.23}$$

(also Balmforth et al., 2006). In the perfect plastic approximation, the yield surface is everywhere coincident with the bed. That is, either an infinitesimal layer of ice or the

bed itself is yielding and the rest of the glacier is intact. This approximation produces a nonlinear first-order differential equation for glacier surface elevation:

$$|h - b|\frac{\partial h}{\partial x} = \mathcal{B}. \tag{2.24}$$

2.2.3 A self-consistent terminus position

In steady state, stresses at the glacier terminus from ice and seawater must balance. That is,

$$\int_{b(x)}^{h(x)} \sigma_{xx}\,\mathrm{d}z = \int_{b(x)}^{0} -\rho_w g z\,\mathrm{d}z. \tag{2.25}$$

If $x = 0$ defines the calving front, positions $x > 0$ lie within the glacier and positions $x < 0$ lie in the water. We assume that across the calving front, where intact ice transitions to yielded, granular ice, there is another yielding surface, such that lateral stress $\tau_{xx} \cong \tau_\mathrm{y}$ for $x \approx 0^+$. Then $\sigma_{xx} = 2\tau_\mathrm{y} - \rho_i g(h - z)$. Integrating and nondimensionalizing, we find an equation relating terminus ice thickness and water depth analogous to that proposed by Bassis and Walker (2012):

$$H_\mathrm{terminus} = 2\mathcal{B}\epsilon + \sqrt{\frac{\rho_w D^2}{\rho_i} + (2\mathcal{B}\epsilon)^2} \tag{2.26}$$

where $H_\mathrm{terminus} \equiv h(x_\mathrm{terminus}) - b(x_\mathrm{terminus})$ is the dimensionless terminus thickness, ρ_w the density of seawater, D dimensionless water depth, and other terms as before. For most cases, the stress-balance requirement is stronger than requiring a grounded terminus—that is, termini that would otherwise thin to flotation instead break and retreat under our model—but we also explicitly require that ice breaks if it thins below flotation thickness:

$$H_\mathrm{float} = D\frac{\rho_i}{\rho_w}. \tag{2.27}$$

Each point (x, z) lies on at most one glacier surface elevation profile. Thus, the terminus position and thickness $(x_\mathrm{terminus}, H_\mathrm{terminus})$ uniquely determine a profile, and we can implement this condition in numerical solution of the model to simulate terminus advance/retreat connected with upstream thickening/thinning. We note that our simple relation does not imply causality in either direction: terminus retreat can trigger thinning upstream or vice versa.

Quantity	Symbol	Representative value	Notes
Yield strength	τ_{y}	150 kPa	Constant or variable (Coulomb condition)
Basal till cohesion	τ_0	130 kPa	Coulomb yield condition $\tau_{\mathrm{y}} = \tau_0 + \mu N$
Coefficient of friction	μ	0.01	Low estimate based on Cohen et al. (2005)
Non-dimensional water depth	D	—	e.g. $D = 0.2$ corresponds to 200 m physical water depth
Characteristic height	H	1000 m	Nondimensionalization constant; does not affect results
Characteristic length	L	10000 m	Nondimensionalization constant; does not affect results
Coefficient of variance (RMS)	CV_{RMS}	—	Indicates model fit with observation

Table 2.1: Key symbols and their representative values for the plastic glacier model.

2.2.4 Numerical solution

The surface elevation equation can be solved analytically for some very simple bed geometries. For more complicated geometries, straightforward numerical integration over a given bed function produces the glacier profile. We evolve the surface elevation function $h(x)$ along a centerline described by points $(x_1, x_2, \ldots, x_N)$ using a discretized version of Eqn. (2.24),

$$h(x_{i+1}) = \frac{\tau_{\mathrm{y}}}{\rho_i g (h(x_i) - b(x_i))} \Delta x + h(x_i), \tag{2.28}$$

where $\Delta x = \|x_{i+1} - x_i\|$, the step size. The bed function $b(x)$ may be defined by an analytical function or by providing observed bed values at the sample points.

We define the coordinate system such that the initial terminus position $x_{\text{terminit}} = 0$. The model may be run: (1) Starting from the terminus and stepping $\Delta x > 0$ upstream, making use of the water balance condition (Eqn. (3.3)) to determine the initial terminus thickness H_{terminit}, or (2) Starting from some upstream position $x_{\text{up}} > 0$ and stepping $\Delta x < 0$ downstream, using Eqn. (3.3) to find the terminus position of the resulting profile.

2.3 Idealized geometries

To test the functionality of the model, we first examine cases for which there is an analytical solution, such as a constant slope $b(x) = mx$, and then explore some simple idealized geometries such as concave slopes, sinusoids, and slopes with Gaussian bumps. The idealized geometries, inspired by Oerlemans (2008), are chosen to be relevant to outlet glaciers.

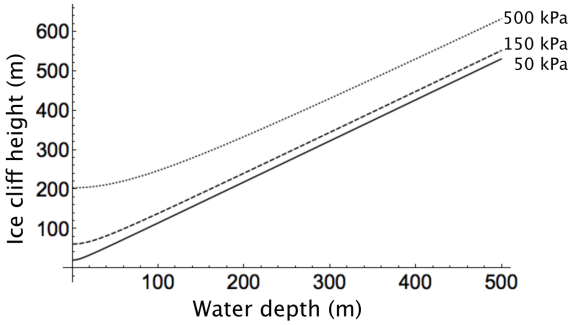

Figure 2.1: Height of ice cliffs at the terminus produced by the model for yield strengths $\tau_y = 50$ kPa (solid), 150 kPa (dashed), and 500 kPa (dotted) and water depths 0 m $\leq D \leq$ 500 m.

We test the model using a realistic range of yield strengths, $50 - 300$ kPa, to examine the effect of τ_y in idealized cases.

The height of ice cliffs at the terminus depends on water depth D and yield strength τ_y. For realistic values of D and τ_y, the model produces terminus thicknesses comparable to diverse observations (e.g. Bassis and Walker, 2012). This is illustrated in Figure 2.1.

To model terminus retreat associated with thinning, we identify an up-glacier reference point on the centerline where thinning will be simulated. We evolve the model from the terminus upstream to create a reference profile and find the reference ice thickness at the chosen point. Then, we vary the ice thickness at the reference point and evolve the model downstream from the reference point, requiring that the ice break if it thins below what is permitted by Eqns. (2.26, 2.27). This allows us to find the terminus position associated with a given amount of thinning.

Our tests show that the plastic model is able to produce realistic glacier profiles and retreat patterns over idealized bed geometries. Figure 2.2a shows snapshots of retreat using the perfect plastic approximation over a constant seaward-sloping bed. We note the familiar "pancake" profile visible in each successive snapshot. With constant upstream thinning of 5 m a^{-1}, the glacier terminus initially retreats quickly: about 12 km in the first 10 years. The initial rapid retreat pulls the terminus above sea level, however, and subsequent retreat is less dramatic.

In Figure 2.2b, we have imposed the same constant upstream thinning rate on a perfectly plastic glacier with an overdeepening and submerged sill in its bed. The initial retreat of this glacier is less rapid; it stabilizes temporarily on the submerged sill before continuing to retreat. Once again, retreat is more pronounced while the terminus is grounded below sea level and becomes more gradual after retreat pulls the terminus above sea level, consistent with observations that only marine (and lake) terminating glaciers retreat rapidly.

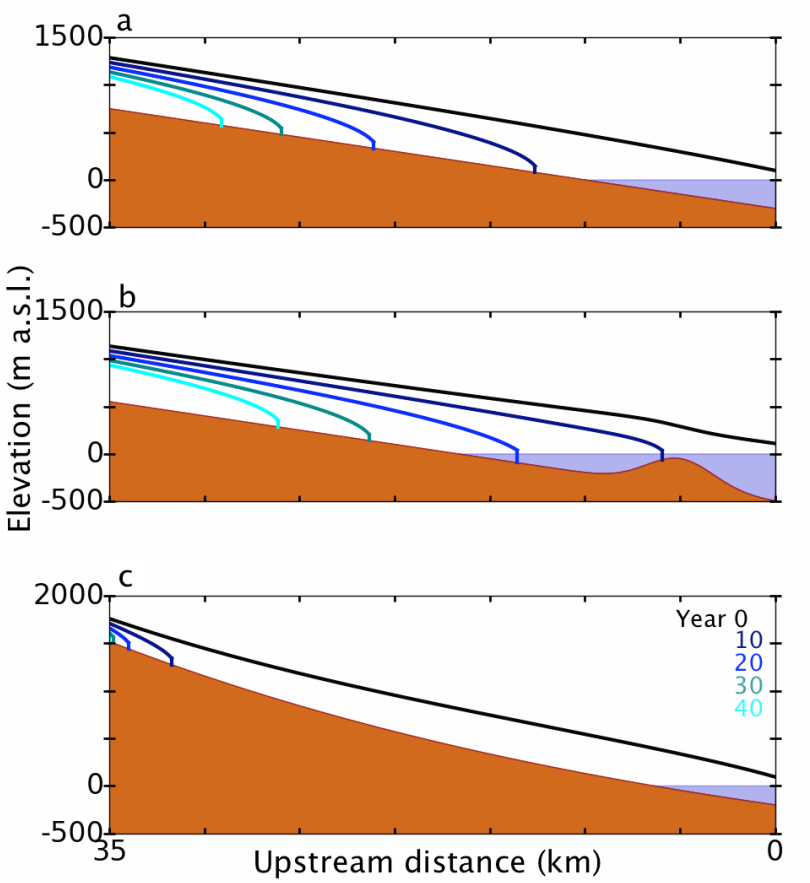

Figure 2.2: Retreat of a perfectly plastic glacier under 5 m a^{-1} constant upstream thinning. Colored curves show initial profile (black) and profiles (blue scale) after 10, 20, 30, and 40 years of thinning. The idealized bed cases (after Oerlemans, 2008) shown are: a) constant seaward-sloping bed, b) seaward-sloping bed with overdeepening and submerged sill, and c) concave bed.

Figure 2.2c shows retreat over a concave bed. The concave idealized bed represents the case of bed slope decreasing downstream, as when a glacier descends from high mountains before traversing a coastal plain (or simply a shallower valley) and terminating in the ocean. The initial steady-state profile shows a long glacier with terminus grounded in 200 m of water. Imposing the same constant thinning as in cases (a) and (b), however, shows markedly different results. After just 10 years, the glacier has retreated more than 30 km, finally stabilizing more than 1000 m above sea level. Subsequent retreat is more gradual, but within 30 years, the glacier has all but disappeared.

2.4 Case study: Columbia Glacier

We next applied our model to the more realistic geometry of the Columbia Glacier, located in south-central Alaska (inset, Fig. 2.3). After several decades of relative stability in the early 20th century, the Columbia Glacier has been changing rapidly since 1980, retreating more than 20 km (McNabb et al., 2012) and thinning up to 20 m yr^{-1} on a regional scale (O'Neel et al., 2005). The extensive data collected since 1957 make the Columbia Glacier one of the most well-studied tidewater glaciers in the world. A dataset published by McNabb et al. (2012) provides reconstructed bed topography and ice thickness, based on velocity observations of the Columbia Glacier and mass conservation. Surface elevation for 1957 is digitized from the USGS National Elevation Dataset, with 2007 surface elevation based on a panchromatic image from the SPOT (Satellite Pour l'Observation de la Terre) satellite. Calculated ice thickness is provided for both 1957 and 2007, effectively showing the state of the glacier before and during its recent major retreat.

The main branch of Columbia begins on high mountains (Fig. 2.3), nearly 2500 m above sea level (a.s.l.). The bed initially slopes steeply downward (as in ideal case (a)), with an especially steep icefall ~ 45 km upstream from the pre-retreat terminus. After the icefall, the bed slope becomes more shallow (as in ideal case (c)) and is grounded below sea level for > 30 km, with several small sills. A prominent sill ~ 20 km upstream from the pre-retreat terminus has been a site of stabilization since 2010 for the main branch retreat (as in ideal case (b)). Key features of the Columbia bed topography, illustrated in brown in Figures 2.4 and 2.5, can be compared with Figure 2.2 above. These features, along with the available bed topography and ice thickness data from several years of study, motivate selection of Columbia Glacier as an initial study site. In this case study, we test our model using realistic bed topography from observations of Columbia and comparing the modeled surface elevation profiles with observed glacier profiles. Figure 2.3 shows the chosen main branch centerline on a map of Columbia Glacier bed topography.

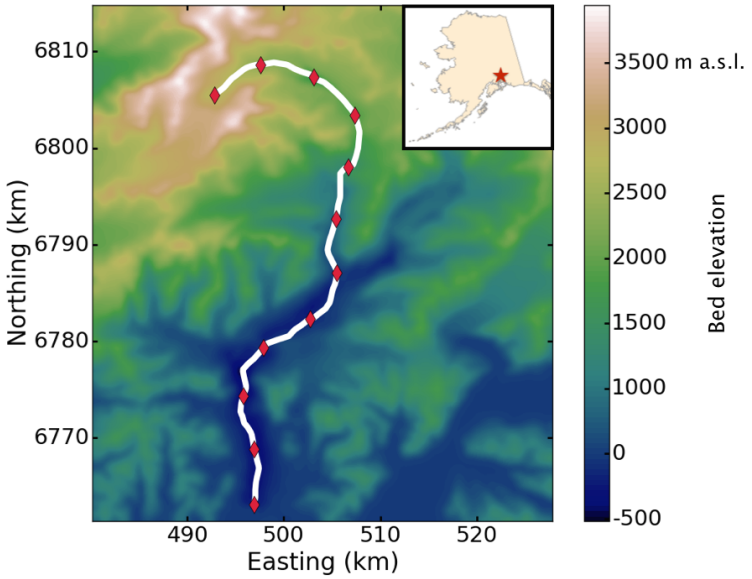

Figure 2.3: Columbia Glacier main centerline shown in white, with red ticks every 5 km, over a map of bed elevation. Inset in top right corner shows the location of Columbia Glacier (red star) over an outline of the state of Alaska.

2.4.1 Steady state profiles

We manually define a centerline along Columbia's main branch by choosing a set of points on a contour plot of 1957 ice thickness, and we interpolate the bed and ice elevation data to 1-D functions in terms of arc length along the centerline. Using the bed function defined by the data, we model the glacier surface elevation along the centerline according to Eqn. (2.28). We apply the model using a range of different yield strengths τ_y. The value is constrained by observations and laboratory experiments; the range $50-200$ kPa considered in the idealized case reflects an appropriate range (Cuffey and Paterson, 2010; O'Neel et al., 2005).

In the simplest case, we assume τ_y is constant. Because τ_y reflects the shear strength at the bed in our approximation, τ_y may vary spatially or with time. For example, there may be soft marine sediments with low τ_y near the terminus and hard bedrock with high τ_y upstream. The effects of subglacial processes such as erosion, sediment deposition, and evolving water drainage suggest temporal variation in τ_y as well. We can introduce a physically-motivated modification to the model by allowing τ_y to be a function of effective water pressure at the glacier base, implemented as follows:

$$\tau_y = \tau_0 + \mu \left(\rho_i g(h-b) - \rho_w g D\right), \tag{2.29}$$

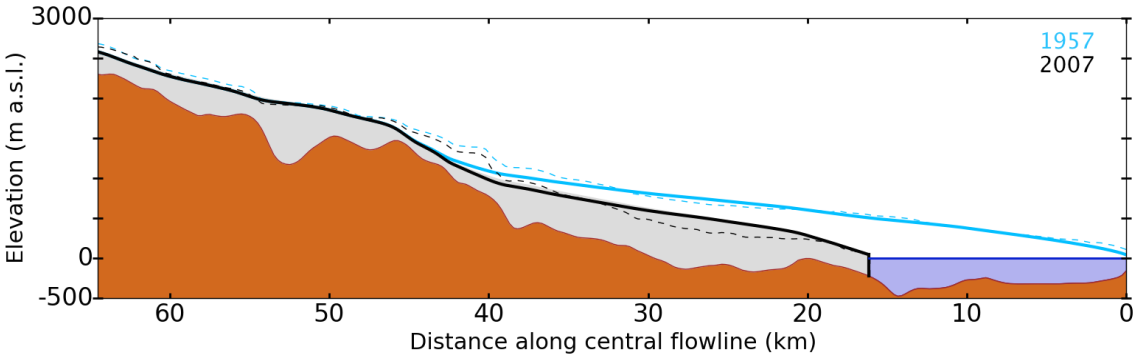

Figure 2.4: Columbia Glacier main centerline: perfect plastic model profiles ($\tau_y = 150$ kPa, solid curves) with 1957/2007 observations (dashed curves). Note 5:1 vertical exaggeration in scale.

with $\mu \approxeq 0.01$ the bulk coefficient of friction and all other symbols as previously defined. Our choice of μ reflects the lower end of the range derived experimentally by Cohen et al. (2005) and is of the appropriate order of magnitude to fit observed Columbia profiles.

The model produces a realistic central profile that can be compared with observations from 1957 and 2007. The shape of the profile is determined by the yield strength, with values of τ_y between $75 - 220$ kPa producing the most realistic profiles. Force balance calculations by O'Neel et al. (2005) suggest a probable range of yield strengths for the Columbia Glacier bed of $50-200$ kPa. The perfect plastic profiles computed with $\tau_y = 150$ kPa for the 1957 and 2007 observed terminus positions are shown in Figure 2.4, with observed 1957 and 2007 profiles presented for comparison.

When observations of surface elevation are available for the entire centerline, as for 1957 and 2007, the CV_{RMS} statistic (coefficient of variation of the RMSE) comparing simulated and observed ice thickness is defined and we may use it for analysis. The CV_{RMS} is related to RMSE but normalized by the mean value of the measurement. This normalization reflects the physical intuition that 100 m of error on a 100 m-thick glacier is more problematic than 100 m of error on a 1000 m-thick glacier.

Allowing yield strength to vary with effective basal pressure produces steady-state profiles with CV_{RMS} comparable with that of constant yield profiles. The shape of variable-τ_y profiles depends on the choice of τ_0 in Eqn. (2.29); CV_{RMS} is minimized using $\tau_0 \approxeq 130$ kPa. Note that the coefficient of friction μ in Eqn. (2.29) also affects the shape of the glacier profiles, but for this study we have held $\mu = 0.01$ constant. Visually, the centerline profiles computed for 1957 and 2007 using $\tau_y = 130\text{kPa} + \mu\left(\rho_i g H - \rho_w g D\right)$ are nearly indistinguishable from the constant-τ_y profiles shown in Figure 2.4.

2.4.2 Retreat

To simulate retreat, we proceed as described for the idealized cases. We assume that the glacier surface elevation was approximately constant during its decades of stability (until about 1980) and that all observed thinning occurred 1982-2007, during the recent period of rapid retreat (O'Neel et al., 2005; Krimmel, 2001). Further, we assume a constant thinning rate between 1982 and 2007 – this works out to an average 8 m a^{-1} at the reference point 35 km upstream. Using this thinning rate, we can estimate the amount of thinning corresponding to a particular month or year during Columbia's retreat and generate a snapshot of the centerline profile at that time. We "evolve" the model in time by producing a series of such snapshots. We then evaluate the model by comparing snapshots from a particular year with surface elevation and terminus position data obtained in that year by the USGS (Krimmel, 2001). Note that while we time-evolve the model by controlling upstream thinning, it could just as well be time-evolved by controlling the terminus retreat rate and solving for upstream thickness. That is, the apparent "causality" in the model could be reversed. We do not presume to comment on the correct direction of causality. Figure 2.5 shows 5-yearly snapshots of the retreat simulated with $\tau_y = 150$ kPa and $\tau_y = 130\text{kPa} + \mu\left(\rho_i g H - \rho_w g D\right)$. Animations of the modeled retreat are available in the Supplementary Information of Ultee and Bassis (2016)

Differences between the yield criteria are more immediately visible in a direct comparison. Figure 2.6 shows the two profiles produced by prescribing the amount of thinning observed in the period 1957-2007 at the reference point. We notice that the profile produced using the effective pressure yield criterion reaches a terminus position ~ 0.6 km farther advanced than the 2007 observation, while the profile from the constant yield criterion has a terminus ~ 3.2 km farther retreated than the 2007 observation. The difference in performance can also be seen in the Supplementary Animations S1 ($\tau_y = 150$ kPa) and S2 ($\tau_y = 130\text{kPa} + \mu\left(\rho_i g H - \rho_w g D\right)$) of Ultee and Bassis (2016).

2.5 Discussion

Results of our idealized simulations compare well with observations of glacier profiles and terminus thicknesses (Bassis and Walker, 2012). We have confirmed that the model is able to reproduce advance and retreat of tidewater glaciers over representative bed topographies, and simulations driven with moderate upstream thinning (5 m a^{-1}) show the corresponding retreat matches observations. Note that the choice of reference point is significant—simulating 5 m a^{-1} of thinning at a point only 10 km upstream from the termi-

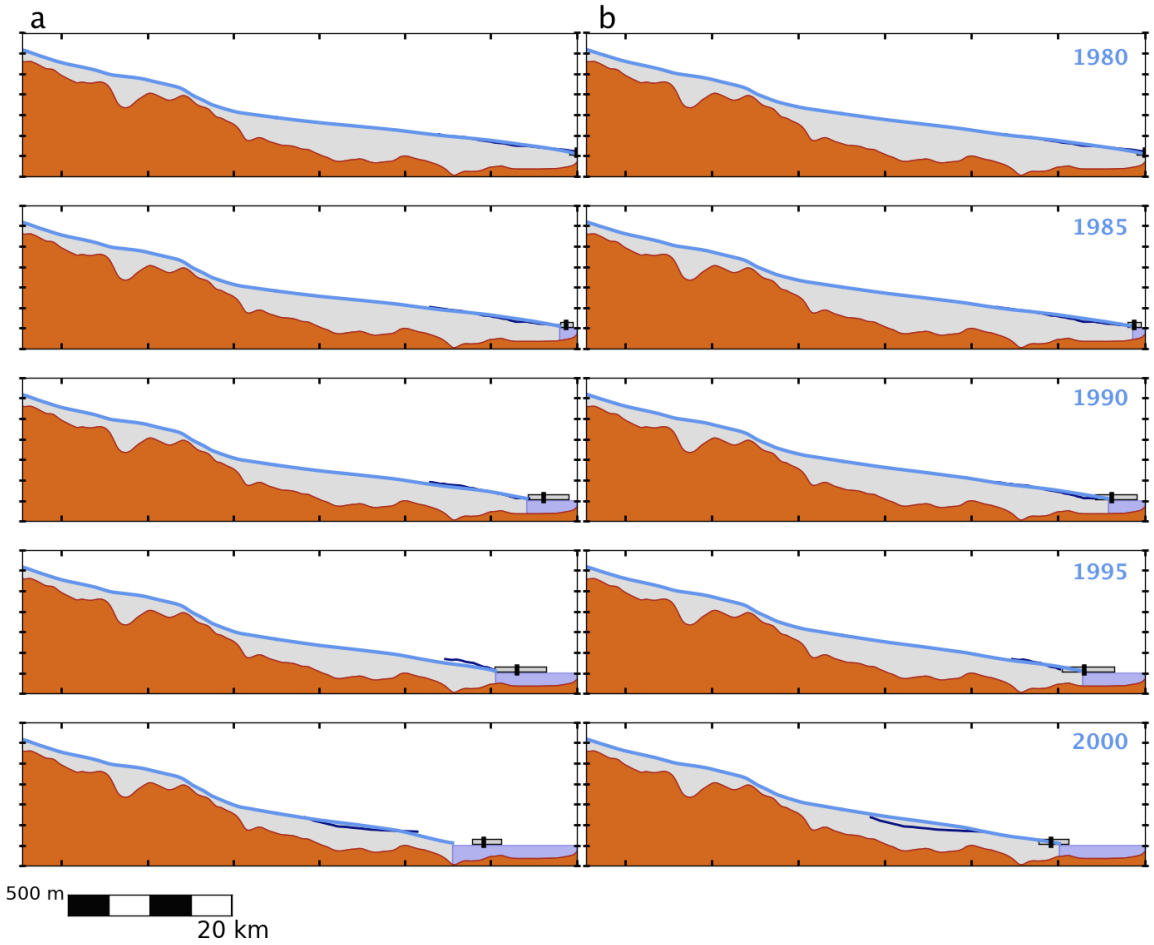

Figure 2.5: 5-yearly snapshots of Columbia Glacier retreat, with the top frames representing 1980 and the bottom frames representing 2000. Model results appear as light blue filled profiles, USGS flightline elevation profiles as navy blue curves, centroid terminus positions as vertical black markers with grey observational range. Scalebar at bottom left shows scales of 20 km in the horizontal and 500 m in the vertical. Panels: (a) Retreat simulated with constant $\tau_{\mathrm{y}} = 150$ kPa; (b) Retreat simulated with the effective pressure criterion, $\tau_{\mathrm{y}} = 130\mathrm{kPa} + \mu\left(\rho_i g H - \rho_w g D\right)$.

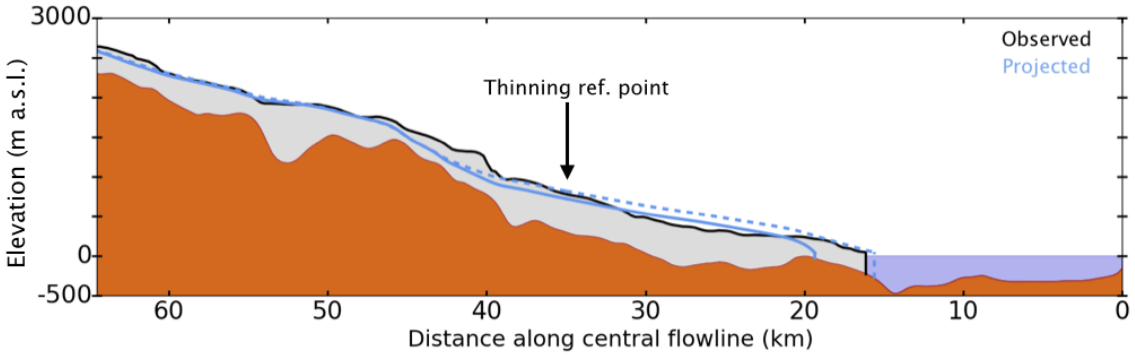

Figure 2.6: Comparison of constant yield and effective-pressure yield criteria in simulating 2007 retreat from prescribing observed amount of thinning (210 m) at reference point (35 km upstream, black arrow). The centerline profile from 2007 observation (McNabb et al., 2012) appears with black outline and grey fill. Profiles projected using $\tau_y = 150$ kPa and $\tau_y = 130\text{kPa} + \mu\left(\rho_i g H - \rho_w g D\right)$ are solid and dashed blue curves, respectively.

nus will produce results quite different from 5 m a^{-1} thinning at the reference point 35 km upstream. Rapid thinning near sea level and rapid thinning at higher elevation correspond to different climate scenarios, however, and the model responds as we would expect: thinning simulated closer to the terminus will produce less rapid terminus retreat than the same amount of thinning simulated farther upstream.

The retreat scenarios shown in Figure 2.2 match physical intuition. In Figure 2.2a, for example, rapid retreat levels off once the glacier terminus is no longer in contact with the ocean. This phenomenon has been documented several times in the literature (Pfeffer, 2007; Pfeffer et al., 2008). In Figure 2.2b, the glacier's initial retreat is modulated by a submarine sill. As the terminus thins in deep water, it no longer satisfies the water-balance conditions of Eqns. (3.3, 2.27) and must retreat. When the terminus retreats onto the submarine sill, however, it is able to stabilize in the shallower water. Figure 2.2c shows an analogous case, though its results may be less intuitive. As the glacier retreats out of the water, the terminus thickness for force-balance decreases (Eqn. (3.3) with $D = 0$). Even though it is thinning upstream, the downstream portion of the glacier is too thick to form a stable ice cliff on the concave bed, so it retreats rapidly and does not stabilize until the terminus is very close to the ice "divide". In a small neighborhood of the ice divide, the concave bed may locally approximate a constant downhill slope, so we see subsequent retreat proceed accordingly. There is not much glacier left for thinning and retreat, though, and the profile after 30 years of thinning shows only a small scrap of glacier ice remaining. This is perhaps unsurprising, as the "ice divide" portion of the glacier of Fig. 2.2c was already thinner than the other idealized cases when constant 5 m a^{-1} thinning began.

The modeled profiles of Columbia Glacier show good agreement with 1957 and 2007

observed ice thickness along the main centerline, and the model reproduces observed retreat and thinning. The model successfully captures the "hinge point" behavior of the Columbia Glacier noted by McNabb et al. (2012); in both the observations and the model, the most drastic changes to the centerline profile are seen in the lower reaches, below a "hinge point" around 40 km up from the terminus, with ice thickness upstream remaining relatively constant. The amount of retreat corresponding to a given amount of thinning (or equilibrium line altitude perturbation) depends on the yield strength, but using the range of τ_y realistic for Columbia we see realistic results. With a constant yield strength of 150 kPa, thinning of the main branch at a reference point just below the hinge point produces retreat consistent with the 1957 and 2007 observations. We also see that the model disagreement with observation (as measured by the CV_{RMS}) is higher for 2007 profiles, and that the model tends to overestimate 2007 thickness when using a single constant yield strength—consistent with what would be seen if the shear strength of the bed decreased due to subglacial processes between 1957 and 2007. This agrees with observations that suggest low shear strength at the bed of Columbia Glacier in 2007 (Walter et al., 2010).

Beyond static profiles, we have also successfully reproduced the general pattern of Columbia's retreat up to 2007, including an acceleration while the terminus retreated off a sill and over an overdeepening in the bed. Both animations (Supplementary Material) capture this behavior, and snapshots can be seen in Figure 2.5. The glacier simulated with $\tau_y = 150$ kPa shows more retreat over the period 1982-2007 than does the simulation with $\tau_y = 130\text{kPa} + \mu\,(\rho_i g H - \rho_w g D)$. For straightforward comparison, Figure 2.6 superimposes the 2007 profiles when retreat is simulated with a constant yield strength and with the effective basal pressure yield criterion. The absolute difference in terminus position between model and 2007 observation is a rough measure of each model variant's skill at simulating retreat. In Figure 2.6 we see a difference in terminus position of modeled and observed profiles of $+0.595$ km for the effective pressure case $\tau_y = 130\text{kPa} + \mu(\rho_i g H - \rho_w g D)$ and -3.171 km for the constant-yield case $\tau_y = 150$ kPa. By this metric, allowing yield strength to vary with effective basal pressure produces a simulation closer to observations.

Simulations using the effective pressure yield criterion more closely match several available observations, and agree with several studies suggesting that effective basal pressure is an important factor governing tidewater glacier retreat (Truffer et al., 2009; Pfeffer, 2007; Vieli et al., 2000). In particular, for the year 2000—the last year for which USGS terminus-position data is available—the terminus position predicted using $\tau_y = 150$ kPa is not within the range of observed terminus positions, while the position predicted using $\tau_y = 130\text{kPa} + \mu(\rho_i g H - \rho_w g D)$ is within that range. For all other years, both simulations place the glacier terminus inside the range given by USGS data. That is, using the slightly

more complicated case $\tau_y = 130\text{kPa} + \mu(\rho_i g H - \rho_w g D)$ does improve the model, but using the constant yield strength $\tau_y = 150$ kPa is an acceptable simplification for the main branch of Columbia Glacier.

Specifying that $\tau_y = 150$ kPa is an acceptable choice *for the main branch of Columbia Glacier* (i.e. perhaps only there) is not trivial. As discussed in Methods, above, we have reason to suspect that τ_y is not constant in space; in particular, its value may be quite different for geographically distant glaciers. Further, in this work we have assumed $\tau_{y_{\text{ice}}} = \tau_{y_{\text{bed}}}$ for simplicity, but a variety of glaciological and geological processes may cause either or both yield strengths to change with time. Laboratory observations and inverse methods from field observations constrain the probable values of $\tau_{y_{\text{ice}}}$; it is more difficult to constrain $\tau_{y_{\text{bed}}}$ on a particular glacier as it requires some knowledge of (or an educated guess about) the subglacial geology. By comparing the observed terminus cliff height with that predicted by our model's water balance condition (Eqn. (2.26)), it is possible to rule out highly improbable values of τ_y for individual glaciers. For example, Columbia Glacier's 1957 terminus was a 108 m ice cliff in 160 m of water, so Figure 2.1 suggests that very high yield strengths approaching 500 kPa would be inappropriate.

Though the simplicity of the model is a great advantage, there are certain oversimplifications that must be addressed. The 1-D centerline approach with yielding at the bed is not suitable in cases where basal drag is not the dominant control on flow: narrow valley glaciers (controlled by wall drag) and floating ice tongues (controlled by longitudinal stresses), for example. Additionally, the present form of the model is too simple to capture the interaction of different stress regimes, and our focus on steady-state solutions ignores shorter-term variability. We note that our case study of Columbia Glacier concludes in 2007, and that between 2007-2012 Columbia Glacier displayed several of these more complicated dynamic features, including the development of a floating ice tongue and short-lived cycles of advance and retreat on the order of 500 m (McNabb et al., 2012; Walter et al., 2010). Our model error is higher in 2007, consistent with the onset of conditions less suitable for the perfect plastic approximation. The model may also miss some longer-term variability associated with feedback between terminus retreat and upstream thinning. Finally, the prominent role of the bed topography $b(x)$ in the surface-elevation equation leaves the model susceptible to errors from poorly-known bed topography as well as sparse sampling of the centerline bed data in estimating an appropriate bed geometry. In the case of Columbia Glacier, however, our results show little sensitivity to introduction of random noise, varying smoothing intervals, or displacement of the centerline over the bed.

In our current formulation, the perfect plastic limit corresponds to a steady-state glacier that is in equilibrium with climate forcing. Counter-intuitively, surface mass balance does

not directly enter into the computation of glacier profiles. In our model formulation, glacier profiles and terminus position evolve in response to a prescribed upstream thinning rate. Mass balance only enters into calculations of mass flux into the ocean, which we have not attempted here. In keeping with the simplicity of the model, one way to introduce climate sensitivity would be extrapolate upstream thinning rates based on current trends or quadratic or exponential growth in thinning rates. This would provide sensitivity and some bounds on rates of retreat for individual glaciers. More satisfyingly, climate dependence could also be introduced by coupling with a dynamic ice sheet upstream. For example, a large-scale, climate-responsive ice sheet model (in which tidewater glaciers are otherwise not resolved) could be used to determine the upstream thickness to input into our model. The two models coupled together will respond to projected changes in climate and resolve individual glacier contributions to sea level rise with minimal additional computational expense. Alternatively, if changes in terminus position are driving increased thinning rates upstream we could instead prescribe a terminus retreat (or advance) rate and use this to determine glacier profiles. This is more challenging because it would require specification of an additional closure relation that specifies calving rate (or rate of terminus advance) and its relation to local climate forcings, such as submarine melt. In the absence of a well-validated calving law, we suggest the first two options as those most consistent with the simplicity of our modeling approach, but we reassert the caveat that the perfect plastic model is unable to distinguish between changes in terminus position due to upstream thinning and changes in upstream thickness due to terminus advance or retreat.

2.6 Conclusion

We have generalized early work in glacier modeling—namely, Nye's 1951 perfect plastic approximation of glacier ice—to present a new, simplified model of tidewater glacier retreat. Results presented here demonstrate that our simple perfect plastic model produces realistic glacier profiles and basic time evolution with very little input data. Using this model, it is straightforward to gain a first-order understanding of tidewater glaciers for which data are extremely limited. This model and slightly more complicated variations such as a full viscoplastic model can be used to inform policy-relevant sea level projections until such time as the state of available data and computational power allows consistent use of state-of-the-art models for that purpose.

Some of the oversimplifications of this perfect plastic model may be addressed using the slightly more complicated viscoplastic rheology. For example, whereas we have approximated intact glacier ice as rigid over our timescales of interest, viscoplastic flow

could account for the viscous creep of intact ice and capture the interaction of different stress regimes in the glacier. However, more complicated models are equally susceptible to errors from poorly-known bed topography and other sparse observations. In the absence of high-resolution data for all the world's glaciers, highly simplified models such as our perfect plastic approximation remain an important tool for constraining 21st century sea level rise. Using only three inputs—bed topography along a centerline, basal shear strength, and change in upstream thickness—the perfect plastic model presented here can produce realistic glacier profiles as well as simulate advance and retreat, offering a first-order understanding of glacial contributions to global mean sea level with negligible computational expense.

CHAPTER 3

Methods to simulate networks of calving glaciers

N.B.: This chapter was published in 2017 as

Ultee, L. and Bassis, J. N. (2017). A plastic network approach to model calving glacier advance and retreat. *Frontiers in Earth Sciences* 5(24). http://dx.doi.org/10.3389/feart.2017.00024.

It outlines the method we have used to simulate "networks" of interacting glacier branches that discharge solid ice (calve icebergs) from a single terminus. This is one of the key innovations our work offers to the field of numerical glacier modelling. In this chapter, we also demonstrate the applicability of our model in diverse contexts: not only Alaska (as in Chapter 2) but also Greenland, not only retreating glaciers but also advancing, not only one glacier branch but also three, five, or more.

3.1 Introduction

The global sea level rise contribution from land ice is large and growing (Rignot et al., 2011; van den Broeke et al., 2016). Much of the increase in the land ice contribution to sea level rise comes from the dynamic response of marine-terminating glaciers, including those draining the Greenland and Antarctic Ice Sheets (Straneo et al., 2013; Vaughan et al., 2013; Church et al., 2013). Where glaciers drain the large ice sheets, there is often a transition from laterally unconfined ice (width $\gtrsim 10^2$ km) to flow through narrow fjords (width ~ 10 km or smaller). For example, most of the 199 widest Greenland outlet glaciers studied by Murray et al. (2015) do not exceed 3 km in width, and many smaller glaciers less than one kilometer in width are excluded from consideration. Where tidewater glaciers drain alpine ice fields, as in coastal Alaska, the ice flux through the terminus may come from tens or hundreds of tributary branches upstream. The largest glaciers with the greatest potential

contribution to sea level rise also have the most tributary branches—more than 400 in the case of Hubbard Glacier, Alaska (Kienholz et al., 2015).

The relatively small scale and large number of outlet glaciers and tributaries present a challenge to effective ice sheet modeling: the fine resolution required to capture small-glacier dynamics is prohibitively expensive to apply in full-Stokes models of entire ice sheets. Adaptive mesh refinement (AMR) has been applied in some models, e.g. BISICLES (Cornford et al., 2013), as a first step toward addressing this challenge. However, the finest-resolution cells (~ 500 m) in AMR grids are generally those nearest the grounding line, potentially leaving upstream tributaries of width ~ 1 km and smaller unresolved. By contrast, simplified centerline models applied to individual glaciers may use grid spacing of < 10 m over the entire glacier length, but such models often ignore tributary branches entirely.

In Ultee and Bassis (2016), we extended the perfect plastic approximation of Nye (1951, 1952, 1953) to a centerline model of tidewater glaciers that self-consistently predicts terminus advance and retreat forced with upstream elevation change. We now generalize this model to account for the intersection of networks of tributaries. Our plastic model is well-suited to this problem because the condition for intersections is straightforward: ice thickness H must match at intersection points between branches. Here, we describe the model's application to intersecting glacier networks through four case studies, including glaciers from both Alaska and Greenland. We also discuss two alternative forcing methods that could bring glacier-wide mass balance—and its changes due to climate—directly into the model.

As illustrative cases, we choose four large, well-studied glaciers: Jakobshavn Isbræ and Helheim Glacier, Greenland, and Columbia and Hubbard Glaciers, Alaska. These glaciers were chosen based on their diversity of behavior and because of the (relatively) abundant data available. For example, geometry of these glaciers varies from Jakobshavn's single major channel to Hubbard's more than 400 mountain tributaries. Moreover, in recent decades Columbia and Jakobshavn have been undergoing sustained retreat (Krimmel, 2001; O'Neel et al., 2005; McNabb et al., 2012; Joughin et al., 2004, 2012, 2014), Hubbard has been advancing (Trabant et al., 2003; Ritchie et al., 2008) and Helheim has experienced both advance and retreat episodes (Howat et al., 2005, 2010; Murray et al., 2010), providing tests of our model's ability to resolve calving dynamics in a range of environments. Further, with the case studies selected here we go beyond the work of Ultee and Bassis (2016) to show that the model can reproduce patterns of retreat and advance in both Greenland and Alaska and that the model can be used to analyze glaciers with more than one branch.

3.2 Method

Our method extends the perfect plastic approximation of Nye (1951, 1952, 1953) to calving glaciers with a network of tributaries. The perfect plastic approximation corresponds to the assumption that glacier ice is perched at a yield strength. Applying the approximation to a glacier centerline as in Ultee and Bassis (2016), we obtain an equation for the surface elevation profile along the centerline:

$$|h - b| \frac{\partial h}{\partial x} = \frac{\tau_\mathrm{b}}{\rho_\mathrm{i} g}, \tag{3.1}$$

where h is glacier surface elevation, b bed elevation, $\rho_\mathrm{i} = 920\,\mathrm{kg\ m^{-3}}$ the density of glacier ice, $g = 9.81\ \mathrm{m\ s^{-2}}$ the acceleration due to gravity, and τ_b the basal yield strength.

At the calving front, we require that tractions balance across the ice-water interface, i.e.

$$\int_{b(x)}^{h(x)} \sigma_{xx}\ \mathrm{d}z = \int_{b(x)}^{0} -\rho_w g z\ \mathrm{d}z, \tag{3.2}$$

with $\rho_\mathrm{w} = 1020\ \mathrm{kg\ m^{-3}}$ the density of sea water. We also require that the ice at the terminus is at the yield strength of ice, τ_y, and integrating as in Ultee and Bassis (2016) provides a corresponding condition on the ice thickness at the terminus:

$$H_\mathrm{terminus} = 2\frac{\tau_\mathrm{y}}{\rho_\mathrm{i} g} + \sqrt{\frac{\rho_\mathrm{w} D^2}{\rho_i} + 2\frac{\tau_\mathrm{y}}{\rho_\mathrm{i} g}} \tag{3.3}$$

where

$$D = \begin{cases} |b(x)| & \text{for } b(x) < 0 \\ 0 & \text{for } b(x) \geq 0 \end{cases} \tag{3.4}$$

represents water depth. For a given terminus position, our model uses Equations 3.1 and 3.3 to construct the surface elevation profile along the glacier centerline with a self-consistent terminus position.

A general plastic model admits two yield strengths: that of the bed, τ_b, and that of the ice, here called τ_y. Generally speaking, $\tau_\mathrm{b} \leq \tau_\mathrm{y}$. When the glacier substrate is weaker than the glacier ice, stress at the calving front (Equation 3.3) is limited by the yield strength of ice, and basal stress (Equation 3.1) is limited by the lower yield strength of the bed. The especially simple solution we present here assumes $\tau_\mathrm{b} = \tau_\mathrm{y}$, which may not be realistic but has shown promising results when applied to Columbia Glacier (Ultee and Bassis, 2016). τ_y thus becomes our single adjustable parameter.

This simple model may be run with a constant yield strength, or with a Coulomb yield criterion:

$$\tau_{\mathrm{y}} = \tau_0 + \mu N, \quad \text{where} \quad N = (\rho_{\mathrm{i}} g H - \rho_{\mathrm{w}} g D) \tag{3.5}$$

with μ a constant cohesion coefficient, $H = h - b$ the ice thickness, other terms as above, and τ_0 replacing τ_{y} as the directly adjustable yield parameter. N in Equation 3.5 represents an effective pressure at the glacier bed, such that basal substrates below sea level can be assumed saturated and promoting faster flow (through a weaker bed and/or more deformation in the adjacent layer of ice). Basal water pressure beneath real glaciers is affected by hydrological factors such as variable meltwater flux and evolution of the basal drainage network, but accounting for such effects is beyond the scope of this simple model. In all four case studies presented here, we keep $\mu = 0.01$ constant to avoid excessive "tuning". This value was chosen to reflect a Mohr-Coulomb condition with low friction angle—as would be found for soft marine sediments near tidewater glacier termini—and consistent with the laboratory estimates of Cohen et al. (2005).

To apply our one-dimensional centerline model to a network of glacier tributaries, we define the network of centerlines, identify an appropriate value of the yield strength τ_{y} for the glacier in question, and simulate upstream thinning/thickening over time.

3.2.1 Define network centerlines

Each centerline comprises a sequence of point coordinates. For relatively simple tributary networks, we manually select centerlines from maps of glacier thickness and bed topography. We save the lists of point coordinates and note which are points of intersection between branches. For general cases, it is more practical to extract point coordinates from automatically-generated sets of centerlines such as those created by Machguth and Huss (2014) or Kienholz et al. (2014). With coordinate sequence in hand, we generate a set of evenly-spaced points from the (common) terminus to the head of each glacier branch and we re-express the points of each line in terms of arc length. Expressing the lines in terms of arc length allows a continuous representation of input quantities along each line, allowing model resolution to be adjusted.

3.2.2 Find best-fit yield strength

Our model rheology depends on a single adjustable parameter: the yield strength τ_{y}. Note once again that, though a general plastic model might include separate yield strengths for

the glacier bed and glacier ice, τ_b and τ_y respectively, we assume here that $\tau_b = \tau_y$.

Where observed surface elevation profiles are available, we can find the best-fit value for yield strength τ_y (or τ_0 of Equation 3.5) by minimizing model mismatch with observation. We run the model only along the main branch, where observations are likely to be higher-quality, for a range of values of τ_y. We quantify the mismatch with observation using the coefficient of variance of the root-mean-square error, CV_{RMS}. We take the value of τ_y corresponding to minimum CV_{RMS} to be the best-fit yield strength, and we apply the same best-fit τ_y to all branches of a given glacier.

For glaciers lacking observations of surface elevation, a best-guess value of τ_y may be used instead. Laboratory and field observations indicate that τ_y should be approximately 50-300 kPa (Cuffey and Paterson, 2010; O'Neel et al., 2005), with lower values for soft, flat beds and higher values for hard, steep beds.

3.2.3 Simulate advance/retreat over time

Using our best-fit or best-guess yield strength, we generate a reference profile along each glacier branch corresponding to an initial terminus position. For the plastic model, terminus retreat corresponds to upstream thinning and advance to thickening. We select an upstream point along the reference profile, ideally a point with good observations available for multiple years, where we will simulate changes in ice thickness. We first simulate main branch thinning/thickening as described in Ultee and Bassis (2016), finding the terminus position satisfying Equation 3.3 for each new glacier profile. Because all tributaries share a common terminus, we use the terminus position identified by the main branch profile and step the plastic model upstream into the tributaries from there. Thus, we generate a consistent set of branch profiles, which by definition agree at the points of intersection, for each time step.

3.2.4 Numerical considerations

We discretize Equation 3.1 with an Euler forward step. The model is fast and can be run with small grid spacing; in the following case studies, grid spacing ranges from 1-5 m to ensure negligible numerical error. Our results are robust and insensitive even to order-of-magnitude increases in grid spacing. We enforce our boundary condition of matching ice thickness at tributary branching points in the model initialization, stepping the model upstream into the tributaries from a common trunk where ice thickness agrees by definition. For more details of our numerical implementation, see Ultee and Bassis (2016)

3.3 Case studies

To demonstrate the application of the network method, we now turn to four case studies, arranged in order of increasing complexity. The case studies include calving glaciers in both Alaska and Greenland, with networks ranging from the very simple single branch of Jakobshavn Isbræ to the highly complex Hubbard Glacier network of more than 400 branches (of which we treat eight). Each case illustrates a different capability of the model: matching average retreat based on relatively sparse data, reproducing more detailed retreat including a network split, simulating retreat and readvance without adjusting model settings, and matching a well-studied terminus advance with a forcing fit to observations. In the final case study, we illustrate the application of the model to automatically generated networks of centerlines, dramatically improving the scalability of this approach for large and complex networks of calving glaciers.

3.3.1 Jakobshavn Isbræ, Greenland—1 centerline

Jakobshavn Isbræ is the fastest-flowing glacier currently known, with summer flow speeds near the terminus reaching 16 km a^{-1} (Joughin et al., 2014). It drains approximately 7% of the Greenland Ice Sheet by volume (Csatho et al., 2008; Joughin et al., 2004) and is a substantial contributor to global sea level rise: nearly 1 mm between 2000 and 2011 (Joughin et al., 2014; Howat et al., 2011). A CReSIS level 3 data product (CReSIS, 2016b) provides gridded ice thickness, surface elevation, and ice-bottom elevation for Jakobshavn Isbræ. The CReSIS product is a composite of data collected between 2006 and 2014, with ice bottom reconstructed by kriging of radar lines. Because Jakobshavn lost its floating ice tongue before the period of the CReSIS product (2006-2014), we assume that the terminus is grounded and that ice-bottom elevation corresponds to bed topography everywhere. Three intersecting troughs are visible in the bed topography, but we consider only the 60 kilometers closest to the terminus, common to all three branches. Thus, we begin our investigation with the simplest possible network geometry: a single centerline. Figure 3.1 shows the selected centerline on a map of Jakobshavn bed topography.

According to the CReSIS data, our centerline terminates (reaches the end of available data) in ice more than 1400 m thick, grounded more than 1100 m below sea level. If this were the true terminus, it would imply an ice cliff 314 m above the water line—much larger than observations suggest (Joughin et al., 2004, 2014; Csatho et al., 2008). For such a cliff to be stable, the yield strength of ice would have to be more than 3.5 MPa, which is an order of magnitude larger than the values we would expect from observation and our previous work (see Ultee and Bassis, 2016; Bassis and Jacobs, 2013; Bassis and Walker,

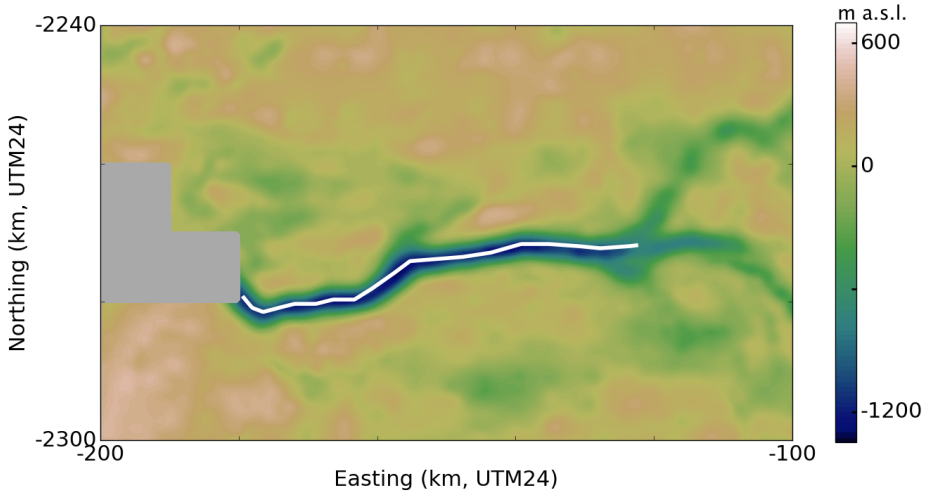

Figure 3.1: CReSIS 2006-2014 composite bed topography of Jakobshavn Isbræ (Sermeq Kujalleq), with hand-selected centerline (white) for terminal 60 km. Note the dark grey area of no data immediately in front of the terminus.

2012; O'Neel et al., 2005). Thus, we suspect that the seaward end of our centerline does not represent a true "terminus" with ice-water interface, making it unsuitable for our optimization procedure initialized with the balance thickness (Eqn 3.3). We instead initialize with the observed terminal thickness and proceed with optimization upstream, finding the best fit with $\tau_y = 355$ kPa. Figure 3.2 compares the centerline profile generated by our plastic model with the observed centerline profile from CReSIS data. The plastic model fit to observation is good, with $CV_{RMS} = 3.3\%$.

In recent years, Jakobshavn has thinned and retreated substantially. Using an average thinning rate based on Csatho et al. (2008), we investigate whether the plastic model produces appropriate retreat. Figure 3.3 shows the simulated change in terminus position with $30\,\mathrm{m\ a^{-1}}$ thinning applied 15 km upstream from the original terminus (reference point marked in blue in Figure 3.2). After a few years of thinning without change in terminus position, retreat begins in the third year of the simulation and accelerates to just over $1\,\mathrm{km\ a^{-1}}$ in years 5-15. Over the entire 15-year period, average retreat rate is 763 m $\mathrm{a^{-1}}$.

Our simulation of the retreat is simplistic, but not unreasonable. Because we initialize from a dataset compositing observations between 2006 and 2014, the onset date of our retreat could be anytime in that range, and comparison with observed retreat is inexact. However, we note that between 1991-2006, Csatho et al. (2008) report a 15-year average retreat rate of 830 m $\mathrm{a^{-1}}$, comparable to the 15-year average retreat rate of 763 m $\mathrm{a^{-1}}$ found in our simulation. Further, for the 5-year period 2001-2006, closer to the probable time of our simulated retreat, the average retreat rate reported by Csatho et al. (2008) is 2.23

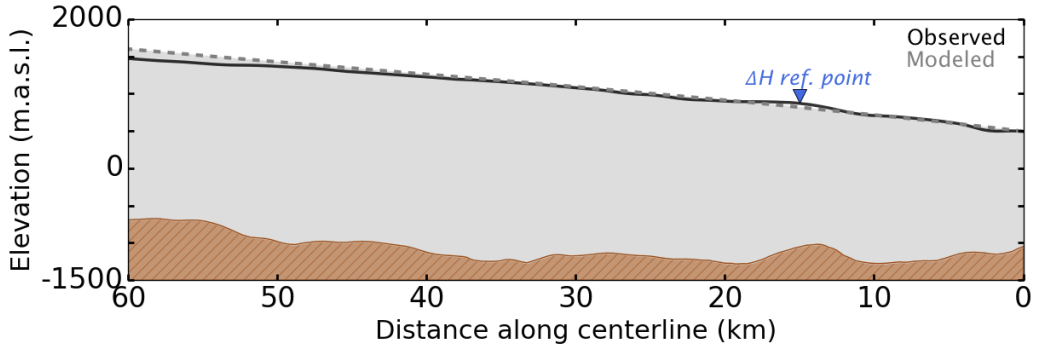

Figure 3.2: Centerline profiles of Jakobshavn Isbræ (Sermeq Kujalleq): CReSIS composite of surface observations 2006-2014 (black curve) and plastic model with $\tau_y = 355$ kPa (grey dashed curve). Blue marker indicates the upstream reference point where forcing was applied to simulate retreat (see Figure 3.3).

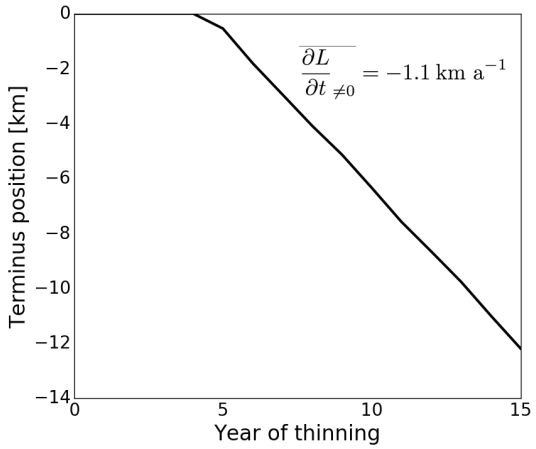

Figure 3.3: Jakobshavn Isbræ (Sermeq Kujalleq) terminus retreat under 15 years of 30 m a^{-1} upstream thinning. Average retreat rate $\overline{\frac{\partial L}{\partial t}}$ is listed for the years after onset of retreat; compare with rates of 0.83–2.23 km a^{-1} reported by Csatho et al. (2008) for a similar time period.

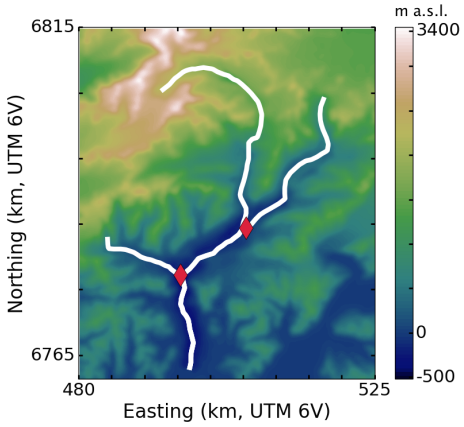

Figure 3.4: Three branches of Columbia Glacier (white) with reconstructed bed topography from McNabb et al. (2012). Red diamonds mark intersections of the branches.

km a^{-1}, on the order of our retreat rate of 1.1 km a^{-1} in the years after onset of retreat in the simulation. Our results are of similar magnitude to those reported in Joughin et al. (2004, 2012, 2014) for the early 2000's as well. Though we do not capture the strong seasonal cycling observed at Jakobshavn's terminus (Joughin et al., 2014) under our constant annual upstream thinning, our results are satisfactory for our primary interest in annual- to decadal-scale change.

3.3.2 Columbia Glacier, Alaska—3 centerlines

Alaska's Columbia Glacier is among the most well-documented cases of tidewater glacier retreat. The glacier has been monitored by the United States Geologic Survey (USGS) since the early 20th century, and over the past 35 years it has undergone rapid terminus retreat and upglacier thinning. Datasets available from McNabb et al. (2012) and Krimmel (2001) document the state of Columbia Glacier before and during its recent retreat. McNabb et al. (2012) offers topography and ice thickness reconstructed for 1957 and 2007 from observations, using a mass-conservation algorithm based on Glen's flow law; Krimmel (2001) gives more frequent flightline observations of the glacier surface elevation.

Figure 3.4 shows the structure of our hand-selected tributary network over Columbia Glacier bed topography. A Coulomb yield criterion with $\tau_0 = 130$ kPa gives the best model fit to observation. Each panel of Figure 3.5 is an aerial view of the same Columbia Glacier network, illustrating different aspects of the model results. Panel (a) shows glacier surface elevation for plastic steady-state profiles generated with the 1957 terminus position; panel (b) shows ice thickness for the same profiles; panel (c) compares the modeled profiles to observation (1957 USGS topographic map, as presented in McNabb et al. (2012)). The

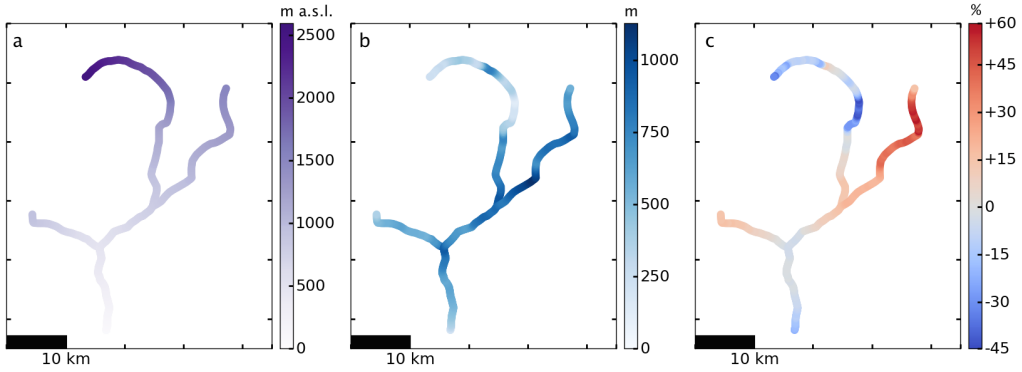

Figure 3.5: Plastic model with $\tau_y = 130\text{kPa} + \mu N$ applied to a network of three major tributaries of Columbia Glacier, aerial view, 1957. (a) Glacier surface elevation, (b) Ice thickness, (c) Percent error model-observation (McNabb et al., 2012). A positive percent error (red colours in panel c) corresponds to model overestimation of observed ice thickness, and a negative percent error (blue colours) corresponds to underestimation.

maximum error is 58% overestimation of ice thickness on parts of the east branch and 44% underestimation of ice thickness on the upper reaches of the main branch, though the percent error in modeled ice thickness is highly spatially variable, as seen in Figure 3.5(c). Overall, the plastic model fit to observed surface elevation as measured by CV_{RMS} is good along the main and west branches ($CV_{RMS} = 6.2\%$ and 9.5%, respectively) but weaker along the east branch (19.9%). The east branch, where our model tends to overestimate ice thickness by 50% or more, has seldom been directly studied (Krimmel, 2001), although recent radar-sounding and bed-mapping efforts (Rignot et al., 2013; Enderlin et al., 2016) have better constrained the bed topography there and can be applied in future use of our model. We note also that the stretch of the main branch with the poorest fit to observation is the location of a sharp drop in the bedrock, where we might expect problems with the plastic model due to its strong dependence on bed topography.

We explore the retreat patterns of Columbia Glacier in detail using a single-branch model in Ultee and Bassis (2016). Here, we apply constant upstream thinning of 8 m a^{-1} for 25 a, 1982-2007, and show the simulated 2007 state of Columbia Glacier in Figure 3.6. The colour schemes in the two figures have been kept the same (with the exception of the percent error plotted in panel (c)) to allow for direct comparison. We note that the most pronounced changes occur in the lower reaches of the glacier, including a striking terminus retreat of more than 20 km. Very little change is visible in the upper reaches of the main branch, which agrees with observations of Columbia's dynamics above and below a "hinge point" (an icefall) approximately 40 km upstream from the 1957 terminus (McNabb et al., 2012)

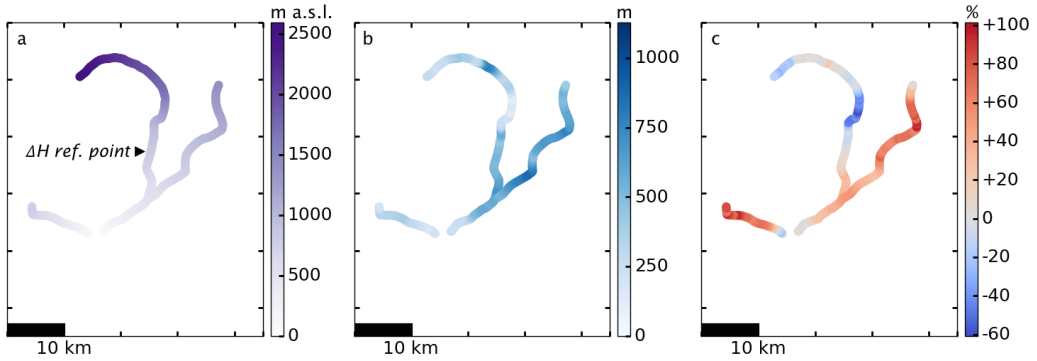

Figure 3.6: Same panels as Figure 3.5, simulated for 2007. Black marker indicates upstream location where forcing was applied to simulate retreat. Note the colour scales: maintained in panels (a) and (b) to facilitate comparison between years, but adjusted in panel (c) to accommodate the greater error of the model in 2007.

During the dramatic retreat between 1957 and 2007, the terminus of Columbia Glacier reached the intersection point of two branches and eventually split into two calving fronts, shedding icebergs from each branch. That split is visible in Figure 3.6. Once the terminus retreated upstream of the intersection point, it was necessary to run the model separately on the two smaller networks comprising the single-branch network to the west and the two-branch network to the east. Our model is able to handle this separation of tributaries with little difficulty.

3.3.3 Helheim Glacier, Greenland—5 centerlines

Helheim Glacier is another of Greenland's largest outlet glaciers, located along its southeast coast. In recent years, Helheim was observed to thin, retreat, and accelerate, then slow its retreat and begin readvancing (Murray et al., 2015; Howat et al., 2010, 2005; Stearns and Hamilton, 2007). A CReSIS level 3 data product (CReSIS, 2016a) provides gridded ice thickness, surface elevation, and ice bottom elevation for Helheim Glacier. The product we are using is a composite of data collected between 2006 and 2014, with the ice bottom reconstructed by kriging of radar lines.

Figure 3.7 shows the ice bottom elevation underlying five branches of Helheim Glacier, with hand-selected centerlines for the branches marked in white. We optimize for the yield strength and find that the Coulomb yield criterion with $\tau_0 = 245$ kPa provides the best fit to observation.

Figure 3.8, analogous to Figure 3.5, shows the plastic model applied to the network of five branches of Helheim. The maximum errors are 47.5% overestimation of ice thickness on parts of the easternmost branch and 5.8% underestimation of ice thickness on upstream

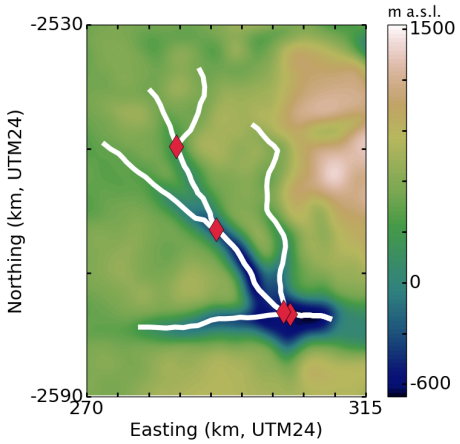

Figure 3.7: Five branches of Helheim Glacier (white) with CReSIS composite ice bottom elevation from 2006-2014. Red diamonds mark intersections of the branches.

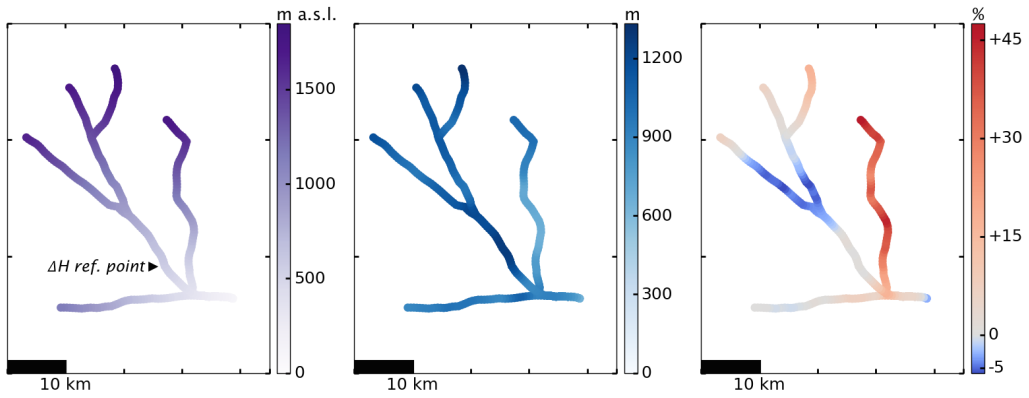

Figure 3.8: Plastic model with $\tau_y = 245\text{kPa} + \mu N$ applied to network of five major tributaries of Helheim Glacier, aerial view, 2006-2014. (a) Glacier surface elevation, (b) Ice thickness, (c) Percent error model-observation (CReSIS, 2016a).

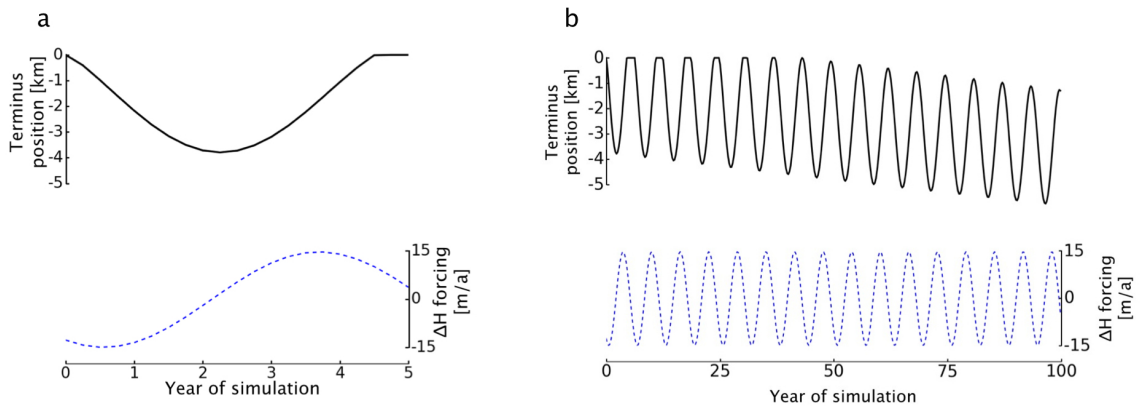

Figure 3.9: Pattern of retreat and readvance of Helheim Glacier simulated with a sinusoidal pattern of thinning-thickening upstream for 5 years (panel a) and 100 years (panel b). Black curves on the upper axes show the changing terminus position, and blue dotted curves below show the forcing over the course of the simulation.

portions of the two central branches. For four of the five branches studied, the plastic model fit to the CReSIS composite is very good ($CV_{RMS} \leq 7.9\%$). For the easternmost branch, the fit is weaker, with $CV_{RMS} = 23.8\%$. This is likely because the best-fit Coulomb yield strength, $\tau_0 = 245$ kPa, was optimized for the main branch and is too high for the easternmost branch. Running the optimization procedure for each branch individually, we find that the best-fit Coulomb yield strength is between $220 - 250$ kPa for all other branches, but only 140 kPa for that easternmost branch. It is possible that ice-dynamical factors unique to that branch, e.g. a different balance of basal/wall drag, affect the optimal yield strength.

Given Helheim's recent pattern of retreat and readvance, we now investigate whether the plastic model can produce retreat and readvance within a single simulation. We fit a sinusoidal function to the upstream surface elevation changes reported in Murray et al. (2015) and run the simulation for 100 years. Figure 3.9a shows the retreat and readvance of the terminus in the first five years of simulation, with figure 3.9b showing the continued oscillation over the 100-year period. Note that positive cumulative changes are not possible, because we have no information about the bed topography for terminus positions more advanced than the initial state. Under the time-varying upstream forcing, our model shows Helheim's terminus undergoing multi-year cycles of retreat and readvance over a longer-term retreat signal. Data limitations preclude a direct comparison between our simulation and observed patterns of advance and retreat, but we note that the simulated retreat is of the correct order of magnitude. For two years, the terminus retreats at an average rate of 1.65 km a^{-1} before slowing its retreat and readvancing, consistent with what was observed

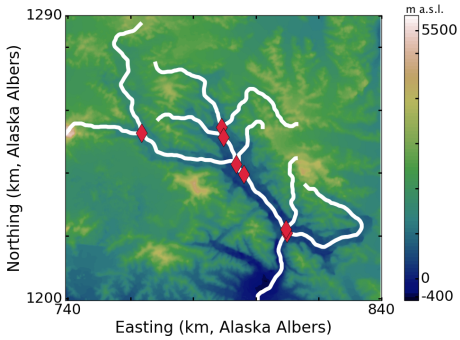

Figure 3.10: Eight branches of Hubbard Glacier, Alaska, (white) selected by Kienholz et al. (2014) with reconstructed bed topography from c. 2007 (Huss and Hock, 2015; Huss and Farinotti, 2012). Red diamonds mark intersections of the branches.

in the early 2000s (Howat et al., 2005; Murray et al., 2015). The 100-year simulation results also demonstrate that the model can capture short-term oscillations over a longer-term retreat, which is promising for eventual treatment of seasonal cycling.

3.3.4 Hubbard Glacier, Alaska—8 auto-selected centerlines

Finally, we explore the performance of the plastic network method for a glacier with more complicated geometry. Hubbard Glacier is Alaska's largest tidewater glacier by area, covering 2450 km^2. Unlike many other tidewater glaciers in the region, and apparently independent of climate forcing, it thickened and advanced throughout the 20th century (Stearns et al., 2015; Trabant et al., 2003; Arendt et al., 2002). The advance has been well-documented due to the glacial outburst flood hazard created when the advancing glacier terminus closes Russell Fjord, which has happened twice in the past 30 years (Ritchie et al., 2008).

Huss and Hock (2015) have reconstructed ice thickness for Alaska glaciers following the method of Huss and Farinotti (2012). We estimate bed topography for Hubbard Glacier by subtracting that reconstructed ice thickness from a digital elevation model of the surface provided by Kienholz et al. (2015). The automated algorithm described by Kienholz et al. (2014) identifies 459 tributary centerlines on Hubbard Glacier, from which we choose the 8 that exceed 20 km in length. Figure 3.10 shows the bed topography underlying the network of eight branches, with automatically-selected centerlines of the branches in white and intersection points marked in red. Following the optimization procedure described above, we find the best model fit with $\tau_y = 200$ kPa.

Figure 3.11 shows the plastic model applied to all eight branches. Note that we have restricted the colorbar of panel c to saturate at 100% error. Overall, model error on Hub-

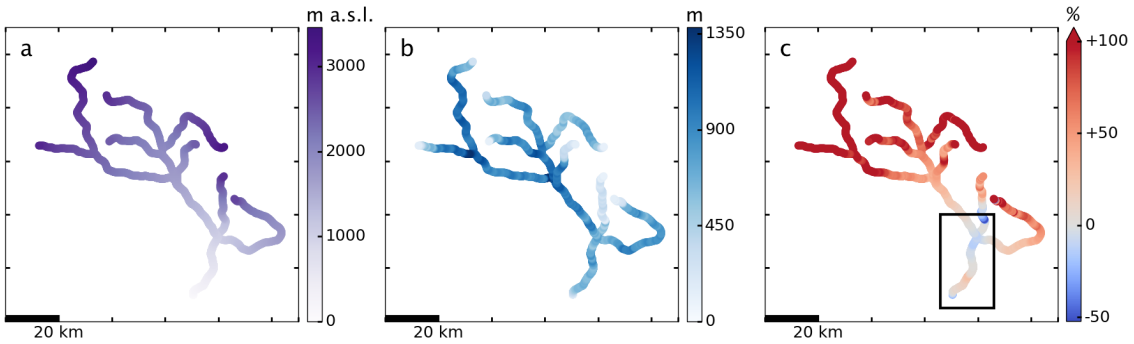

Figure 3.11: Plastic model with $\tau_y = 200$kPa applied to network of eight major tributaries of Hubbard Glacier, aerial view, c. 2007. (a) Glacier surface elevation, (b) Ice thickness, (c) Percent error model-reconstruction (Huss and Hock, 2015; Huss and Farinotti, 2012). Black box on panel (c) indicates the region shown in Figure 3.12.

bard Glacier is comparable to other cases, with mean error of +52% and median of +27%. The maximum underestimation of ice thickness is 52%, also comparable to other cases. However, the upper reaches of several branches show high error, with five points reaching 1000% error and an anomalously high 4237% overestimation of ice thickness found at one point in the main branch. The reconstruction method of Huss and Farinotti (2012) constrains ice thickness to be 0 at the ice divide , which likely accounts for such large increases in model error upstream ($\%_{\text{error}} = 100(H_{\text{model}} - H_{\text{recon}})/H_{\text{recon}}$). Indeed, the point with the highest percent error corresponds to a 747 m overestimation of ice thickness, which is only about 70% of the maximum observed ice thickness for Hubbard Glacier. We expect the plastic model to be more applicable close to the terminus—where stresses are higher and the ice is flowing faster—and the increasing error far upstream agrees with this expectation.

Observations of Hubbard Glacier are sparse above the lowest 15 km (Trabant et al., 2003) and the highest model error coincides with poorly-constrained areas of the glacier. Further, our optimization procedure shows that optimizing for τ_y over the lower 30 km of Hubbard Glacier provides the best, least sensitive fit to observation. For these reasons, we focus our attention on the better-constrained downstream portion of the glacier. Figure 3.12 shows the plastic model results on the lower 30 km of Hubbard Glacier. The percent error of the model with respect to the reconstruction of Huss and Hock (2015) in this region is quite low, comparable to percent error on other glaciers. The maximum errors are 27.7% overestimation and 22.3% underestimation of ice thickness, a marked improvement on the error seen on the full eight-branch network.

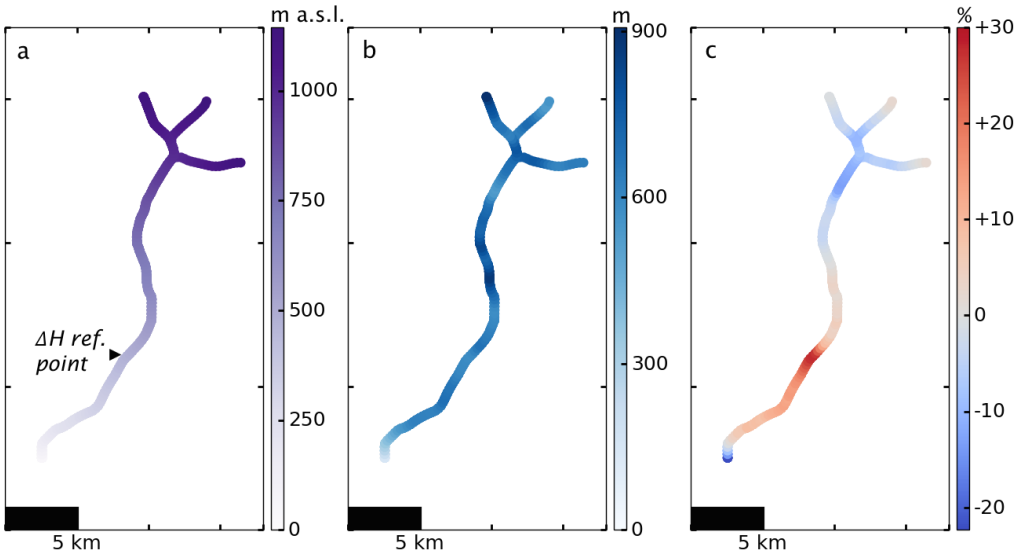

Figure 3.12: Plastic model with $\tau_y = 200$kPa applied to lower 30 km of network of Hubbard Glacier tributaries, aerial view, c. 2007. (a) Glacier surface elevation, (b) Ice thickness, (c) Percent error model-reconstruction (Huss and Hock, 2015). Note that Figures 3.11 and 3.12 use different colorbars to best highlight the features of each.

3.3.4.1 Advance 1948-present

Previous case studies, as well as our earlier work on Columbia Glacier, documented that our plastic model reproduces observed patterns of retreat (Ultee and Bassis, 2016) as well as rudimentary multi-year cycles of advance and retreat. Now, using observations of the lowest 10 km of Hubbard Glacier from 1948 to the present, we investigate how well the model can reproduce observed tidewater glacier advance. Several published studies (McNabb and Hock, 2014; Trabant et al., 2003; U. S. Geological Survey, 2003) and a US Geological Survey dataset documenting the observed advance provide a useful basis for evaluation. We choose a reference point 6 km upstream, where the successive longitudinal profiles of Trabant et al. (2003) show a total of 70 m of thickening between 1948 and 2000. The rate of thickening was not constant, but for simplicity we impose a constant rate equal to the 1948-2000 mean—approximately $1.3\,\mathrm{m\ a^{-1}}$ at the reference point. We run the model for every year 1948-2000 with constant annual thickening, and find the terminus advance plotted in Figure 3.13. Mean terminus advance rate over the entire period is $29.7\ \mathrm{m\ a^{-1}}$, and total advance 1948-2000 is 1.55 km. For comparison, black diamonds in Figure 3.13 show the advance reported by the USGS. The modeled total advance of 1.54 km 1948-2000 agrees with the total advance of 1.4 km reported by Trabant et al. (2003), as well as the 1.75 km advance reported for 1948-2012 by McNabb and Hock (2014). The mean advance rate of $29.7\mathrm{m\ a^{-1}}$ agrees with the $28\mathrm{m\ a^{-1}}$ rate reported by Trabant et al. (2003)

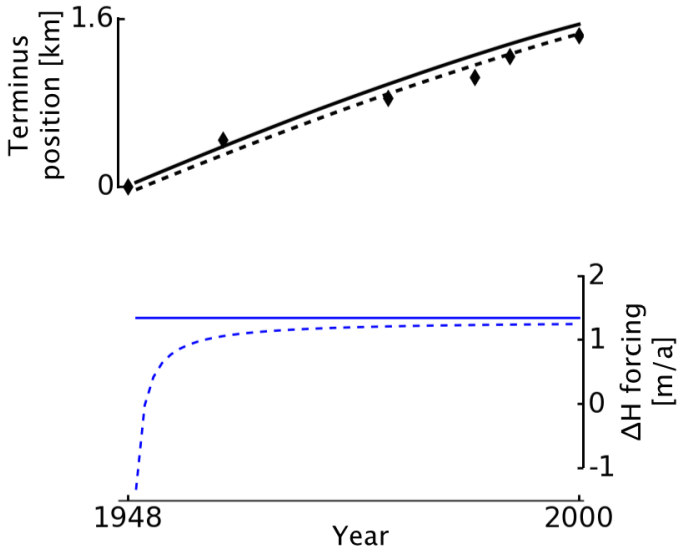

Figure 3.13: Simulated terminus advance of Hubbard Glacier, 1948-2000, under two different forcings. Black curves show plastic model advance under constant upstream thickening (solid) and under a fit to observed upstream thickening (dashed). Black diamonds give observed change in terminus position from USGS longitudinal profiles. Blue curves show the annual thickening rate imposed as an upstream forcing: constant (solid) and fit to observations (dashed).

and the $23 - 36$m a^{-1} reported by Stearns et al. (2015).

Finally, we explore what can be gained by running the model with a more realistic forcing, deriving the upstream thickening from a fit to observations rather than the 52-year mean. We run the model with variable upstream thickening fit to observations and find the terminus advance shown by the dashed curve in Figure 3.13. The variable forcing produces more realistic advance, but only marginally so. Mean terminus advance rate over the entire period is 28.0 m a^{-1}, very similar to the mean advance rate found using a constant forcing. We conclude that using a constant average forcing is an acceptable simplification. For both forcings, our model shows advance rate decreasing over time, while observations show an increasing rate of advance punctuated by one slow period c.1972-1984 (Stearns et al., 2015). The construction of a moraine shoal through sediment buildup has been shown to be fundamentally important for tidewater glacier advance (Meier and Post, 1987; Oerlemans and Nick, 2006; Goff et al., 2012); we suspect that the lack of sediment transport in our plastic model prevents it from maintaining or accelerating rapid advance as a real glacier could.

3.4 Discussion

The yield strength τ_y, as the sole adjustable parameter of our model, merits careful examination. We note that there is not one single value of τ_y that works equally well for all observed glaciers; rather, there is variation in the best-fit values. The two Alaska glaciers studied are best fit by lower yield strengths (130-200 kPa), while the Greenland glaciers are best fit by higher yield strengths (245-355 kPa). We hypothesized that the greater physical sophistication of the Coulomb yield criterion would better match observed glacier profiles, but the results of our case studies are inconsistent on this point. For example, CV_{RMS} between modeled and observed main branch profiles is minimized with the Coulomb criterion for Columbia and Helheim Glaciers, but with the constant-yield-strength criterion for Jakobshavn Isbræ and Hubbard Glacier. We suggest that some of the diversity of yield-strength regimes found in our case studies is a reflection of glacier physics, and some is a side effect of the plastic model's simplicity. For example, the two Alaskan glaciers are temperate and receive much more precipitation than the Greenland outlet glaciers, which may contribute to the lower yield strengths of the former. If the model could be adjusted for ice-dynamical factors such as fjord width, temperature, presence of proglacial mélange or ice tongue, etc., we might expect to adjust for those factors with their own parameters and find a more consistent best-fit yield criterion across all observed glaciers. With τ_y as the only parameter of the model, however, it is reasonable that a diverse set of glaciers with unique characteristics would have similar diversity in their best-fit yield strengths. This phenomenon is also recognizable in the inter-branch yield strength disparity found for Helheim Glacier. Nevertheless, we note that the range of τ_y in our case studies is well within the range of laboratory and field observations (roughly 75-500 kPa).

For networks of two or more branches, we must also consider the inter-branch variability in best-fit τ_y. On Helheim Glacier, that variability is especially noteworthy, with more than 100 kPa difference in the best-fit Coulomb yield strength τ_0 between the small north-easternmost branch and the larger, deeper main branch. In the case studies presented here, we used a single value of τ_y (constant yield strength) or τ_0 (Coulomb yield condition) for all branches of a given glacier network, but future model development could include varying the yield strength by branch. To avoid discontinuities in surface slope, it would be necessary to vary the yield strength smoothly across the junction between branches rather than allowing a step change at the branch point.

Though our plastic network model fits observed profiles of tidewater glaciers remarkably well given its simplicity, some clear model weaknesses remain. For example, the simplest version of the model, making use of a single constant yield strength τ_y, cannot re-

produce retreat that occurs while the glacier is thickening, nor advance that occurs while the glacier is thinning. In observed glaciers, upstream thinning usually corresponds to terminus retreat, and thickening to advance, but not always. For example, about 10% of the Alaska glaciers sampled by Arendt et al. (2002) exhibited thickening-retreat or thinning-advance. Further, the model response to forcing is instantaneous. Driving the model upstream produces instant change in terminus position, and driving the model at the terminus produces instant change in the upstream elevation profile. Therefore, we remain unable to comment on the causal relationship between retreat and thinning (see also Ultee and Bassis, 2016). More fundamentally, lack of a sediment transport mechanism hampers our model's simulation of realistic tidewater glacier advance, as illustrated by the Hubbard Glacier case study. Another obstacle to wide implementation of our model is the input data required: bed topography and bathymetry, which are not globally available. We have treated case studies of Columbia and Hubbard Glaciers, which are among the best-constrained Alaska tidewater glaciers. While extending the model to other Alaska tidewater glaciers seems a natural next step, further study is hampered by limited observational constraints on glacier bed topography.

3.4.1 Introducing climate forcing

The highly simplified model implementation presented here relies on manual input of an upstream thickening or thinning rate for each glacier. Manual input may be constrained by observational data, but it is a poor substitute for true climate forcing. Further, the technique is not scalable to the hundreds of tidewater glaciers worldwide, limiting the utility of the model. Two options exist to remedy this situation: introducing climate forcing directly into the plastic model, for example by adding functionality to treat changes in surface mass balance, or coupling upstream with a more sophisticated model that handles climate forcing itself. We discuss the first tactic in Bassis and Ultee (2017, submitted manuscript) and focus our attention here on the second tactic.

Coupling with a more complex glacier dynamics model (e.g. Marzeion et al., 2012) may be possible, but will require judicious choice of coupling location x_{couple}. We need only require that ice thickness remains continuous at the junction, but the best x_{couple} may depend on the glacier and the choice of upstream model. Without the benefit of coupling experiments to guide us, we suggest that the most consistent choice of x_{couple} will match not only ice thickness, but basal shear stress at the junction point. The plastic model assumes that basal stress over the entire glacier is exactly the yield strength of ice, τ_{y}, which may vary spatially according to the Coulomb condition of Equation 3.5 (see also Ultee and

Bassis, 2016). In theory, basal stress of a tidewater glacier flowing down a valley without large pinning points should increase downstream throughout the accumulation area, which should be reflected in the glacier models with which our model could couple. The appropriate location to induce coupling, x_{couple}, is the point along the centerline of the main glacier branch where the basal stress according to the upstream model matches our model's yield strength of ice to within a certain tolerance. Large, abrupt features such as upstream ice falls—like the one on Columbia Glacier's main branch—may affect selection of x_{couple}. Careful initial experiments will help in designing a general method of avoiding such problems.

At x_{couple}, we require that the ice thickness of the plastic glacier, $H_{\text{couple}} \equiv H(x_{\text{couple}})$, match that found by the upstream model. As the upstream model evolves in time, the plastic glacier downstream will respond to changes in H_{couple}. In this way, the plastic model can respond to changes in climate forcing applied upstream. We note that the climate forcing relevant to tidewater glaciers includes not only atmosphere forcing, but ocean forcing as well. However, coupling our model to an ocean model at the calving front would be considerably more complicated to implement, and we have not explored that possibility.

3.5 Conclusion

We have presented a model that balances the simplicity of one-dimensional flowline modeling with the power of explicitly representing intersections between glacier branches. Our case studies indicate that the model can produce surface elevation profiles of multiple branches with low error, as well as realistically simulate the advance and retreat of Alaska and Greenland tidewater glaciers. Though our method gains important validation from detailed application to individual glaciers, its true appeal is in scaling up to large networks of tidewater glaciers, such as those draining the Greenland Ice Sheet. Simulation of those larger networks can be enhanced by explicit inclusion of surface mass balance—as described in Bassis & Ultee (2017, submitted manuscript)—or coupling to a more sophisticated model upstream.

Our initial case studies, performed without high-quality local climate data or coupling to a sophisticated ice dynamics model, give reason for optimism. In particular, the cases of Columbia Glacier (see Ultee and Bassis, 2016) and Hubbard Glacier demonstrate that a simple constant upstream forcing can reproduce terminus advance and retreat with surprising accuracy. More precise forcing based on observations of the glacier or the local climate does offer marginal improvement in model performance, as demonstrated for Hubbard Glacier above, but it is not essential. Thus, our model offers useful projections despite

the inherent uncertainty in models of future climate.

CHAPTER 4

Future projections of calving flux from Greenland outlet glaciers

This chapter is a draft manuscript in preparation for publication. It applies the model developed in Chapters 2 and 3 under several forcing scenarios to estimate upper bounds on the calving contribution to sea level rise from the largest Greenland outlet glaciers.

4.1 Introduction

The ice that makes up the Greenland Ice Sheet has the potential to raise global mean sea level by 7 meters (Greve, 2000; Gregory et al., 2004) and dramatically reshape Earth's coastal regions. Current annual ice loss from the Greenland Ice Sheet is responsible for almost 1 mm of global sea level rise per year (Jacob et al., 2012; Forsberg et al., 2017), a contribution that exceeds that from Antarctica and has accelerated in recent decades (Velicogna et al., 2014; van den Broeke et al., 2016). About half of the acceleration in mass loss is attributable to ice dynamic changes (Straneo et al., 2013; Benn et al., 2017b). Accurate projections of global mean sea level must include the contribution from ice dynamics, but capturing that contribution in models remains challenging.

One of the major challenges is that the fracture process preceding iceberg calving is fundamentally incompatible with the assumption of continuum deformation in most ice sheet models. There has been recent progress to reconcile this issue; for example, Borstad et al. (2012) and Duddu et al. (2013) have represented ice damage as a continuum variable, though there is disagreement about how ice damage should evolve in time. Benn et al. (2017a) have coupled a granular model that allows calving to a finite-element model that solves the Stokes equations for viscous deformation, offering a very promising basis for eventual fully-dynamic calving. For the time being, however, their approach is too computationally expensive to be widely implemented.

Simpler models can produce constraints on dynamic mass loss to inform more sophisticated models and sea level scenarios. Pfeffer et al. (2008) deduced low-end and high-end constraints of 21st century sea-level contribution from Greenland and Antarctica based on average and extreme observations of present outlet glacier flow rates. Their constraints provide useful context to evaluate model parameterizations of dynamic mass loss, but their connection to future climate scenarios is unclear and they do not account for changing physical context (e.g. fjord geometry). Similarly, Nick et al. (2013a) simulate a single glacier flowline for each catchment basin, leaving their model unable to account for changing glacier geometry as tributary branches separate. The model Nick et al. (2013a) use for their projections does parametrize several processes known to be important to outlet glacier dynamics. However, the tuning parameters vary by an order of magnitude between glaciers (Nick et al., 2013b), limiting its broader applicability.

We have previously derived a simple model that extends the perfect plastic approximation of Nye (1951, 1952, 1953) to networks of calving glaciers (Ultee and Bassis, 2016, 2017). Our approach uses the plastic rheology to produce centerline profiles of glaciers whose fronts can lose mass by rapid calving events. In its simplest form, the model relies on only one adjustable parameter—the yield strength of ice, τ_{y}—which is constrained by observation and laboratory experiments. The more sophisticated implementation we describe here adds one more adjustable parameter, the flow law creep factor A, which has been similarly constrained by observations (Cuffey and Paterson, 2010, and references therein).

The perfect plastic approximation is a limiting case of other rheologies commonly applied to glacier ice, including viscous creep with disarticulation above a yield strength (Balmforth et al., 2006). It produces thicker and steeper glacier profiles than other rheologies, maximizing the volume of ice stored at each point along a profile of a given length. Our implementation also responds instantaneously to the forcing we apply, maximizing the rate of terminus retreat that results from a given forcing. The plastic approximation's maximized rate of retreat and stored-ice volume along each flowline combine to produce upper bounds on the dynamic discharge of ice associated with a given forcing.

Here, we apply our model as a limiting case of viscoplastic creep flow to produce upper-extreme projections of dynamic fluxes from Greenland outlet glaciers under five different forcing scenarios. Our projections can be used together with projections of meltwater runoff to constrain these glaciers' contribution to global sea level in the coming century.

Network name	Branches	Initial terminus (lat, lon)	Ice flux [Gt a^{-1}]
Sermeq Kujalleq (main)	1	(69.132053, -49.509957)	48.5 $\pm$ 10.5
Sermeq Kujalleq (central)	1	(69.291579, -49.273543)	N/A
Sermeq Kujalleq (north)	1	(69.301572, -49.697977)	N/A
Koge Bugt	1	(65.164437, -41.12781)	15.2 $\pm$ 4.1
Helheim Glacier	3	(66.38222, -38.182096)	31.0 $\pm$ 6.6
Kangerlussuaq Glacier	4	(68.61339, -32.920968)	30.0 $\pm$ 6.5

Table 4.1: Glacier networks appearing in this study. "Branches" refers to the number of branches we simulate in this work, "initial terminus" the coordinates of the center of the terminus as of our initialization with BedMachine v3 (Morlighem et al., 2017), and "ice flux" annual ice flux from the network in Gt a^{-1} as estimated in Aschwanden et al. (2016). The three single-branch networks of Sermeq Kujalleq, all of which calve into Ilulissat Icefjord, were previously connected and are not reported separately by Aschwanden et al. (2016).

4.2 Methods

We apply the plastic network model described in Ultee and Bassis (2016, 2017) to six of the highest-flux glacier networks in Greenland. We first identify glacier termini using the boundaries of the "grounded ice" mask of BedMachine v3 (Morlighem et al., 2017). Then, we identify branch flowlines by tracing ice velocities observed by Sentinel (ENVEO, 2017) upstream from a set of points that spans each terminus. Our networks are therefore defined to be dynamically connected and calving from a single terminus at initialization. The condition of dynamic connection from a single terminus leads us to define three separate networks for the three branches of Sermeq Kujalleq (Danish: Jakobshavn Isbræ).

The networks we simulate are shown in Figure 4.1 and outlined in Table 4.1.

4.2.1 Motion of a calving glacier terminus

Let $x = 0$ represent the ice divide and $x = L$ the terminus, where $L = L(t)$ is the length of the glacier. The time derivative dL/dt then represents the change in terminus position over time. We use mass continuity and a condition on terminus thickness to derive an expression for dL/dt of a plastic calving glacier.

In our plastic model, the glacier terminus is a yield surface (see Ultee and Bassis, 2016). This imposes a condition on the ice thickness at the terminus, $H|_{x=L} = H_\mathrm{y}$, where

$$H_\mathrm{y} = 2\frac{\tau_\mathrm{y}}{\rho_\mathrm{i} g} + \sqrt{\frac{\rho_\mathrm{w} D^2}{\rho_\mathrm{i}} + 2\frac{\tau_\mathrm{y}}{\rho_\mathrm{i} g}} \tag{4.1}$$

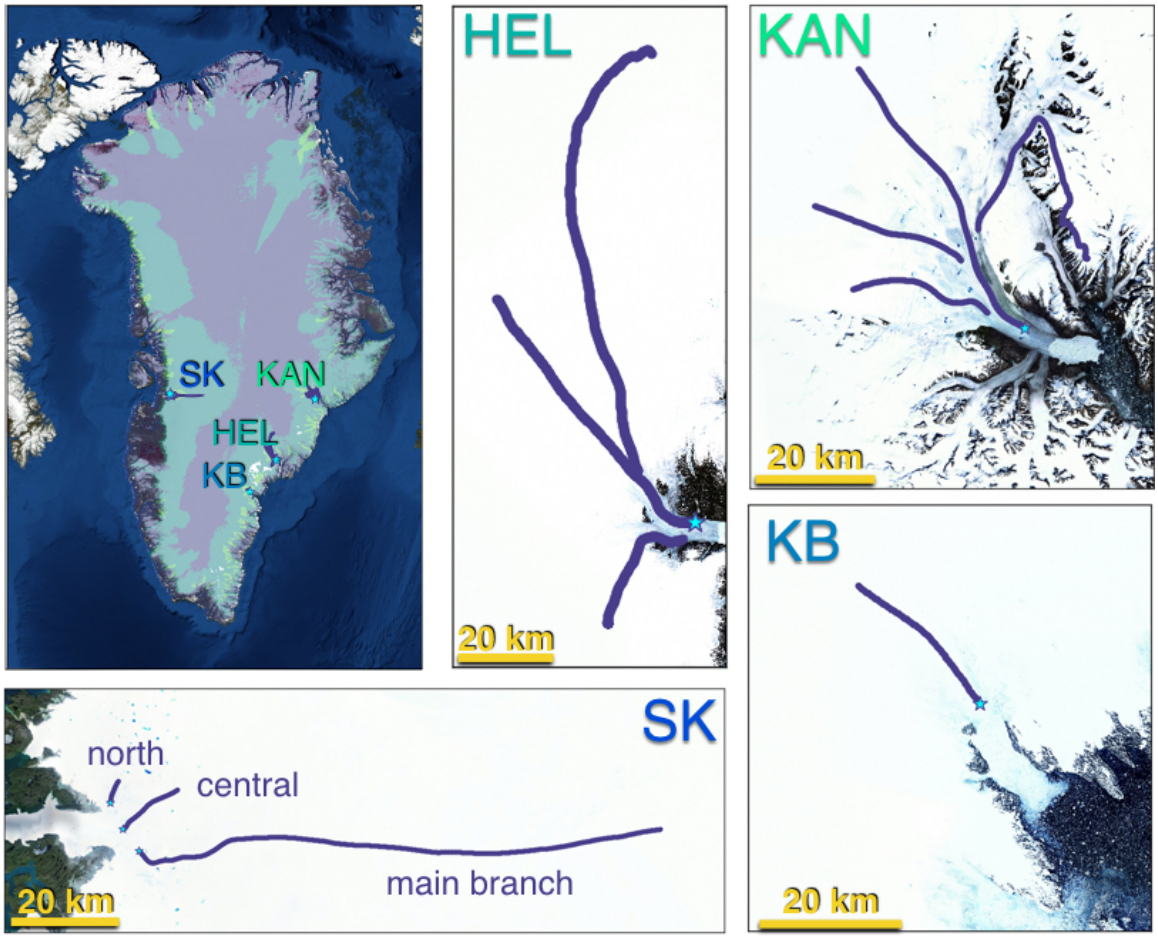

Figure 4.1: Greenland outlet glacier networks included in this study. (a) Location of glacier networks indicated on ESRI imagery of Greenland, overlaid with 2016-2017 ice velocity from Sentinel (ENVEO, 2017). (b) Three single-branch networks of Sermeq Kujalleq, previously connected but now calving from dynamically disconnected termini. (c) Three-branch network of Helheim Glacier. (d) Four-branch network of Kangerlussuaq Glacier. (e) Single-branch network of Koge Bugt. Spatial scales have been chosen to best illustrate network geometry and are not consistent across subplots (b)-(e).

In equation (4.1), τ_y is the yield strength of ice, $\rho_i = 916\,\text{kg m}^{-3}$ the density of glacier ice, $g = 9.81\,\text{m s}^{-2}$ acceleration due to gravity, $\rho_w = 1020\,\text{kg m}^{-3}$ the density of seawater, and D the water depth at the terminus. Taking the material derivative of the terminus ice thickness, we find

$$\frac{DH}{Dt}|_{x=L} = \frac{DH_y}{Dt} \tag{4.2}$$

$$\left[\frac{\partial H}{\partial t} + \frac{dL}{dt}\frac{\partial H}{\partial x}\right]_{x=L} = \frac{\partial H_y}{\partial t} + \frac{dL}{dt}\frac{\partial H_y}{\partial x} \tag{4.3}$$

$$\frac{\partial H}{\partial t}|_{x=L} = \frac{dL}{dt}\left[\frac{\partial H_y}{\partial x} - \frac{\partial H}{\partial x}\right]_{x=L}. \tag{4.4}$$

Mass continuity requires

$$\frac{\partial H}{\partial t} + \frac{\partial}{\partial x}(HU) = \dot{a} \tag{4.5}$$

where $H = H(x,t)$ is the ice thickness, $U = U(x,t)$ the ice velocity, and $\dot{a} = \dot{a}(x,t)$ the net ice accumulation rate, for all (x,t).

Substituting equation (4.5) into (4.4), we find

$$\dot{a} - H\frac{\partial U}{\partial x} - U\frac{\partial H}{\partial x} = \frac{dL}{dt}\left[\frac{\partial H_y}{\partial x} - \frac{\partial H}{\partial x}\right]_{x=L} \tag{4.6}$$

$$\therefore \frac{dL}{dt} = \frac{\dot{a} - H\frac{\partial U}{\partial x} - U\frac{\partial H}{\partial x}}{\frac{\partial H_y}{\partial x} - \frac{\partial H}{\partial x}}, \tag{4.7}$$

with all terms of equation (4.7) evaluated at $x = L$, the terminus of the glacier. With the exception of ice accumulation rate $\dot{a}$, all terms are determined by the rheology of ice.

Upstream from the terminus, we assume a plastic yielding layer at the bed of the glacier. A perfectly plastic glacier would have a rigid ice plug above the yielding layer, but the perfect plastic approximation is a limiting case of several other rheologies that could be used to describe the slow deformation of ice in a pseudo-plug (e.g. Balmforth et al., 2006). Here we choose to describe the slow deformation of intact ice with the familiar Glen's flow law. At the terminus, as in Ultee and Bassis (2016, 2017), we require a vertical yield surface to describe the more rapid motion of fractured, disarticulated ice as it calves away from the intact glacier. This implies that the effective stress in a region of length δ upstream from the terminus is within ϵ of the yield strength τ_y. Near the terminus, we have

$$\begin{aligned}\frac{\partial U}{\partial x} = \dot{\varepsilon}_{xx} &= A\tau_{xx}^n \\ &= A\tau_y^n,\end{aligned} \tag{4.8}$$

where flow law exponent $n = 3$ and A is the flow rate parameter of Glen's flow law.

We integrate equation (4.5) in x to find

$$\int_0^L \frac{\partial H}{\partial t}\,\mathrm{d}x + (HU)|_{x=L} = \int_0^L \dot{a}\,\mathrm{d}x \tag{4.9}$$

$$U(x=L) = \frac{1}{H_{\text{terminus}}}\int_0^L \left[\dot{a} - \frac{\partial H}{\partial t}\right]\,\mathrm{d}x, \tag{4.10}$$

and by the chain rule $\frac{\partial H}{\partial t} = \frac{\partial H}{\partial L}\frac{dL}{dt}$. Separating the integral in equation (4.10) and expanding $\frac{\partial H}{\partial t}$ gives

$$U(x=L) = \frac{\dot{\alpha}L}{H_{\text{terminus}}} - \frac{dL}{dt}\frac{1}{H_{\text{terminus}}}\int_0^L \frac{\partial H}{\partial L}\,\mathrm{d}x, \tag{4.11}$$

where $\dot{\alpha} = \frac{1}{L}\int_0^L \dot{a}\mathrm{d}x$ is the spatially-averaged ice accumulation rate along the flowline.

We now substitute our expressions (4.8, 4.11) in to equation (4.5) and rearrange to find

$$\frac{dL}{dt} = \frac{\dot{a} - A\tau_y^3 H_{\text{terminus}} + \frac{\dot{\alpha}L}{H_{\text{terminus}}}\frac{\partial H}{\partial x}}{\frac{\partial H_y}{\partial x} - \frac{\partial H}{\partial x}\left(1 - \frac{1}{H_{\text{terminus}}}\int_0^L \frac{\partial H}{\partial L}\right)}. \tag{4.12}$$

Equation (4.12), with the terminus ice thickness requirement of equation (4.1) and the upstream ice thickness as described in Ultee and Bassis (2016, 2017), fully specifies the time evolution of our model.

4.2.2 Climate forcing

Changes in the ice accumulation rate $\dot{a}(x,t)$ over time provide a climate forcing. Because our model does not account for firn densification or other processes between precipitation and eventual ice accumulation, we use ice surface elevation change data from Cryosat (Flevinson et al., 2013) to define an initial $\dot{a}(x)$. Our use of surface elevation change forcing to drive our model of ice dynamics assumes that all surface elevation change is due to mass balance rather than dynamic thinning. This assumption will lead our model to overestimate the dynamic response to non-dynamic thinning, which is consistent with producing an upper bound on future ice mass loss from the glaciers we study.

We simulate a range of forcing scenarios. Our baseline scenarios (cold baseline "CB", warm baseline "WB") set $\dot{\alpha} = \dot{a} = 0$, thus representing only changes due to ice-dynamic adjustment. To this we add two scenarios forced by persistence of the 2011-2017 mean surface elevation change: one with warm ice ("WP") and one with cold ice ("CP"). Finally, we include one scenario of strong warming ("WX") in which the surface elevation change forcing is slowly ramped up to double its initial value. Table 4.2.2 summarizes

Scenario	Ice temp [°C]	A [Pa^{-3}s^{-1}]	$\dot{\alpha}$
Cold baseline (CB)	-30	3.7×10^{-26}	0
Warm baseline (WB)	-2	1.7×10^{-24}	0
Cold persistence (CP)	-30	3.7×10^{-26}	Persistence of 2011-2017 mean[1]
Cold persistence modif. (CPm)	*-30*	3.7×10^{-26}	*Persistence of 2011-2017 mean*[2]
Warm persistence (WP)	-2	1.7×10^{-24}	Persistence of 2011-2017 mean
Strong warming (WX)	-2	1.7×10^{-24}	Linear doubling of 2011-2017 mean

Table 4.2: Model settings for the scenarios we study here. A is the flow rate parameter of Glen's flow law and $\dot{\alpha}$ is the surface elevation change forcing of equation (4.12).
Note 1: 2011-2017 mean refers here to the spatial average for each flowline, calculated from the gridded 5-year mean of Greenland surface elevation change, one of the Essential Climate Variables reported by the European Space Agency Climate Change Initiative (Flevinson et al., 2013). The persistence assumption maintains a constant value of $\dot{\alpha}$ for each glacier for the entire simulation. Linear doubling slowly increases the strength of the $\dot{\alpha}$ forcing so that $\dot{\alpha}_{\text{final}} = 2\dot{\alpha}_{\text{initial}}$.
Note 2: Modified persistence scenario "CPm" is identical to scenario CP for all networks except Sermeq Kujalleq [main]. For Sermeq Kujalleq [main], we reduce the surface forcing to 80% strength to highlight a numerical issue—see section 4.3.

these scenarios. The cold baseline scenario uses the most conservative assumptions about ice physics and future climate, which will produce the lowest estimates of dynamic ice flux from our model. These low estimates should not be interpreted as a lower bound or minimum possible ice loss; rather, they are an upper bound on ice loss given very conservative forcing.

4.2.3 Calculating mass loss and sea level contribution

We calculate the change in pure ice mass from our selected glaciers. That is, we assume a constant density of ice, $\rho_{\text{i}} = 920\,\text{kg m}^{-3}$ in our model formulation and use the same ρ_{i} to convert changes in ice volume to mass flux. Estimating only the change in pure ice mass allows us to separate firn processes and other surface mass balance effects from the effect of iceberg calving.

As in Ultee and Bassis (2016, 2017), we find a centerline profile for each glacier branch at each time step. Here, we calculate change in ice volume ΔV by integrating the difference between successive profiles,

$$\Delta V = \int_0^L \left(H(x, t_{n+1}) - H(x, t_n)\right) w(x)\, \mathrm{d}x \tag{4.13}$$

where $H(x,t)$ is ice thickness as a function of position and time, and $w(x)$ is the width of

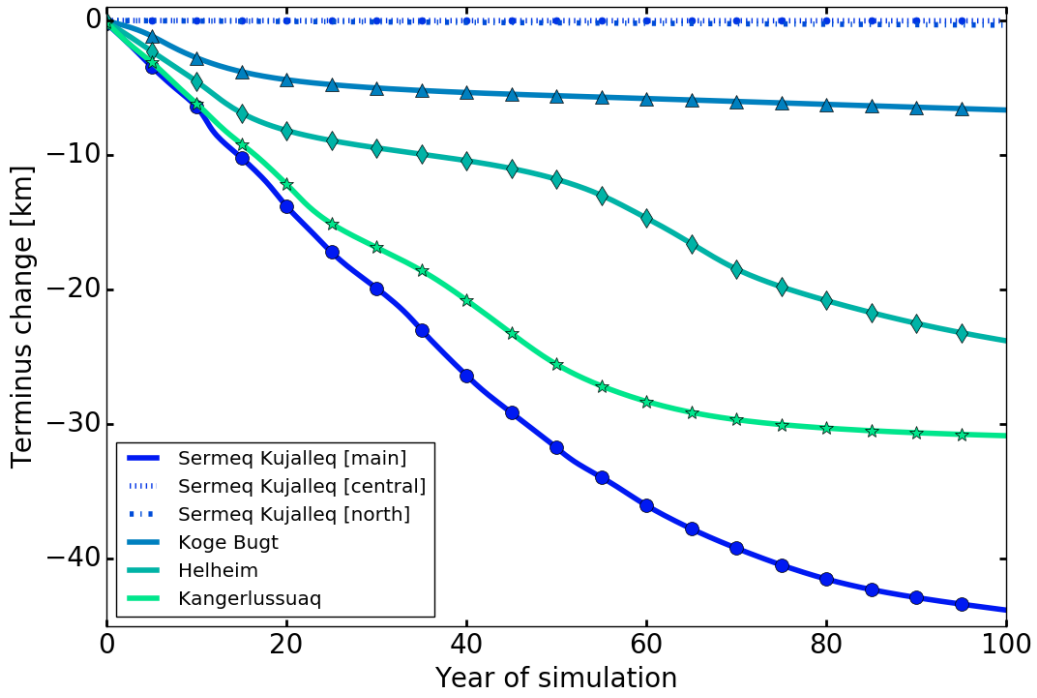

Figure 4.2: Change in main terminus position of 6 glacier networks for 100 years of the "Cold baseline" scenario described in Table 4.2.2.

the glacier branch as a function of position along the flowline[1]. For a pure-ice, constant density glacier, mass flux $\Delta M = \rho_{\text{ice}} \Delta V$.

Not all of the mass lost from calving glaciers contributes to global sea level, as Bamber et al. (2018) point out. Where glaciers are grounded below sea level, as many of our study set are for some portion of their catchment, only the portion of ice initially above sea level makes a sea level contribution. We include only the above-sea-level portion of ice lost from iceberg calving in our calculated sea level contribution. However, a substantial portion of the ice flux in our simulations comes from upstream glacier thinning (dynamic drawdown), all of which contributes to sea level change.

4.3 Results

We find strong terminus retreat for all of the scenarios described in Table 4.2.2. Even under the most conservative "Cold baseline" scenario, the main branch of Sermeq Kujalleq retreats by more than 40 km in 100 years, as illustrated in Figure 4.2. Most of the main termini we simulate retreat by several kilometers under scenario CB, but the single-branch

[1]The glacier branch width refers to the region where surface speed is at least $1\,\text{m}\,\text{d}^{-1}$ and direction of flow is aligned within $60°$ of centerline flow direction.

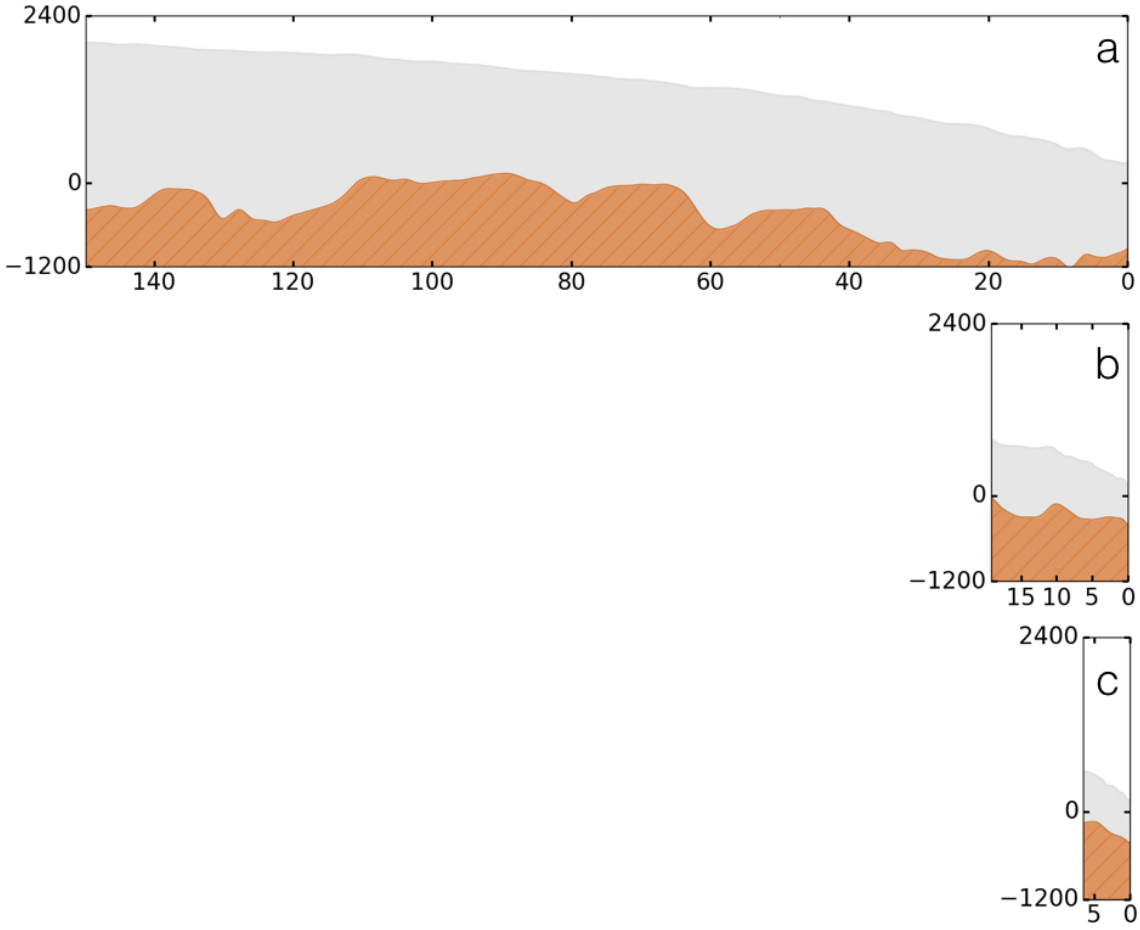

Figure 4.3: Bed topography of three formerly-connected branches of Sermeq Kujalleq: (a) main, (b) central, and (c) north. Horizontal and vertical scale are kept approximately consistent across the three subplots.

networks Sermeq Kujalleq [central] and Sermeq Kujalleq [north] are nearly static. Both networks have shallow, seaward-sloping beds, which tend to slow retreat. Figure 4.3 compares the bed topography of the three Sermeq Kujalleq networks. The deep trough beneath Sermeq Kujalleq [main], shown in Figure 4.3a, contributes to its faster rate of retreat and stronger sea level contribution. Figure 4.4 shows the sea level contribution from each of our six glacier networks for scenario CB.

Upper bounds on sea level contribution from our 6 networks range from 11.3 mm (CB) - 28.2 mm (WX) within the next 100 years. Figure 4.5 summarizes sea level contribution under each forcing scenario. We reiterate that our low estimate from scenario CB should not be interpreted as a lower bound or minimum possible ice loss from these glaciers—it is simply the estimate produced with the most conservative ice physics assumptions. Interestingly, our high-end scenarios WP and WX produce nearly identical sea level contributions: 28.0 and 28.2 mm, respectively. Under scenario CP, the terminus of Sermeq Kujalleq

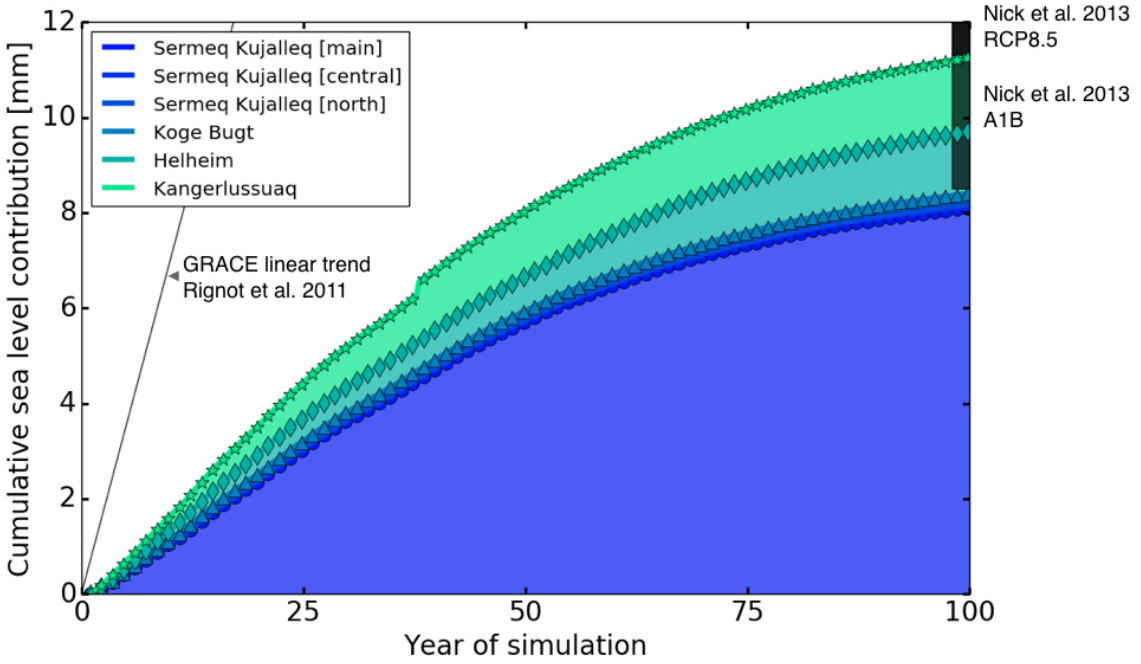

Figure 4.4: Cumulative dynamic-flux contribution to global sea level resulting from the terminus retreat shown in Figure 4.2. Included for comparison are the present-day linear trend of Greenland sea level contribution from observations (grey line; Rignot et al., 2011) and the projections of Nick et al. (2013a) for sea level contribution from four main Greenland outlet glaciers under two forcing scenarios (dark grey bars).

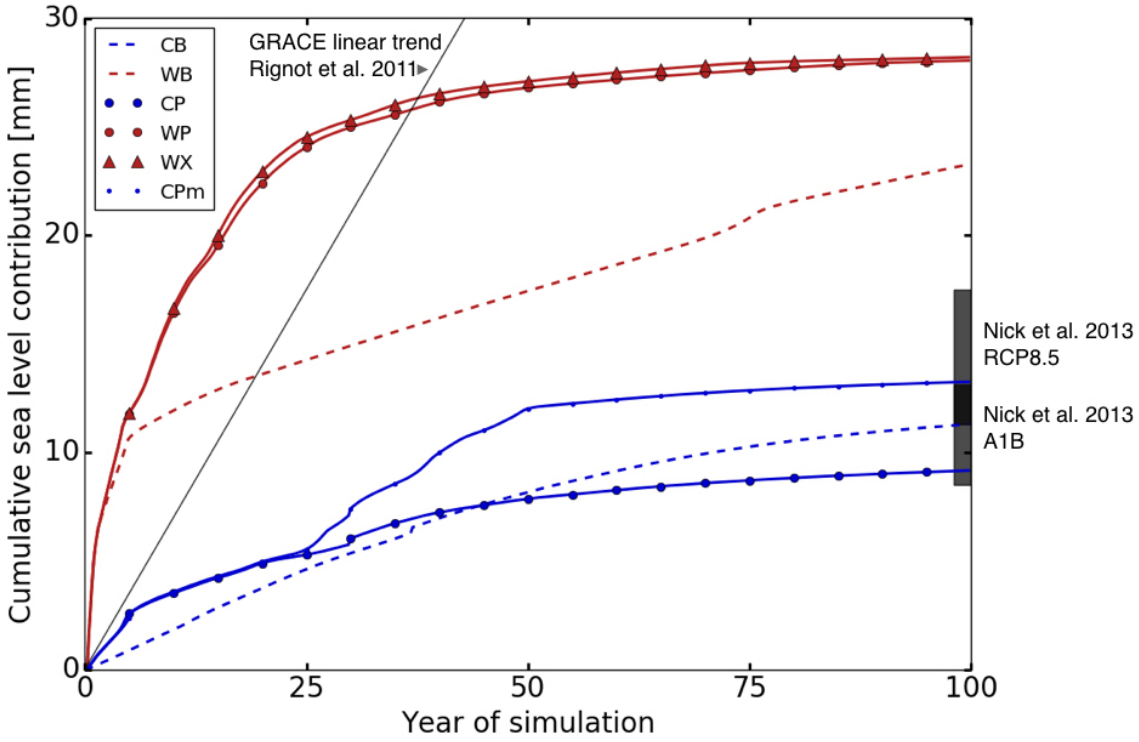

Figure 4.5: Comparison of total sea-level contribution from our six glacier networks under the scenarios outlined in Table 4.2.2. Once again, we include the present-day linear trend of Greenland sea level contribution from observations (grey line; Rignot et al., 2011) and projections of sea level contribution from four main Greenland outlet glaciers under two forcing scenarios (dark grey bars; Nick et al., 2013a).

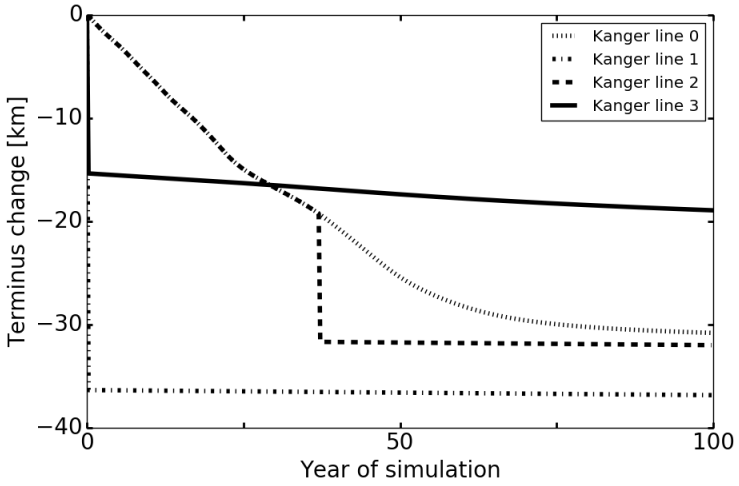

Figure 4.6: Terminus retreat of Kangerlussuaq glacier network simulated for 100 years of scenario CB. The network begins with a single shared terminus, but has separated into four independently-evolving termini by the end of the simulation.

[main] reaches a bedrock rise and stagnates early on in the simulation. Under the modified scenario CPm, in which we keep the forcing identical for most networks but multiply by 0.8 for Sermeq Kujalleq [main]—representing slightly weaker surface thinning—the terminus retreat is slightly smoother and manages to continue past the bedrock rise. Figure 4.5 shows this bifurcation.

Unlike single-flowline models, our model is able to handle networks that separate into multiple termini over the course of simulations. Figure 4.6 shows the separation of Kangerlussuaq glacier network from one terminus into three. Line 0 is our "main" flowline, whose course is similar to the single flowline defined for Kangerlussuaq glacier by Nick et al. (2013a). The terminus of line 0 retreats a total of 30.84 km during the 100-year simulation, while the termini of lines 1, 2, and 3 retreat 36.88, 32.03, and 18.97 km, respectively. Our network model handles such separations automatically, without prescription from the user, and tracks dynamic flux from each new terminus as soon as it separates from other branches. We are not aware of any flowline models with similar capability.

4.4 Discussion

We have included two independent comparisons for qualitative validation of these results: the model projections of Nick et al. (2013a) and the average annual mass loss of the entire Greenland Ice Sheet for the period 2002-2010 as calculated by the Gravity Recovery and Climate Experiment (Rignot et al., 2011). Both are plotted on Figures 4.4 and 4.5.

Nick et al. (2013a) simulated the 100-year response to assorted forcing scenarios for four glaciers: Jakobshavn Isbræ (Sermeq Kujalleq [main]), Helheim Glacier, Kangerlussuaq Glacier, and Petermann Glacier. The overlap of their study set with ours makes their projections a valuable comparison. Our upper-bound dynamic sea level contribution for the conservative scenarios CB, CP, and CPm fall within the range of the projections of Nick et al. (2013a), which demonstrates that our cumulative estimates are of the correct order of magnitude. Meanwhile, the slope of the grey line in Figures 4.4 and 4.5 indicating rate of mass loss from all of Greenland, through both ice dynamics and surface mass balance processes (Rignot et al., 2011), serves as a comparison for the rate of mass loss associated with our upper-bound calculations. In warmer scenarios, the rate of mass loss from our six glacier networks initially exceeds the average annual rate of mass loss from all of Greenland, but decreases throughout the simulation. Red lines in Figure 4.5 illustrate this pattern. Our upper-bound cumulative dynamic contribution to sea level from all scenarios falls below the simple forward projection of the observed trend for all of Greenland. This agrees with what we expect given that the mass loss from all of Greenland should exceed the mass loss from a subset of its outlet glaciers. Both of these comparisons are qualitative validation of our results. Simulating historical evolution of the six glacier networks appearing in this Chapter and comparing them with available observations from past decades would provide stronger evidence of our model's validity; we have done so for Sermeq Kujalleq and Helheim Glacier in Chapter 3 of this dissertation and intend to produce remaining hindcasts in the near future.

Our findings demonstrate the importance of glacier fjord topography in controlling retreat, in agreement with previous observational, theoretical, and numerical studies (Benn et al., 2017b; Schoof, 2007; Vieli et al., 2001; Warren, 1991). The main branch of Sermeq Kujalleq, which is grounded in a trough nearly 1000 m below sea level, retreats the fastest of all networks studied and makes a strong contribution to global sea level in all of our simulations, while adjacent branches with seaward-sloping beds show much weaker response to all forcing scenarios. The marine portion of Sermeq Kujalleq is responsible for the majority of its sea level contribution and undergoes complete collapse by midway through the 100-year simulation in all scenarios except "Cold baseline", the most conservative. The sensitivity of Equation 4.12 to bed topography produces physically-realistic time evolution of glacier termini on varied beds, but it also produces numerical trouble in some cases. In particular, the unmodified forcing scenario CP shows a dubious terminus stagnation of the main branch of Sermeq Kujalleq in water 1100 m deep, resulting in cumulative sea level contribution below that of the more weakly forced CB and CPm scenarios (Figure 4.5).

We also capture the distinct sea level contributions of multi-tributary glacier networks.

The "Sermeq Kujalleq [main]" network makes a contribution to sea level two orders of magnitude greater than that of the two other Sermeq Kujalleq networks, partly as a result of the deep bedrock trough of the main branch. However, the sea level contribution of Helheim Glacier tributary 1 is comparable to that of the main branch. Similarly, two of the three tributaries of Kangerlussuaq Glacier make sea level contributions comparable to or exceeding that of the main branch. Our model's automatic handling of dynamically decoupling glacier branches during prolonged retreat accounts for the influence of glacier geometry that may differ among branches of a formerly-connected network. This effect has proven important in the terminus evolution of recently-separated Columbia and Post Glaciers in Alaska (Enderlin et al., 2018) and on branches of Upernavik Isstrøm, Greenland (Kjær et al., 2012).

In contrast with the forcing method we employed in Ultee and Bassis (2016, 2017), which required the user to specify a single upstream point where forcing would be applied, here we have derived a self-consistent equation for terminus evolution (4.12) that requires no such specification. Equation (4.12) can accept upstream forcing that varies in time and space along an entire glacier flowline. The forcing method we have developed and applied here connects our simulations more closely with climate variables and future scenarios, and it allows us to use more sophisticated data products such as Flevinson et al. (2013). Further, our previous method lost effectiveness when glacier termini retreated past the upstream location where the forcing was being applied, while the new method allows simulations to proceed for terminus positions anywhere along the flowline. This dramatically improves our model applicability.

The scenarios we examine do not account for the effect of ocean thermal forcing, which is known to be important for outlet glacier dynamics (e.g. Motyka et al., 2003; O'Leary and Christoffersen, 2013; Petlicki et al., 2015). Ocean water in Greenland fjords is generally warm, reaching temperatures > 3°C even in the winter at Helheim Glacier (Straneo et al., 2012), and summer submarine melt rates up to 3.9 ± 0.8 m day^{-1} have been calculated from observations at Greenland glacier termini (Rignot et al., 2010). Adding submarine melt forcing to our model is likely to increase the projected sea level contribution from low-end scenarios, especially for glaciers grounded below sea level for large parts of their catchment. The main branch of Sermeq Kujalleq, for example, is grounded below sea level for 84.4 km upstream from its present terminus, while the bed of Koge Bugt rises above sea level only 5.8 km upstream from its present terminus. For more extreme warming scenarios such as WP and WB, almost all the termini of our glacier networks have retreated by year 50 to positions grounded above sea level or in very shallow water, where the effect of submarine melt would be limited. This suggests that the addition of submarine melt

forcing to our warmer scenarios might increase the rate of retreat and dynamic flux in the early years of the simulation but would not affect cumulative contribution to sea level rise on the century time scale.

4.5 Conclusions

We have developed and applied a dynamically consistent model that constrains century-scale dynamic mass loss for Greenland outlet glaciers. Our simple model accounts for the effects of iceberg calving without resolving individual calving events. It is applicable to networks of interacting glacier branches and allows new calving termini to emerge when branches separate. Dynamic ice flux from newly emerged termini is nontrivial in our simulations and sometimes exceeds flux from the "main" glacier branch identified in this and other modelling studies. Accounting for flux from glacier tributaries is especially consequential for warmer climate scenarios.

The role of basal topography in controlling glacier advance and retreat remains evident. Glacier branches grounded far below sea level retreat rapidly (in excess of 1 km a^{-1}) and make the strongest contribution to sea level change regardless of forcing scenario. The effect of submarine melt forcing, which we do not include here, would also be modulated by glacier bed/fjord topography; glaciers whose termini sit on land or in shallow water are much less susceptible to retreat driven by warm ocean water. This suggests that constraints generated by our warm scenarios WP and WX truly are constraints, in that adding submarine melt is unlikely to increase their cumulative sea level contribution.

Under the most conservative assumptions—very cold ice, no external climate forcing, with retreat a response to near-terminus stretching and ice yield—our upper constraint on dynamic mass loss from the six glacier networks here studied is the equivalent of 11.3 mm global mean sea level rise within 100 years. Under our strongest forcing scenario, the constraint is a 28.2 mm contribution to global mean sea level rise in the same time period. The doubling of our upper constraint from scenario CB to scenario WX illustrates dependence of our results, like other projections of glacier change, on future climate forcing.

CHAPTER 5

Attending to the use and usability of our research

N.B.: This chapter was published in 2018 as

Ultee, L., Arnott, J. C., Bassis, J. N., and Lemos, M. C. (2018). From ice sheets to main streets: Intermediaries connect climate scientists to coastal adaptation. *Earth's Future* 6(3): 299–304. doi: 10.1002/2018EF000827

In envisioning the eventual use of our numerical model to inform decision-making, the chapter transcends this work to examine the broader purpose of sea-level research in society. We argue that sea-level research, including numerical modelling efforts such as this dissertation, may support coastal communities' adaptation to sea-level change, but that scientific knowledge produced without those communities in mind may not match their actual needs. We present three possible avenues of engagement for researchers to produce more decision-relevant information in collaboration with different kinds of "science intermediaries".

5.1 Enhancing the decision relevance of our science

There is tremendous popular interest in our changing planet. Media coverage highlights huge, faraway events, like the recent calving of a large iceberg from the Larsen C ice shelf in Antarctica (Figure 5.1a), as well as more persistent local changes like frequent flooding in coastal communities (Figure 5.1b). Meanwhile, climate researchers and scientific organizations have called on their peers to intensify engagement with policy-makers and the broader public (e.g. Lubchenco, 2015; Achakulwisut, 2017; American Association for the Advancement of Science [AAAS], 2017), emphasizing the policy relevance of their work. Climate change touches many sectors of society that could benefit from science-based knowledge, yet in many cases research expertise does not make it out of academic

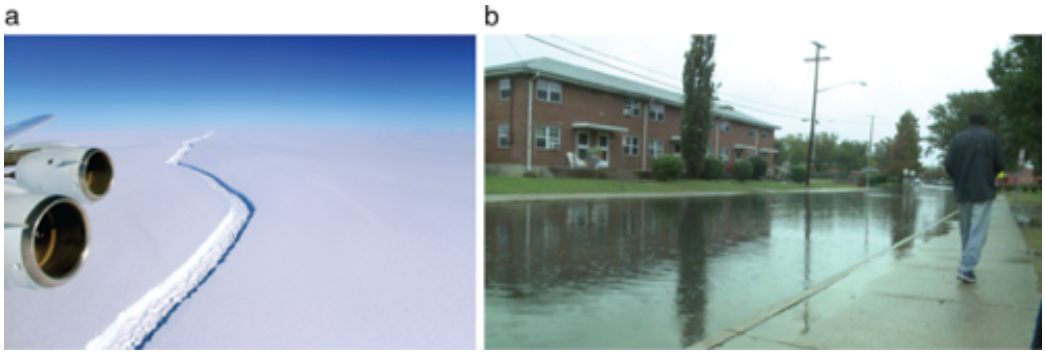

Figure 5.1: (a) Rift appearing in Larsen C Ice Shelf as photographed November 10, 2016. Credit: John Sonntag, NASA. (b) High-tide flooding in Norfolk, VA in November 2017. Credit: WTKR News 3 Norfolk.

literature and into decision-making (McNie, 2007; Lemos et al., 2012; Asrar et al., 2013; Moss et al., 2013). To fully realize the promise of science for the betterment of society, we must narrow the knowledge-to-action gap (Meyer, 2011). The task is made more urgent by decisions already being made that ignore or sidestep the best climate information available, potentially compromising future lives, livelihoods, and adaptation options (National Research Council [NRC], 2010; Intergovernmental Panel on Climate Change [IPCC], 2012). As climate change researchers, we suggest that we need to take advantage of the growing body of knowledge on how to make climate information more usable and how to better engage with decision-makers across spatial and political scales of decision-making. In this commentary, we describe three relevant styles of intermediation between science and decision-making: networks of public extension agents, climate consulting firms, and organizations established to bridge the science-policy divide (boundary organizations).

The problem we see is one of potential mismatch between the available science and the needs of decision-makers. We are particularly interested in researchers' engagement with adaptation to sea-level rise, as projections of future sea-level changes draw on various areas of expertise such that it is difficult to know which area matches what decision-makers need. For example, glaciologists can estimate how much ice from the world's glaciers and ice sheets will be transferred to the ocean, but expertise on changing ocean currents and the thermal expansion of ocean water would come from oceanographers. Knowledge of the spatially heterogeneous sea-level effects of a changing gravitational field and the Earth's rotational wobble would come from geophysicists. At the local scale, experts including geologists, coastal engineers, and climatologists work to understand factors including land subsidence (or uplift), coastal erosion, prevailing wind patterns, and extreme flooding, which can modulate changes in global sea level by an order of magnitude. A full picture of sea-level change along with the associated risks for decision-makers to consider

requires expertise from diverse fields. Further, the highly local nature of sea-level adaptation and the connected spatial scales of decision-making presage a high volume of demand for sea-level projections and expertise, which the scientific community might not be able to meet. This diversity of knowledge and needs suggest that for information to be usable, it will need to be customized to different decision contexts. Customized information availability, in turn, is a function of the number of people actively working on problems related to sea-level rise, the amount of free time they can offer to engage with decision-makers, and professional incentive structures to do so (Kirchhoff et al., 2013).

In some instances, researchers seeking to engage more with the practical application of their work find that success in this domain is not valued by traditional academic recognition systems such as the tenure process (e.g. Ellison and Eatman, 2008). Moreover, to communicate information that informs a complex decision may require both special skills and an extended interaction between scientists and decision-makers to build trust. Such extended interactions drive up the transaction costs of engagement (Lemos et al., 2014), which can tend to detract from the level of effort required to conduct lab research, simulations, or field observation.

Finally, adaptation planning and implementation involve different social, political, and economic structures at different scales, which may obscure or delay tangible outcomes and frustrate researchers. Engagement at one scale, e.g. a city planning process, might not translate to eventual outcomes at other scales, e.g. regional or national plans. We believe intermediation can help scientists and decision-makers to overcome these challenges.

5.2 Styles of intermediation

Sea-level rise is not the only domain of climate science where demand for information outpaces researcher capacity. Empirical research that explores intermediation in other areas, especially agriculture and water management, is growing (e.g. Klenk et al., 2015; Haigh et al., 2015). Research in this area suggests that intermediary actors and organizations can be invaluable to ensuring a sound scientific and engineering basis for decision-making (Bessant and Rush, 1995; Guston, 2001), be an important partner in climate information dissemination (Prokopy et al., 2015), facilitate the use of climate information (Cash et al., 2003; Hoppe et al., 2013) and reach decision-makers more efficiently than scientists could (Brugger and Crimmins, 2015).

Here we suggest three possible styles of intermediated engagement that may enhance sea-level adaptation decision-making: public intermediation, boundary organizations, and private intermediation.

Public intermediation relies on a large network of extension agents who interact with researchers and disseminate knowledge to large numbers of users and the public. For example, each of the National Oceanic and Atmospheric Administration's National Estuarine Research Reserve sites supports a Coastal Training Coordinator, who performs an intermediary function between relevant coastal management science and regional coastal managers (http://coast.noaa.gov/nerrs/training/). Public intermediation recognizes the value of longer-term relationship building with and embeddedness in communities that are the end points for knowledge application (Brugger and Crimmins, 2015): Specialized local agents in public intermediation networks can build on their social ties with end users to tailor scientific information for their specific needs.

Boundary organizations bring together researchers and decision makers to co-create usable knowledge (Guston, 2001) The NOAA Regional Integrated Sciences and Assessments (RISA) program exemplifies the boundary organization approach (see e.g. Kirchhoff et al., 2013; Stevenson et al., 2016), and an extensive empirical literature has documented boundary organizations' effectiveness in climate decision-making (e.g. Cash et al., 2003; Sarewitz and Pielke, 2007; Tribbia and Moser, 2008). Nonprofits with relationships across science and practice are another example of boundary organizations. For example, researchers working with the Consortium for Climate Risk in the Urban Northeast have collaborated with the City of New York to model and evaluate coastal adaptation options for the city.

Private intermediation occurs when researchers contribute their expertise to the work of for-profit consultants and engineering companies. Private intermediary companies may be contracted to advise decision-making in the public or private sectors, or they may be encouraged to design and carry out adaptation actions themselves, as in the example of Lagos, Nigeria below. Commercial actors may be more empowered than their public counterparts for rapid decision-making under uncertainty. However, the primary objectives of for-profit consulting are self-evident—to make a profit—and thus the price paid by public entities for these services may be higher and less publicly accountable. However, private intermediation may be appropriate where very site-specific science is required and thus more general tools and resources are inadequate.

All three styles of intermediation offer resources beyond standard research grants for scientists and engineers to make their work more usable for decision-makers. For example, extension agents in public intermediation networks can help researchers frame new studies

that respond broadly to user needs, and can further help to tailor that broadly relevant information for localized adaptation. Boundary organizations can provide funding, physical space, and structure for productive interactions between researchers and coastal communities. Private companies may invite researchers to consult on specific adaptation projects, or they may offer full-time career opportunities. The different styles of intermediation also give rise to different modes of researcher involvement, with more or less direct interaction between researchers and community stakeholders. Boundary organizations, with their explicit focus on co-production of knowledge, involve the most direct interaction. The costs involved (e.g. finances, time and trust building) for all parties involved are relatively higher. Public intermediation, by contrast, relies on researchers' indirect interaction with end users via a large network of locally specialized extension agents, which can lower costs for both scientists and decision-makers.

All forms of intermediated engagement raise ethical concerns that ought to be addressed. When researcher involvement with decision processes is indirect, lines of accountability become less clear. In cases of private intermediation, research findings may support narrow interests specific to the client, at the expense of the broader public good. The scope of need for informing decisions related to sea-level rise is so vast that efficient, scalable approaches of all styles, including client-driven private sector approaches, are likely to be essential and commonplace. Ethical guidelines are therefore urgently needed. Currently, there are few formalized standards of ethical practice for applying research expertise to climate adaptation planning purposes, though professional groups such as the American Society of Adaptation Practitioners are working to develop such standards.

5.3 Intermediaries in practice: a few experiences

To illustrate the process of applying science to plan for sea-level rise, we examine examples of sea-level adaptation at three different scales—an international boundary organization, a nationwide program that can engage both public and private intermediaries, and an urban revitalization plan utilizing private intermediation. The three types of intermediation outlined above are present to differing degrees in each. The examples shed light on the kinds of opportunities and complications arising from different styles of intermediation as implemented in practice.

5.3.1 The IPCC

At the international level, the Intergovernmental Panel on Climate Change (IPCC) is a prominent example boundary organization that, among its other tasks, assesses global projections of sea-level rise and articulates implications for coastal regions. The IPCC draws together scientists and policy-makers from all over the world—though developing nations have historically been under-represented (Hulme and Mahony, 2010; Biermann, 2002)—to produce policy-relevant assessments and special reports on the state of climate science. Representatives of national governments contribute to determining report outlines (i.e. what topics will be covered) and approving Summaries for Policymakers, but the design of the report-drafting phase in practice limits interactions between scientists and policy-makers (Siebenhüner, 2003). As a United Nations-sponsored organization, the IPCC is governed by elaborate and internationally-agreed procedures. Such extensive institutionalization around the science-policy interface is designed to promote accountability between scientists and policy-makers. However, the IPCC's high standard of scientific accountability may sometimes be counterproductive. For example, the large estimated sea level contribution from ice sheet dynamics was excluded until the Fifth Assessment (2013) because the physical processes involved were considered too new and too uncertain (Meehl et al., 2007; Church et al., 2013). Time commitment for scientists participating in the IPCC is high, which may trade off with professional commitments in other areas if not managed well, but offers the potential for societal impact on a very broad spatial scale. While the work of the IPCC may inform National Adaptation Plans of Action, including those of island nations for which sea level is a forefront concern, sea-level change is extremely variable at local scale, and the flow of knowledge from IPCC reports to local implementation is less clear (e.g. Viner and Howarth, 2014; Petersen et al., 2015). This murky path to implementation, along with the low participation of scientists and policy-makers from the global South (e.g. Hulme and Mahony, 2010; Biermann, 2002), raises questions regarding the most equitable avenues for public engagement. We suggest that sea-level researchers could be more effective by seeking out local- or regional-scale boundary organizations.

5.3.2 Coastal communities and insurance

United States coastal communities participating in the National Flood Insurance Program can apply for discounted insurance rates by completing a selection of eligible risk-mitigating actions under the Community Rating System. The local actions supported by the nationwide Community Rating System may use private (for-profit consultancy) or public (extension agent) intermediation, both of which can facilitate decision-making based

on highly tailored information but risk losing a transparent scientific basis. For example, action 410 described in the Coordinator's Manual (National Flood Insurance Program Community Rating System [NFIP-CRS], 2017), "Floodplain Mapping", asks planners to demonstrate that they have developed new maps of flood hazard for their area; action 440, "Flood Data Maintenance", asks planners to "use better base maps" (with no indication of what "better" means); and action 510, "Floodplain Management Planning", asks communities to develop and maintain "a comprehensive flood hazard mitigation plan using a standard planning process". The true risk-mitigating capacity of these actions depends strongly on the quality of scientific knowledge they employ. In particular, intermediaries who supply communities with out-of-date or poorly-supported information may help secure lower insurance rates but fail to fully characterize actual flood and other hazard risk. By working with public intermediaries, however, sea-level researchers could train extension agents to incorporate a broader understanding of the physical processes responsible for sea-level rise in their engagement with communities, potentially amplifying the role of research in decision-making. Public intermediation also offers clearer lines of accountability, both between scientist and intermediary and between intermediary and local communities, which in turn may promote more equitable outcomes among residents of adapting communities.

5.3.3 Privatizing risk

In Lagos, Nigeria, where millions reside on coastlines exposed to sea-level rise and resulting enhancement of dangerous storm surges, a large adaptation project is being led by the private sector. Nigerian business conglomerate, The Chagoury Group, with the assistance of Dutch engineering firm Royal HaskoningDHV, has begun construction of a new luxury district, "Eko Atlantic", atop 10 square kilometers of land reclaimed from the Atlantic Ocean and protected by a seawall. The project's sea defenses do not extend to other heavily-populated parts of Lagos; indeed, residents and external observers have expressed concern that the Eko Atlantic development might increase flood risk in other parts of Lagos (Adelekan, 2013). Nevertheless, the Lagos State Commissioner for Waterfront Infrastructure Development describes Eko Atlantic as a "life-saver" sea defense for the wealthy and economically important Victoria Island (Ayeyemi, 2013). In this example, Royal HaskoningDHV acts as a commercial intermediary for sea-level science, working under contract for the Chagoury Group, whose sole stated aims are "developing industrial links between Africa and China as well as Latin America" (http://www.chagourygoup.com/about). As a private intermediary, Royal HaskoningDHV is only directly accountable to the party who hired them—the Chagoury Group—

and not to broader Lagos society. Accordingly, actions prioritize the economic and industrial aims of the Chagoury Group rather than general public welfare, raising important equity issues (Adelekan, 2013). Hence while working with private intermediaries can be unencumbered and quick, perhaps conferring more immediate professional benefit of seeing one's work applied, realizing the public value of science may be less straightforward. The inequity looming behind the Eko Atlantic seawall should serve as a cautionary tale, urging scientists and private intermediaries to carefully consider the equity implications of actions we inform.

5.4 Conclusions

Engaging with intermediaries for sea-level adaptation comes with a variety of trade-offs. Where public decision-making is often paralyzed by the inherent uncertainty in sea-level projections, the work of private intermediaries may circumvent inaction, as demonstrated in Lagos's Eko Atlantic project. In contrast, with the benefits of adaptation more likely to accrue to wealthier stakeholders, the private intermediation employed in Lagos contributes to environmental injustice. Private and public intermediation both allow researchers to spread their expertise more widely with lower relative transaction costs, but intermediaries may communicate sea-level exposure differently than those researchers would. For example, economic metrics such as "assets at risk" or the local price of insurance under the National Flood Insurance Program depend on many more factors than the projected rate of sea-level rise alone, which may or may not align with coastal residents' priorities and serve to obscure the scientific basis of sea-level projections. Formal boundary organizations promote the most direct interaction between scientists and community stakeholders, enabling decision-making with a very clear basis in current science and giving researchers the most control over application. However, boundary organizations operate at various scales, not all of which translate easily to local decision-making, and the intensive time commitment required for direct interaction may act as a constraint.

Based on the above examples and the broader academic literature, we suggest that maximizing the social utility of sea-level research, and climate change research more broadly, requires us to consider the adaptation needs of diverse communities and the tradeoffs involved in supporting them. While this effort is often resource intensive and context-specific, engagement through intermediaries can mitigate costs and amplify the impact of science and engineering in preventing negative impacts of sea-level rise. Each of the three styles of intermediation has its place in furthering our community engagement, but we stress the need for deeper understanding of the implications of each style for society in general and

adaptation in particular. As such investigation continues, we must strive to promote both accountability and equity in our decisions about societal engagement.

CHAPTER 6

Conclusions

Motivated by the societal concern for global sea level change, we have sought to constrain one of the major contributions to 21st-century sea level. First, we extended an early analytical model of glacier flow to allow iceberg calving from glacier termini. We applied the new model to simulate the 20th century retreat of Columbia Glacier, Alaska, and showed that it could capture glacier surface profiles and terminus positions within the range of USGS observations [Chapter 2]. Next, we demonstrated implementation of the model on networks of interacting glacier branches. We validated the model with observations of terminus advance, retreat, and multi-annual advance-retreat cycling from glaciers in Alaska and Greenland [Chapter 3]. Then, noting that this model is a limiting-case glacier rheology that produces maximum dynamic ice loss, we generated constraints on the contribution to 21st-century sea level rise from major Greenland outlet glaciers [Chapter 4]. Finally, we revisited societal concern for sea level change and probed how the modelling work of the earlier chapters could more directly address the needs of coastal communities [Chapter 5].

By applying our network model derived in Chapters 3 and 2 to large Greenland outlet glacier networks in Chapter 4, we found that tributary glaciers can make a nontrivial contribution to sea level. This contribution is not well captured by single-flowline models and would require fine spatial resolution (< 2 km) to capture in higher-dimensional ice sheet models. We also demonstrate in Chapters 3 and 4 that our model handles dynamic separation of glacier networks as well as coupled network dynamics.

The simulations presented in Chapter 4 suggest that calving from the Greenland outlet glaciers I studied is unlikely to contribute more than 30 mm to global sea level in the next 100 years. Our two strongest forcing scenarios, WP and WX, converge to an upper bound of 28.2 mm dynamic sea level contribution. These constraints project the future evolution of only six of the $\sim$200 marine-terminating outlets of the Greenland Ice Sheet. The six study glaciers are among the highest-flux Greenland outlet glaciers, but we cannot assume that their dynamics reflect the future of the tens of smaller outlets encircling the ice sheet. A more satisfying constraint on Greenland's dynamic contribution to 21st-century sea level

would require simulating a larger fraction of its outlet glaciers—for example, the 30 outlets captured by Aschwanden et al. (2016).

Producing ever more specific constraints on the calving contribution to sea level is not necessarily a response to societal concerns, however. Such constraints are of glaciological interest, but it is unlikely that they will directly inform any societal action. Treating this topic with the appropriate moral seriousness requires me to make this distinction. I may come closer to addressing the societal motivation of this dissertation by working with science intermediaries, as described in Chapter 5, to support coastal adaptation efforts. I may also explore scientific collaborations to produce sea level projections that better address expressed societal needs, e.g. for probabilistic and regionally-specific estimates (Walsh et al., 2004).

The function of this dissertation is not to produce sea level projections for immediate implementation in coastal planning. Rather, it is to build a foundation of scientific credibility for ongoing work. Moving forward, I will shore up that foundation by simulating a wider selection of Greenland outlet glaciers to inform our upper bounds on dynamic ice loss. Ultimately, I hope to work more closely with planners to co-create the knowledge needed to respond to 21st-century sea level rise.

BIBLIOGRAPHY

P. Achakulwisut. Why are scientists so averse to public engagement? Scientific American [blog post], March 8 2017. URL https://blogs.scientificamerican.com/guest-blog/why-are-scientists-so-averse-to-public-engagement/.

I. Adelekan. Private sector investment decisions in building and construction: increasing, managing and transferring risks: Case study of Lagos, Nigeria. Technical report, United Nations Office for Disaster Risk Reduction, Geneva, Switzerland, 2013.

T. Albrecht and A. Levermann. Fracture field for large-scale ice dynamics. *Journal of Glaciology*, 58(207):165–176, 2012. doi: 10.3189/2012JoG11J191.

American Association for the Advancement of Science [AAAS]. Why public engagement matters. https://www.aaas.org/pes/what-public-engagement, 2017.

J. M. Amundson and M. Truffer. A unifying framework for iceberg-calving models. *Journal of Glaciology*, 56(199):822–830, 2010. doi: 10.3189/002214310794457173.

A. A. Arendt, K. A. Echelmeyer, W. D. Harrison, C. S. Lingle, and V. B. Valentine. Rapid wastage of Alaska glaciers and their contribution to rising sea level. *Science*, 297(5580): 382–386, 2002. ISSN 0036-8075. doi: 10.1126/science.1072497.

A. Aschwanden, M. A. Fahnestock, and M. Truffer. Complex Greenland outlet glacier flow captured. *Nature Communications*, 7:10524 EP, 2016. doi: 10.1038/ncomms10524.

G. R. Asrar, J. W. Hurrell, and A. J. Busalacchi. A need for "actionable" climate science and information: Summary of WCRP open science conference. *Bulletin of the American Meteorological Society*, 94(2):ES8–ES12, 2013. doi: 10.1175/BAMS-D-12-00011.1.

J. A. Åström, T. I. Riikilä, T. Tallinen, T. Zwinger, D. Benn, J. C. Moore, and J. Timonen. A particle based simulation model for glacier dynamics. *The Cryosphere*, 7(5):1591–1602, 2013. doi: 10.5194/tc-7-1591-2013.

J. A. Astrom, D. Vallot, M. Schafer, E. Z. Welty, S. O/'Neel, T. C. Bartholomaus, Y. Liu, T. I. Riikila, T. Zwinger, J. Timonen, and J. C. Moore. Termini of calving glaciers as self-organized critical systems. *Nature Geosci*, 7(12):874–878, 12 2014. doi: 10.1038/ngeo2290.

D. Ayeyemi. FG should make money available to coastal states to combat erosion – Oniru. *National Mirror [Nigeria]*, 5 November 2013. URL https://goo.gl/Y49Hgs.

N. J. Balmforth, R. V. Craster, A. C. Rust, and R. Sassi. Viscoplastic flow over an inclined surface. *Journal of Non-Newtonian Fluid Mechanics*, 139(1–2):103 – 127, 2006. doi: 10.1016/j.jnnfm.2006.07.010.

J. L. Bamber, R. M. Westaway, B. Marzeion, and B. Wouters. The land ice contribution to sea level during the satellite era. *Environmental Research Letters*, 13:063008, 2018. doi: 10.1088/1748-9326/aac2f0.

J. N. Bassis. The statistical physics of iceberg calving and the emergence of universal calving laws. *Journal of Glaciology*, 57(201):3–16, 2011. doi: 10.3189/002214311795306745.

J. N. Bassis and S. Jacobs. Diverse calving patterns linked to glacier geometry. *Nature Geoscience*, 6(10):833–836, 2013. doi: 10.1038/ngeo1887.

J. N. Bassis and C. C. Walker. Upper and lower limits on the stability of calving glaciers from the yield strength envelope of ice. *Proceedings of the Royal Society of London A: Mathematical, Physical and Engineering Sciences*, 468(2140):913–931, 2012. doi: 10.1098/rspa.2011.0422.

D. I. Benn, C. R. Warren, and R. H. Mottram. Calving processes and the dynamics of calving glaciers. *Earth-Science Reviews*, 82(3–4):143 – 179, 2007. doi: 10.1016/j.earscirev.2007.02.002.

D. I. Benn, J. Åström, T. Zwinger, J. Todd, F. M. Nick, S. Cook, N. R. J. Hulton, and A. Luckman. Melt-under-cutting and buoyancy-driven calving from tidewater glaciers: new insights from discrete element and continuum model simulations. *Journal of Glaciology*, 63(240):691–702, 2017a. doi: 10.1017/jog.2017.41.

D. I. Benn, T. Cowton, J. Todd, and A. Luckman. Glacier calving in Greenland. *Current Climate Change Reports*, 3(4):282–290, 2017b. doi: 10.1007/s40641-017-0070-1.

J. Bessant and H. Rush. Building bridges for innovation: the role of consultants in technology transfer. *Research Policy*, 24(1):97 – 114, 1995. doi: 10.1016/0048-7333(93)00751-E.

F. Biermann. Institutions for scientific advice: Global environmental assessments and their influence in developing countries. *Global Governance*, 8(2):195–219, 2002. URL http://www.jstor.org/stable/27800338.

C. P. Borstad, A. Khazendar, E. Larour, M. Morlighem, E. Rignot, M. P. Schodlok, and H. Seroussi. A damage mechanics assessment of the Larsen B ice shelf prior to collapse: Toward a physically-based calving law. *Geophysical Research Letters*, 39(18):L18502, 2012. doi: 10.1029/2012GL053317.

J. Brugger and M. Crimmins. Designing institutions to support local-level climate change adaptation: Insights from a case study of the U.S. cooperative extension system. *Weather, Climate, and Society*, 7(1):18–38, 2015. doi: 10.1175/WCAS-D-13-00036.1.

D. W. Cash, W. C. Clark, F. Alcock, N. M. Dickson, N. Eckley, D. H. Guston, J. Jäger, and R. B. Mitchell. Knowledge systems for sustainable development. *Proceedings of the National Academy of Sciences*, 100(14):8086–8091, 2003. doi: 10.1073/pnas.1231332100.

J. A. Church, P. U. Clark, J. M. Cazenave, S. Jevrejeva, A. Levermann, M. A. Merrifield, G. A. Milne, R. S. Nerem, P. D. Nunn, A. J. Payne, W. T. Pfeffer, D. Stammer, and A. S. Unnikrishnan. Sea Level Change. In T. F. Stocker, D. Qin, G. K. Plattner, M. Tignor, S. K. Allen, J. Boschung, A. Nauels, Y. Xia, V. Bex, and P. M. Midgley, editors, *Climate Change 2013: The Physical Science Basis*, pages 1137–1216. Cambridge University Press, Cambridge, United Kingdom and New York, NY, USA, 2013.

D. Cohen, N. R. Iverson, T. S. Hooyer, U. H. Fischer, M. Jackson, and P. L. Moore. Debris-bed friction of hard-bedded glaciers. *Journal of Geophysical Research: Earth Surface*, 110(F2):F02007, 2005. doi: 10.1029/2004JF000228.

W. Colgan, H. Rajaram, W. Abdalati, C. McCutchan, R. H. Mottram, M. S. Moussavi, and S. Grigsby. Glacier crevasses: Observations, models, and mass balance implications. *Reviews of Geophysics*, S4:119–161, 2016. doi: 10.1002/2015RG000504.

S. L. Cornford, D. F. Martin, D. T. Graves, D. F. Ranken, A. M. L. Brocq, R. M. Gladstone, A. J. Payne, E. G. Ng, and W. H. Lipscomb. Adaptive mesh, finite volume modeling of marine ice sheets. *Journal of Computational Physics*, 232(1):529 – 549, 2013. doi: 10.1016/j.jcp.2012.08.037.

CReSIS. CReSIS L3 radar depth sounder data: Helheim Glacier. http://data.cresis.ku.edu/, 2016a.

CReSIS. CReSIS L3 radar depth sounder data: Jakobshavn Isbræ. http://data.cresis.ku.edu/, 2016b. URL http://data.cresis.ku.edu/.

B. Csatho, T. Schenk, C. van der Veen, and W. B. Krabill. Intermittent thinning of Jakobshavn Isbræ, West Greenland, since the Little Ice Age. *Journal of Glaciology*, 54(184): 131–144, January 2008. doi: 10.3189/002214308784409035.

K. Cuffey and W. Paterson. *The Physics of Glaciers*. Elsevier Science, Burlington, MA and Kidlington, United Kingdom, 4^{th} edition, 2010. ISBN 9780080919126.

C. Davenport and C. Robertson. Resettling the first American 'climate refugees'. *The New York Times*. Available from https://www.nytimes.com/2016/05/03/us/resettling-the-first-american-climate-refugees.html, May 2016.

R. M. DeConto and D. Pollard. Contribution of Antarctica to past and future sea-level rise. *Nature*, 531(7596):591–597, Mar. 2016.

R. Duddu, J. N. Bassis, and H. Waisman. A numerical investigation of surface crevasse propagation in glaciers using nonlocal continuum damage mechanics. *Geophysical Research Letters*, 40(12):3064–3068, 2013. doi: 10.1002/grl.50602.

J. Ellison and T. K. Eatman. Scholarship in public: Knowledge creation and tenure policy in the engaged university. *Imagining America*, 16, 2008. URL https://surface.syr.edu/ia/16.

E. M. Enderlin, G. S. Hamilton, S. O'Neel, T. C. Bartholomaus, M. Morlighem, and J. W. Holt. An empirical approach for estimating stress-coupling lengths for marine-terminating glaciers. *Frontiers in Earth Science*, 4:104, 2016. doi: 10.3389/feart.2016.00104.

E. M. Enderlin, S. O'Neel, T. C. Bartholomaus, and I. Joughin. Evolving environmental and geometric controls on Columbia Glacier's continued retreat. *Journal of Geophysical Research: Earth Surface*, [Accepted article online], 2018/06/17 2018. doi: 10.1029/2017JF004541.

ENVEO. Greenland ice velocity map 2016/2017 from Sentinel-1 [version 1.0]. http://products.esa-icesheets-cci.org/products/details/greenland_ice_velocity_map_winter_2016_2017_v1_0.zip/, 2017.

J. Flevinson, K. Khvorostovsky, F. Ticconi, A. Shepherd, R. Forsberg, L. S. Sorenson, and M. Kleinherenbrink. ESA's Ice Sheets CCI: validation and inter-comparison of surface elevation changes derived from laser and radar altimetry over Jakobshavn Isbræ, Greenland – Round Robin results. *The Cryosphere Discussions*, 7:5433–5460, 2013.

R. Forsberg, L. Sørensen, and S. Simonsen. Greenland and Antarctica ice sheet mass changes and effects on global sea level. *Surveys in Geophysics*, 38(1):89–104, 2017. doi: 10.1007/s10712-016-9398-7.

O. Gagliardini, T. Zwinger, F. Gillet-Chaulet, G. Durand, L. Favier, B. de Fleurian, R. Greve, M. Malinen, C. Martín, P. Råback, J. Ruokolainen, M. Sacchettini, M. Schäfer, H. Seddik, and J. Thies. Capabilities and performance of Elmer/Ice, a new-generation ice sheet model. *Geoscientific Model Development*, 6(4):1299–1318, 2013. doi: 10.5194/gmd-6-1299-2013.

A. S. Gardner, G. Moholdt, J. G. Cogley, B. Wouters, A. A. Arendt, J. Wahr, E. Berthier, R. Hock, W. T. Pfeffer, G. Kaser, S. R. M. Ligtenberg, T. Bolch, M. J. Sharp, J. O. Hagen, M. R. van den Broeke, and F. Paul. A reconciled estimate of glacier contributions to sea level rise: 2003 to 2009. *Science*, 340(6134):852–857, 2013. ISSN 0036-8075. doi: 10.1126/science.1234532. URL http://science.sciencemag.org/content/340/6134/852.

J. A. Goff, D. E. Lawson, B. A. Willems, M. Davis, and S. P. S. Gulick. Morainal bank progradation and sediment accumulation in Disenchantment Bay, Alaska: Response to advancing Hubbard Glacier. *Journal of Geophysical Research: Earth Surface*, 117(F2):F02031, 2012. doi: 10.1029/2011JF002312.

J. M. Gregory, P. Huybrechts, and S. C. B. Raper. Threatened loss of the Greenland ice-sheet. *Nature*, 428:616 EP, 04 2004. doi: 10.1038/428616a.

R. Greve. On the response of the Greenland Ice Sheet to greenhouse climate change. *Climatic Change*, 46(3):289–303, Aug 2000. doi: 10.1023/A:1005647226590.

R. Greve and K. Hutter. Polythermal three-dimensional modelling of the Greenland ice sheet with varied geothermal heat flux. *Annals of Glaciology*, 21(1):8–12, 1995. doi: 10.3198/1995AoG21-1-8-12.

D. H. Guston. Boundary organizations in environmental policy and science: An introduction. *Science, Technology, & Human Values*, 26(4):399–408, 2001. doi: 10.1177/016224390102600401.

T. Haigh, L. W. Morton, M. C. Lemos, C. Knutson, L. S. Prokopy, Y. J. Lo, and J. Angel. Agricultural advisors as climate information intermediaries: Exploring differences in capacity to communicate climate. *Weather, Climate, and Society*, 7(1):83–93, 2015. doi: 10.1175/WCAS-D-14-00015.1.

C. C. Hay, E. Morrow, R. E. Kopp, and J. X. Mitrovica. Probabilistic reanalysis of twentieth-century sea-level rise. *Nature*, 517(7535):481–484, Jan. 2015.

R. Hoppe, A. Wesselink, and R. Cairns. Lost in the problem: the role of boundary organisations in the governance of climate change. *Wiley Interdisciplinary Reviews: Climate Change*, 4(4):283–300, 2013. doi: 10.1002/wcc.225.

R. Horton, C. Little, V. Gornitz, D. Bader, and M. Oppenheimer. New York City Panel on Climate Change 2015 report chapter 2: Sea level rise and coastal storms. *Annals of the New York Academy of Sciences*, 1336(1):36–44, 2015. doi: 10.1111/nyas.12593.

I. M. Howat, I. Joughin, S. Tulaczyk, and S. Gogineni. Rapid retreat and acceleration of Helheim Glacier, east Greenland. *Geophysical Research Letters*, 32(22):L22502, 2005. doi: 10.1029/2005GL024737.

I. M. Howat, J. E. Box, Y. Ahn, A. Herrington, and E. M. McFadden. Seasonal variability in the dynamics of marine-terminating outlet glaciers in Greenland. *Journal of Glaciology*, 56(198):601–613, October 2010. doi: 10.3189/002214310793146232.

I. M. Howat, Y. Ahn, I. Joughin, M. R. van den Broeke, J. T. M. Lenaerts, and B. Smith. Mass balance of Greenland's three largest outlet glaciers, 2000–2010. *Geophysical Research Letters*, 38(12):L12501, 2011. doi: 10.1029/2011GL047565.

M. Hulme and M. Mahony. Climate change: What do we know about the IPCC? *Progress in Physical Geography: Earth and Environment*, 34(5):705–718, 2010. doi: 10.1177/0309133310373719.

M. Huss and D. Farinotti. Distributed ice thickness and volume of all glaciers around the globe. *Journal of Geophysical Research: Earth Surface*, 117(F4):F04010, 2012. doi: 10.1029/2012JF002523.

M. Huss and R. Hock. A new model for global glacier change and sea-level rise. *Frontiers in Earth Science*, 3:382–22, Sept. 2015. doi: 10.3389/feart.2015.00054.

Intergovernmental Panel on Climate Change [IPCC]. Managing the risks of extreme events and disasters to advance climate change adaptation. In C. B. Field, V. Barros, T. F. Stocker, D. Qin, D. J. Dokken, K. L. Ebi, M. D. Mastrandrea, K. J. Mach, G.-K. Plattner, S. K. Allen, M. Tignor, and P. M. Midgley, editors, *A Special Report of Working Groups I and II of the Intergovernmental Panel on Climate Change*. Cambridge University Press, Cambridge, United Kingdom and New York, NY, USA, 2012.

T. Jacob, J. Wahr, W. T. Pfeffer, and S. Swenson. Recent contributions of glaciers and ice caps to sea level rise. *Nature*, 482(7386):514–518, 02 2012. doi: 10.1038/nature10847.

I. Joughin, W. Abdalati, and M. Fahnestock. Large fluctuations in speed on Greenland's Jakobshavn Isbrae glacier. *Nature*, 432(7017):608–610, 2004. doi: 10.1038/nature03130.

I. Joughin, B. E. Smith, I. M. Howat, D. Floricioiu, R. B. Alley, M. Truffer, and M. Fahnestock. Seasonal to decadal scale variations in the surface velocity of Jakobshavn Isbræ, Greenland: Observation and model-based analysis. *Journal of Geophysical Research: Earth Surface*, 117(F2):F02030, 2012. doi: 10.1029/2011JF002110.

I. Joughin, B. E. Smith, D. E. Shean, and D. Floricioiu. Brief communication: Further summer speedup of Jakobshavn Isbræ. *The Cryosphere*, 8(1):209–214, 2014. doi: 10.5194/tc-8-209-2014.

S. A. Khan, K. H. Kjær, M. Bevis, J. L. Bamber, J. Wahr, K. K. Kjeldsen, A. A. Bjørk, N. J. Korsgaard, L. A. Stearns, M. R. van den Broeke, L. Liu, N. K. Larsen, and I. S. Muresan. Sustained mass loss of the northeast Greenland ice sheet triggered by regional warming. *Nature Climate Change*, 4:292 EP, 2014. doi: 10.1038/nclimate2161.

S. A. Khan, A. Aschwanden, A. A. Bjørk, J. Wahr, K. K. Kjeldsen, and K. H. Kjær. Greenland ice sheet mass balance: a review. *Reports on Progress in Physics*, 78(4):046801, 2015.

C. Kienholz, J. L. Rich, A. A. Arendt, and R. Hock. A new method for deriving glacier centerlines applied to glaciers in Alaska and northwest Canada. *The Cryosphere*, 8(2):503–519, 2014. doi: 10.5194/tc-8-503-2014.

C. Kienholz, S. Herreid, J. L. Rich, A. A. Arendt, R. Hock, and E. W. Burgess. Derivation and analysis of a complete modern-date glacier inventory for Alaska and northwest Canada. *Journal of Glaciology*, 61(227):403–420, 2015. doi: 10.3189/2015JoG14J230.

C. J. Kirchhoff, M. C. Lemos, and S. Dessai. Actionable knowledge for environmental decision-making: Broadening the usability of climate science. *Annual Review of Environment and Resources*, 38:393–414, October 2013. doi: 10.1146/annurev-environ-022112-112828.

K. H. Kjær, S. A. Khan, N. J. Korsgaard, J. Wahr, J. L. Bamber, R. Hurkmans, M. van den Broeke, L. H. Timm, K. K. Kjeldsen, A. A. Bjørk, N. K. Larsen, L. T. Jørgensen, A. Færch-Jensen, and E. Willerslev. Aerial photographs reveal late-20th-Century dynamic ice loss in northwestern Greenland. *Science*, 337(6094):569, 08 2012. doi: 10.1126/science.1220614.

N. L. Klenk, K. Meehan, S. L. Pinel, F. Mendez, P. T. Lima, and D. M. Kammen. Stakeholders in climate science: Beyond lip service? *Science*, 350(6262):743–744, 2015. doi: 10.1126/science.aab1495.

R. M. Krimmel. *Photogrammetric data set, 1957-2000, and bathymetric measurements for Columbia Glacier, Alaska*. US Geological Survey Reston, VA, 2001.

E. Larour, H. Seroussi, M. Morlighem, and E. Rignot. Continental scale, high order, high spatial resolution, ice sheet modeling using the Ice Sheet System Model (ISSM). *Journal of Geophysical Research: Earth Surface*, 117(F1):F01022, 2012. doi: 10.1029/2011JF002140.

C. Larsen, E. Burgess, A. Arendt, S. O'Neel, A. Johnson, and C. Kienholz. Surface melt dominates Alaska glacier mass balance. *Geophysical Research Letters*, 42(14):5902–5908, 2015. doi: 10.1002/2015GL064349.

C. F. Larsen, R. J. Motyka, A. A. Arendt, K. A. Echelmeyer, and P. E. Geissler. Glacier changes in southeast Alaska and northwest British Columbia and contribution to sea level rise. *Journal of Geophysical Research: Earth Surface*, 112(F1):F01007, 2007. ISSN 2156-2202. doi: 10.1029/2006JF000586.

M. C. Lemos, C. J. Kirchhoff, and V. Ramprasad. Narrowing the climate information usability gap. *Nature Clim. Change*, 2(11):789–794, 2012. doi: 10.1038/nclimate1614.

M. C. Lemos, C. J. Kirchhoff, S. E. Kalafatis, D. Scavia, and R. B. Rood. Moving climate information off the shelf: Boundary chains and the role of RISAs as adaptive organizations. *Weather, Climate, and Society*, 6(2):273–285, 2014. doi: 10.1175/WCAS-D-13-00044.1.

J. Lubchenco. Delivering on science's social contract. In A. J. Hoffmann, K. Ashworth, C. Dwelle, P. Goldberg, A. Henderson, L. Merlin, Y. Muzyrya, N.-J. Simon, V. Taylor, C. Weisheit, and S. Wilson, editors, *Academic engagement in public and political discourse: Proceedings of the Michigan Meeting, May 2015*, 2015. doi: 10.3998/mm.13950883.0001.001.

H. Machguth and M. Huss. The length of the world's glaciers—a new approach for the global calculation of center lines. *The Cryosphere*, 8(5):1741–1755, 2014. doi: 10.5194/tc-8-1741-2014.

B. Marzeion, A. H. Jarosch, and M. Hofer. Past and future sea-level change from the surface mass balance of glaciers. *The Cryosphere*, 6(6):1295–1322, 2012. doi: 10.5194/tc-6-1295-2012.

R. McNabb, R. Hock, S. O'Neel, L. Rasmussen, Y. Ahn, M. Braun, H. Conway, S. Herreid, I. Joughin, W. Pfeffer, B. Smith, and M. Truffer. Using surface velocities to calculate ice thickness and bed topography: A case study at Columbia Glacier, Alaska, USA. *Journal of Glaciology*, 58(212):1151–1164, 2012. doi: 10.3189/2012JoG11J249.

R. W. McNabb and R. Hock. Alaska tidewater glacier terminus positions, 1948–2012. *Journal of Geophysical Research: Earth Surface*, 119(2):153–167, 2014. doi: 10.1002/2013JF002915.

E. C. McNie. Reconciling the supply of scientific information with user demands: an analysis of the problem and review of the literature. *Environmental Science & Policy*, 10 (1):17 – 38, 2007. doi: 10.1016/j.envsci.2006.10.004.

G. A. Meehl, T. F. Stocker, W. D. Collins, P. Friedlingstein, A. T. Gaye, J. M. Gregory, A. Kitoh, R. Knutti, J. M. Murphy, A. Noda, S. C. B. Raper, I. G. Watterson, A. J. Weaver, and Z.-C. Zhao. Global climate projections. In S. Solomon, D. Qin, M. Manning, Z. Chen, M. Marquis, K. B. Averyt, M. Tignor, and H. L. Miller, editors, *Climate Change 2007: The Physical Science Basis. Contribution of Working Group I to the Fourth Assessment Report of the Intergovernmental Panel on Climate Change*. Cambridge University Press, Cambridge, United Kingdom and New York, NY, USA, 2007.

M. F. Meier and A. Post. Fast tidewater glaciers. *Journal of Geophysical Research: Solid Earth*, 92(B9):9051–9058, 1987. doi: 10.1029/JB092iB09p09051.

J. Melillo, T. C. Richmond, and G. Yohe. Climate change impacts in the United States: The third national climate assessment. doi:10.7930/J0Z31WJ2, 2014.

R. Meyer. The public values failures of climate science in the US. *Minerva*, 49(1):47–70, 2011. doi: 10.1007/s11024-011-9164-4.

M. Morlighem, C. N. Williams, E. Rignot, L. An, J. E. Arndt, J. L. Bamber, G. Catania, N. Chauché, J. A. Dowdeswell, B. Dorschel, I. Fenty, K. Hogan, I. Howat, A. Hubbard, M. Jakobsson, T. M. Jordan, K. K. Kjeldsen, R. Millan, L. Mayer, J. Mouginot, B. P. Y. Noël, C. O'Cofaigh, S. Palmer, S. Rysgaard, H. Seroussi, M. J. Siegert, P. Slabon, F. Straneo, M. R. van den Broeke, W. Weinrebe, M. Wood, and K. B. Zinglersen. BedMachine v3: Complete bed topography and ocean bathymetry mapping of Greenland from multibeam echo sounding combined with mass conservation. *Geophysical Research Letters*, 44(21):11,051–11,061, 2017. doi: 10.1002/2017GL074954.

R. H. Moss, G. A. Meehl, M. C. Lemos, J. B. Smith, J. R. Arnold, J. C. Arnott, D. Behar, G. P. Brasseur, S. B. Broomell, A. J. Busalacchi, S. Dessai, K. L. Ebi, J. A. Edmonds, J. Furlow, L. Goddard, H. C. Hartmann, J. W. Hurrell, J. W. Katzenberger, D. M. Liverman, P. W. Mote, S. C. Moser, A. Kumar, R. S. Pulwarty, E. A. Seyller, B. L. Turner, W. M. Washington, and T. J. Wilbanks. Hell and high water: Practice-relevant adaptation science. *Science*, 342(6159):696–698, 2013. doi: 10.1126/science.1239569.

R. J. Motyka, L. Hunter, K. A. Echelmeyer, and C. Connor. Submarine melting at the terminus of a temperate tidewater glacier, LeConte Glacier, Alaska, U.S.A. *Annals of Glaciology*, 36:57–65, 2003. doi: 10.3189/172756403781816374.

T. Murray, K. Scharrer, T. D. James, S. R. Dye, E. Hanna, A. D. Booth, N. Selmes, A. Luckman, A. L. C. Hughes, S. Cook, and P. Huybrechts. Ocean regulation hypothesis for glacier dynamics in southeast greenland and implications for ice sheet mass changes. *Journal of Geophysical Research: Earth Surface*, 115(F3):F03026, 2010. doi: 10.1029/2009JF001522.

T. Murray, K. Scharrer, N. Selmes, A. D. Booth, T. D. James, S. L. Bevan, J. Bradley, S. Cook, L. C. Llana, Y. Drocourt, L. Dyke, A. Goldsack, A. L. Hughes, A. J. Luckman, and J. McGovern. Extensive retreat of Greenland tidewater glaciers, 2000–2010. *Arctic, Antarctic, and Alpine Research*, 47(3):427–447, 2015. doi: 10.1657/AAAR0014-049.

National Flood Insurance Program Community Rating System [NFIP-CRS]. Coordinator's manual. Available from https://www.fema.gov/media-library/assets/documents/8768, 2017.

National Research Council [NRC]. *Informing an Effective Response to Climate Change*, chapter America's climate choices: Panel on informing effective decisions and actions related to climate change. The National Academies Press, Washington, DC, 2010. ISBN 978-0-309-14594-7. doi: 10.17226/12784.

F. Nick, C. van der Veen, A. Vieli, and D. Benn. A physically based calving model applied to marine outlet glaciers and implications for the glacier dynamics. *Journal of Glaciology*, 56(199):781–794, 2010. doi: 10.3189/002214310794457344.

F. M. Nick, A. Vieli, M. L. Andersen, I. Joughin, A. Payne, T. L. Edwards, F. Pattyn, and R. S. W. van de Wal. Future sea-level rise from Greenland's main outlet glaciers in a warming climate. *Nature*, 497(7448):235–238, 2013a. doi: 10.1038/nature12068.

F. M. Nick, A. Vieli, M. L. Andersen, I. Joughin, A. Payne, T. L. Edwards, F. Pattyn, and R. S. W. van de Wal. Supplementary information to article: Future sea-level rise from Greenland's main outlet glaciers in a warming climate. *Nature*, 497(7448):235–238, 2013b. doi: 10.1038/nature12068.

J. F. Nye. The flow of glaciers and ice-sheets as a problem in plasticity. *Proceedings of the Royal Society of London A: Mathematical, Physical and Engineering Sciences*, 207 (1091):554–572, 1951. doi: 10.1098/rspa.1951.0140.

J. F. Nye. The mechanics of glacier flow. *Journal of Glaciology*, 2(12):82–93, November 1952. doi: 10.3189/2015JoG15J164.

J. F. Nye. The flow law of ice from measurements in glacier tunnels, laboratory experiments and the Jungfraufirn borehole experiment. *Proceedings of the Royal Society of London A: Mathematical, Physical and Engineering Sciences*, 219(1139):477–489, 1953. doi: 10.1098/rspa.1953.0161.

J. Oerlemans. *Minimal glacier models*. Igitur, Universiteitsbibliotheek Utrecht, 2008. ISBN 978-90-6701-022-1.

J. Oerlemans and F. Nick. Modelling the advance–retreat cycle of a tidewater glacier with simple sediment dynamics. *Global and Planetary Change*, 50(3–4):148 – 160, 2006. doi: 10.1016/j.gloplacha.2005.12.002.

M. O'Leary and P. Christoffersen. Calving on tidewater glaciers amplified by submarine frontal melting. *The Cryosphere*, 7(1):119–128, 2013. doi: 10.5194/tc-7-119-2013.

S. O'Neel, K. A. Echelmeyer, and R. J. Motyka. Short-term variations in calving of a tidewater glacier: LeConte Glacier, Alaska, USA. *Journal of Glaciology*, 49(167):587–598, 2003. doi: 10.3189/172756503781830430.

S. O'Neel, W. T. Pfeffer, R. Krimmel, and M. Meier. Evolving force balance at Columbia Glacier, Alaska, during its rapid retreat. *Journal of Geophysical Research: Earth Surface*, 110(F3):F03012, 2005. doi: 10.1029/2005JF000292.

A. Petersen, J. Blackstock, and N. Morisetti. New leadership for a user-friendly IPCC. *Nature Climate Change*, 5:909 EP, 2015. doi: 10.1038/nclimate2766.

M. Petlicki, M. Ciepły, J. A. Jania, A. Promińska, and C. Kinnard. Calving of a tidewater glacier driven by melting at the waterline. *Journal of Glaciology*, 61(229):851–863, 2015. doi: doi:10.3189/2015JoG15J062.

V. Peyaud, C. Ritz, and G. Krinner. Modelling the Early Weichselian Eurasian Ice Sheets: role of ice shelves and influence of ice-dammed lakes. *Climate of the Past Discussions*, 3(1):221–247, Jan. 2007. URL https://hal.archives-ouvertes.fr/hal-00330724.

W. T. Pfeffer. A simple mechanism for irreversible tidewater glacier retreat. *Journal of Geophysical Research: Earth Surface*, 112(F3):F03S25, 2007. doi: 10.1029/2006JF000590.

W. T. Pfeffer, J. T. Harper, and S. O'Neel. Kinematic constraints on glacier contributions to 21st-century sea-level rise. *Science*, 321(5894):1340–1343, 2008. doi: 10.1126/science.1159099.

A. Pralong and M. Funk. Dynamic damage model of crevasse opening and application to glacier calving. *Journal of Geophysical Research: Solid Earth*, 110(B1):B01309, 2005. doi: 10.1029/2004JB003104.

S. F. Price, W. Lipscomb, M. Hoffman, M. Hagdorn, I. Rutt, T. Payne, F. Hebeler, and J. H. Kennedy. CISM 2.0.5 Documentation. http://oceans11.lanl.gov/trac/CISM/data/cism_documentation_v2.0.pdf, 2015.

L. S. Prokopy, J. S. Carlton, J. G. Arbuckle, T. Haigh, M. C. Lemos, A. S. Mase, N. Babin, M. Dunn, J. Andresen, J. Angel, C. Hart, and R. Power. Extension's role in disseminating information about climate change to agricultural stakeholders in the united states. *Climatic Change*, 130(2):261–272, 2015. doi: 10.1007/s10584-015-1339-9.

N. Reeh. On the calving of ice from floating glaciers and ice shelves. *Journal of Glaciology*, 7(50):215–232, 1968. doi: 10.3189/S0022143000031014.

A. Remaître, J.-P. Malet, O. Maquaire, C. Ancey, and J. Locat. Flow behaviour and runout modelling of a complex debris flow in a clay-shale basin. *Earth Surface Processes and Landforms*, 30(4):479–488, Apr. 2005. doi: 10.1002/esp.1162.

J. R. Rice. *Fracture: An advanced treatise*, volume 2, chapter 3. Mathematical analysis in the mechanics of fracture, pages 191–311. Academic Press, 1968.

E. Rignot, M. Koppes, and I. Velicogna. Rapid submarine melting of the calving faces of West Greenland glaciers. *Nature Geoscience*, 3:187 EP, 2010. doi: 10.1038/ngeo765.

E. Rignot, I. Velicogna, M. R. van den Broeke, A. Monaghan, and J. T. M. Lenaerts. Acceleration of the contribution of the Greenland and Antarctic ice sheets to sea level rise. *Geophysical Research Letters*, 38(5):L05503, 2011. doi: 10.1029/2011GL046583.

E. Rignot, J. Mouginot, C. F. Larsen, Y. Gim, and D. Kirchner. Low-frequency radar sounding of temperate ice masses in southern Alaska. *Geophysical Research Letters*, 40 (20):5399–5405, 2013. doi: 10.1002/2013GL057452.

J. B. Ritchie, C. S. Lingle, R. J. Motyka, and M. Truffer. Seasonal fluctuations in the advance of a tidewater glacier and potential causes: Hubbard Glacier, Alaska, USA. *Journal of Glaciology*, 54(186):401–411, July 2008. doi: 10.3189/002214308785836977.

M. Rytz. Anote's ark. [Documentary film], 2018.

D. Sarewitz and R. A. Pielke. The neglected heart of science policy: reconciling supply of and demand for science. *Environmental Science & Policy*, 10(1):5 – 16, 2007. doi: https://doi.org/10.1016/j.envsci.2006.10.001.

C. Schoof. Marine ice-sheet dynamics. Part 1. The case of rapid sliding. *Journal of Fluid Mechanics*, 573:27–55, 2007. doi: 10.1017/S0022112006003570.

B. Siebenhüner. The changing role of nation states in international environmental assessments—the case of the IPCC. *Global Environmental Change*, 13(2):113 – 123, 2003. doi: 10.1016/S0959-3780(03)00023-2.

L. A. Stearns and G. S. Hamilton. Rapid volume loss from two East Greenland outlet glaciers quantified using repeat stereo satellite imagery. *Geophysical Research Letters*, 34(5):L05503, 2007. doi: 10.1029/2006GL028982.

L. A. Stearns, G. S. Hamilton, C. J. vander Veen, D. C. Finnegan, S. O'Neel, J. B. Scheick, and D. E. Lawson. Glaciological and marine geological controls on terminus dynamics of Hubbard Glacier, southeast Alaska. *Journal of Geophysical Research: Earth Surface*, 120(6):1065–1081, 2015. doi: 10.1002/2014JF003341.

J. Stevenson, M. Crimmins, J. Whitehead, J. Brugger, and C. Fraisse. *Connecting climate information with practical uses: Extension and the NOAA RISA program*, chapter 4, pages 75–98. Wiley-Blackwell, Oxford, UK, 2016. ISBN 9781118474785. doi: 10.1002/9781118474785.ch4.

F. Straneo, D. A. Sutherland, D. Holland, C. Gladish, G. S. Hamilton, H. L. Johnson, E. Rignot, Y. Xu, and M. Koppes. Characteristics of ocean waters reaching Greenland's glaciers. *Annals of Glaciology*, 53(60):202–210, 2012. doi: 10.3189/2012AoG60A059.

F. Straneo, P. Heimbach, O. Sergienko, G. Hamilton, G. Catania, S. Griffies, R. Hallberg, A. Jenkins, I. Joughin, R. Motyka, W. T. Pfeffer, S. F. Price, E. Rignot, T. Scambos, M. Truffer, and A. Vieli. Challenges to understanding the dynamic response of Greenland's marine terminating glaciers to oceanic and atmospheric forcing. *Bulletin of the American Meteorological Society*, 94(8):1131–1144, 2013. doi: 10.1175/BAMS-D-12-00100.1.

D. C. Trabant, R. M. Krimmel, K. A. Echelmeyer, S. L. Zirnheld, and D. H. Elsberg. The slow advance of a calving glacier: Hubbard Glacier, Alaska, U.S.A. *Annals of Glaciology*, 36(1):45–50, January 2003. doi: 10.3189/172756403781816400.

J. Tribbia and S. C. Moser. More than information: what coastal managers need to plan for climate change. *Environmental Science & Policy*, 11(4):315 – 328, 2008. doi: https://doi.org/10.1016/j.envsci.2008.01.003.

M. Truffer, R. J. Motyka, M. Hekkers, I. M. Howat, and M. A. King. Terminus dynamics at an advancing glacier: Taku Glacier, Alaska. *Journal of Glaciology*, 55(194):1052–1060, 2009. doi: 10.3189/002214309790794887.

U. S. Geological Survey. Hubbard Glacier, Alaska: Growing and advancing in spite of global climate change and the 1986 and 2002 Russell Lake outburst floods. USGS Fact Sheet 001-03, January 2003.

L. Ultee and J. N. Bassis. The future is Nye: An extension of the perfect plastic approximation to tidewater glaciers. *Journal of Glaciology*, 62(236):1143–1152, 2016. doi: 10.1017/jog.2016.108.

L. Ultee and J. N. Bassis. A plastic network approach to model calving glacier advance and retreat. *Frontiers in Earth Science*, 5(24), 2017. doi: 10.3389/feart.2017.00024.

M. van den Broeke, J. Bamber, J. Ettema, E. Rignot, E. Schrama, W. J. van de Berg, E. van Meijgaard, I. Velicogna, and B. Wouters. Partitioning recent Greenland mass loss. *Science*, 326(5955):984 – 986, 2009. doi: 10.1126/science.1178176.

M. R. van den Broeke, E. M. Enderlin, I. M. Howat, P. Kuipers Munneke, B. P. Y. Noël, W. J. van de Berg, E. van Meijgaard, and B. Wouters. On the recent contribution of the greenland ice sheet to sea level change. *The Cryosphere*, 10(5):1933–1946, 2016. doi: 10.5194/tc-10-1933-2016. URL http://www.the-cryosphere.net/10/1933/2016/.

D. G. Vaughan. Relating the occurrence of crevasses to surface strain rates. *Journal of Glaciology*, 39(132):255–266, 1993. doi: 10.3189/S0022143000015926.

D. G. Vaughan, J. Comiso, I. Allison, J. Carrasco, G. Kaser, R. Kwok, P. W. Mote, T. Murray, F. Paul, J. Ren, E. Rignot, O. Solomina, K. Steffen, and T. Zhang. Observations: Cryosphere. In T. F. Stocker, D. Qin, G. K. Plattner, M. Tignor, S. K. Allen, J. Boschung, A. Nauels, Y. Xia, V. Bex, and P. M. Midgley, editors, *Climate Change 2013: The Physical Science Basis*, pages 317–382. Cambridge University Press, Cambridge, United Kingdom and New York, NY, USA, 2013.

I. Velicogna, T. C. Sutterley, and M. R. vanden Broeke. Regional acceleration in ice mass loss from Greenland and Antarctica using GRACE time-variable gravity data. *Geophysical Research Letters*, 41(22):8130–8137, 2014. doi: 10.1002/2014GL061052.

A. Vieli, M. Funk, and H. Blatter. Tidewater glaciers: Frontal flow acceleration and basal sliding. *Annals of Glaciology*, 31(1):217–221, 2000. doi: 10.3189/172756400781820417.

A. Vieli, M. Funk, and H. Blatter. Flow dynamics of tidewater glaciers: a numerical modelling approach. *Journal of Glaciology*, 47(159):595–606, 2001. doi: 10.3189/172756501781831747.

D. Viner and C. Howarth. Practitioners' work and evidence in IPCC reports. *Nature Climate Change*, 4:848 EP, 2014. doi: 10.1038/nclimate2362.

K. Walsh, H. Betts, J. Church, and A. B. Pittock. Using sea level rise projections for urban planning in Australia. *Journal of Coastal Research*, 20(2):586–598, 2004.

F. Walter, S. O'Neel, D. McNamara, W. T. Pfeffer, J. N. Bassis, and H. A. Fricker. Iceberg calving during transition from grounded to floating ice: Columbia Glacier, Alaska. *Geophysical Research Letters*, 37(15):L15501, 2010. doi: 10.1029/2010GL043201.

C. R. Warren. Terminal environment, topographic control and fluctuations of west greenland glaciers. *Boreas*, 20(1):1–15, 1991. doi: 10.1111/j.1502-3885.1991.tb00453.x.

R. Winkelmann, M. A. Martin, M. Haseloff, T. Albrecht, E. Bueler, C. Khroulev, and A. Levermann. The Potsdam Parallel Ice Sheet Model (PISM-PIK) – Part 1: Model description. *The Cryosphere*, 5(3):715–726, 2011. doi: 10.5194/tc-5-715-2011.